ASSESSMENT OF UNCERTAINTIES IN BED LOAD RATE AND WATER SURFACE PROFILE COMPUTATIONS

A THESIS SUBMITTED TO
THE GRADUATE SCHOOL OF NATURAL AND APPLIED SCIENCES
OF
MIDDLE EAST TECHNICAL UNIVERSITY

BY

GİZEM GENÇ

IN PARTIAL FULFILLMENT OF THE REQUIREMENTS
FOR
THE DEGREE OF MASTER OF SCIENCE
IN
CIVIL ENGINEERING

JANUARY 2023

Approval of the thesis:

ASSESSMENT OF UNCERTAINTIES IN BED LOAD RATE AND WATER SURFACE PROFILE COMPUTATIONS

submitted by **GİZEM GENÇ** in partial fulfillment of the requirements for the degree of **Master of Science** i**n Civil Engineering, Middle East Technical University** by,

Prof. Dr. Halil Kalıpçılar
Dean, Graduate School of **Natural and Applied Sciences** _____

Prof. Dr. Erdem Canbay
Head of the Department, **Civil Engineering** _____

Prof. Dr. A. Melih Yanmaz
Supervisor, **Civil Engineering, METU** _____

Examining Committee Members:

Prof. Dr. A. Burcu Altan Sakarya
Civil Engineering, METU _____

Prof. Dr. A. Melih Yanmaz
Civil Engineering, METU _____

Prof. Dr. Elçin Kentel Erdoğan
Civil Engineering, METU _____

Prof. Dr. İsmail Yücel
Civil Engineering, METU _____

Assoc. Prof. Dr. Müsteyde Baduna Koçyiğit
Civil Engineering, Gazi University _____

Date: 12.01.2023

I hereby declare that all information in this document has been obtained and presented in accordance with academic rules and ethical conduct. I also declare that, as required by these rules and conduct, I have fully cited and referenced all material and results that are not original to this work.

Name Last name : Gizem Genç

Signature :

ABSTRACT

ASSESSMENT OF UNCERTAINTIES IN BED LOAD RATE AND WATER SURFACE PROFILE COMPUTATIONS

Genç, Gizem
Master of Science, Civil Engineering
Supervisor : Prof. Dr. A. Melih Yanmaz

January 2023, 109 pages

Many processes in water resources engineering are disposed to uncertainty due to the inherent variation of many inputs and parameters in time and place. This study mainly consists of two parts. In the first part, probabilistic variations of bed load rates are examined using Meyer-Peter Müller and Einstein-Brown approaches under the effect of different bed slopes, bed materials, and flow rates in the Miliç Basin. The results of the first part offer an insight into the probabilistic nature of bed resistance. With this awareness, the changes in the water surface profile are analyzed in the second part of the study. The Monte Carlo simulation method is utilized to carry out the uncertainty analysis of bed load rate and water surface profile computations. The recommended Probability Density Function and coefficient of variation for hydraulic variables reported in the literature are designated for the milestone of the simulation. To appraise the outcomes, the Chi-Square and Kolmogorov-Smirnov tests are applied as part of the Goodness of Fit test. Consequently, mainly Beta and Gamma distributions are observed for the bed load transport rate in the study area. As the expanse of the second part, Manning's roughness coefficient and the flow rate are

investigated by integrating Monte Carlo simulation with the HEC-RAS model for Taşlıdere Creek. Consequently, when uncertainty analysis is conducted for flow rate and Manning's roughness coefficient jointly, mainly Gamma and Log-normal distributions are observed for the bed load transport rate.

Keywords: Uncertainty, Bed load rate, Monte Carlo simulation, flow depth, Manning's roughness coefficient

ÖZ

SÜRÜNTÜ YÜKÜ VE SU YÜZÜ PROFİLİ HESAPLARINDA BELİRSİZLİKLERİN DEĞERLENDİRİLMESİ

Genç, Gizem
Yüksek Lisans, İnşaat Mühendisliği
Tez Yöneticisi: Prof. Dr. A. Melih Yanmaz

Ocak 2023, 109 sayfa

Su kaynakları mühendisliğindeki çoğu süreç birçok girdinin ve parametrenin zaman ve mekandaki doğal değişkenliğinden dolayı belirsizliğe eğilimlidir. Bu çalışma başlıca iki kısımdan oluşmaktadır. İlk kısımda Miliç Irmağı ve kollarında farklı taban eğimi, taban malzemesi ve debi etkisi altında Meyer-Peter Müller ve Einstein-Brown bağıntıları kullanılarak hesaplanan sürüntü yükünün olasılıksal değişimleri incelenmiş ve bunları temsil eden olasılık yoğunluk fonsiyonları bulunmuştur. İlk bölümün sonuçları, taban pürüzlülüğünün olasılıksal doğasına ışık tutmaktadır. Bu bilinçle çalışmanın ikinci kısmında su yüzü profilindeki değişimler incelenmiştir. Monte Carlo simülasyon yöntemi, sürüntü yükü ve su yüzeyi profili hesaplamalarının belirsizlik analizini gerçekleştirmek için kullanılmıştır. Literatürde önerilen olasılık yoğunluk fonksiyonu ve değişim katsayısı değerleri hidrolik değişkenler için simülasyonlarda kullanılmıştır. Sonuçları değerlendirmek için uygunluk testi kapsamında Chi-Kare ve Kolmogorov-Smirnov testleri uygulanmıştır. Sonuçlar göz önüne alındığında, çalışma bölgesinde sürüntü yükü için çoğunlukla Beta ve Gamma dağılımları gözlenmiştir. İkinci bölüm kapsamında Taşlıdere için Monte Carlo simülasyonu HEC-RAS modeline entegre edilerek

Manning pürüzlülük katsayısı ve debi etkisi incelenmiştir. Sonuçlar göz önüne alındığında, hem debi hem de Manning pürüzlülük katsayısı için birlikte belirsizlik analizi yapıldığında akım derinliği için çoğunlukla Gamma ve Log-normal dağılımları gözlenmektedir.

Anahtar Kelimeler: Belirsizlik, sürüntü yükü, Monte Carlo simülasyonu, akım derinliği, Manning pürüzlülük katsayısı

To my family…

ACKNOWLEDGMENTS

I would like to express my deepest appreciation to my supervisor Prof. Dr. A. Melih Yanmaz for bringing the weight of his considerable experience, wisdom, and knowledge to this study. He always stands with his flashlight whenever I felt in the dark. I would not have been able to complete this thesis without his support and valuable comments. I am grateful for his guidance, patience, and faith through the conduction of this study.

I am grateful to Assist. Prof. Dr. Mehdi Hesami Afshar for always supporting me and being a door to knock on whenever I have a question. I appreciate Berkay Akpınar and Can Şanlıtürk for their help and for being a phone call away every time I stumbled upon my study. Constructive criticism of Prof. Dr. Elçin Kentel Erdoğan is appreciated.

I would like to thank my colleagues one by one. Many thanks to Serdar Binzet, Jean Baptiste Etienne, Emrah Demirtaş, Seda Mercan, and everyone whose names I could not write. I am grateful to them for always allowing me to create a space for my thesis despite our busy meetings and workloads.

Special and profound thanks to my sister İrem, and my parents, Asiye and Erhan Genç. All this time, I had a full-time job and a thesis study. They always welcomed me with understanding during all this busy rush, and the precious time I could not spare for them. Their motivational speeches and supports are invaluable to me.

Thanks to my dear friends Beril Aydın and Ceren Durğut, who shared the same path with me. We started this adventure together and we are going to finish it together. With their instant support, I always had a foothold.

Final and endless thanks to my partner and my best friend, Naim Kıldırgıcı who is always with me when I need him. I would not have been able to complete this path without his support.

TABLE OF CONTENTS

LIST OF TABLES

TABLES

LIST OF FIGURES

FIGURES

LIST OF SYMBOLS

SYMBOLS

A	Flow area
C	Chezy coefficient
C'	Chezy coefficient for the skin friction effect
D	Sediment particle size
$D_n^{\propto}$	Kolmogorov-Smirnov Test statistics
D_g	Geometric mean size of bed material
D_{50}	Median grain size
D_{90}	Diameter at which 90% of the particle size distribution is less than it
f	Degree of freedom
F(x)	Cumulative distribution function for Kolmogorov-Smirnov test
f_i	Observed frequency for Chi-Square Test
g	Acceleration of gravity
h_o	Initial water level
H_a	Alternative hypothesis
H_0	Null hypothesis
i	Rainfall intensity
k	Number of parameters for Chi-Square Test
m	Number of class intervals

n	Manning's roughness coefficient
n_b	Basic value for the straight, uniform, smooth channel in the natural materials involved
n_1	Correction factor for effect of surface irregularities
n_2	Correction factor for variations in shape and size of the channel cross-section
n_3	Correction factor for value of obstructions
n_4	Correction factor for vegetation and flow conditions
m	Correction factor for meandering of channel
P_i	Estimated frequency for Chi-Square Test
q_B	Bed load transport rate
Q	Flow rate
S_h	Harmonic slope
S_n	Empirical distribution function for the Kolmogorov-Smirnov test
u	Average flow velocity
v	Kinematic viscosity
W_f	Fall velocity of bed material
χ^2	Chi-Square Test statistics
y	Average hydraulic depth
α	Significance level
γ_s	Sediment specific weight

Δ	Relative density
μ	Bed shape factor
σ	Standard deviation

CHAPTER 1

INTRODUCTION

1.1 General

Hydrology, which is the study of Earth's water, is a fundamental phenomenon for the environment and human beings. It deals with the generation of design parameters for hydraulic structures, management of water resources, sediment transportation, reservoir routing, flood control, forecasting of hydrological events and time series, and modeling various processes (Jajarmizadeh et al., 2012; Wilson, 1990). While dealing with all these main subjects, hydrology is subject to uncertainty. Hydrology can only be sufficient for mathematical representation due to a lack of knowledge, such as the essential dynamics of water processes and the geometry of systems (Montanari et al., 2009). At the point of representation, the deterministic approach is used for formulating the variables in nature with an accurate method. In the deterministic approach, the same set of outputs is obtained by using the inputs in a time-invariant manner. Despite this approach being the most effective and easiest way to analyze the system, hydrological systems are exposed to unstable cases, which always occur in nature (Verhoeven et al., 2003). At this point, it becomes difficult or not realistic to formulate the deterministic approaches; therefore, the stochastic approach is required. The stochastic approach explains the randomness and distributions of variables instead of providing unique values and it fills the blank points in the system (Renard et al., 2013). Since all hydrologic variables from nature are stochastic, hydrological models are disposed to uncertainty (Iskra and Droste, 2008). For example, when reservoir sedimentation is analyzed for many hydrological studies, they have uncertainties arising from parameters, such as the rate of streamflow, the quantity of sediment inflow into a reservoir, sediment particle size

distribution, and reservoir size (Salas and Shin, 1999). Other examples, such as designing dams and storm drainage systems and assessing the water supply facilities are disposed to uncertainty because of characteristics of flow simulation models, supplies, and operating processes (Yen, 2010). In order to present a study that is close to being certain, analyzing and modeling processes should be conducted regarding uncertainty analysis of hydraulic variables, such as hydraulic parameters (flow rate, headloss, etc.), inputs (meteorological time series, river geometry, etc.), or factors (design flood frequency, etc.) (Iskra and Droste, 2008). Correspondingly, dealing with uncertainties is an essential step for hydrology and water resources. Working with precise hydraulic variables is beneficial for engineers in decision-making, sediment transportation analysis, data processing, cost-effective designs, and more accurate inputs and outputs for prediction and simulation models (Johnson, 1996; Yen, 2010). Hence, it is stated that a wide range of engineering perspectives and interpretations is presented by introducing a stochastic approach.

1.2 Assessment of Uncertainty

In planning and design steps carried out in water resources engineering, systems are exposed to uncertainty for many reasons. Hydrologic or hydraulic uncertainties in these systems can be given as leading examples. Hydrologic uncertainty can be classified as natural, model, and parameter uncertainties. Natural uncertainty occurs due to nature which is unmanageable and variable. Model uncertainty appears because of the estimations made in the equations integrated into the model, and correction factors can be used to limit these uncertainties. Parameter uncertainty arises due to the randomness of the coefficients used in the mathematical statements. The uncertainty arising from the structure, model, and flow description is hydraulic uncertainty. An evaluation of the general uncertainty of the phenomenon is required to evaluate the system properly (Yanmaz, 2022a).

1.3 Literature Review

Generally, uncertainty defines a situation that includes defective or unknown information (Corotis, 2015). Before investigating the uncertainty analyses and methods, the factors and sources causing uncertainty should be known. The uncertainty of hydraulic analyses and modeling could be affected by the following reasons (Chang et al., 1993; Montanari et al., 2009):

1. The inherent variability of natural phenomena.
2. The structural error of the model (difficulty in reflecting the same behavior in nature).
3. Uncertainty of parameter due to quantification problems.
4. Uncertainty of data due to measurement error and heterogeneity of samples.
5. Uncertainties arising from the possibility of operator and human error during the model and analysis phase.

In hydrology and water resources, many studies have been carried out to clarify the uncertainty subjects, such as monitoring the variables that impact uncertainty most and identifying the most efficient, costly beneficial, and easily applicable methods to eliminate uncertainties.

Hieu et al. (2015) applied three different methods to investigate uncertainty quantification through the bed level of the river for TELEMAC/2D simulation to a 10 km long reach of River Rhine. The Monte Carlo simulation, First Order Second Moment method, and algorithmic differentiation methods were selected to identify the most applicable approach and to determine the effect of uncertainty analysis in river engineering. Manning's roughness coefficient and the various grain sizes were selected as uncertain parameters. It is concluded that three methods are successful to conduct uncertainty analysis and the most sensitive parameter for analysis is Manning's roughness coefficient for the main channel. Consequently, the study presented the advantages and opportunities of uncertainty analysis for numerical calculations in river engineering.

Iskra and Droste (2008) performed a study based on parameter uncertainty by using three different methods in the watershed model. The 18 different hydrologic parameters were analyzed by Methods of Moments, Monte Carlo simulation, and Response Surface. According to the study, the Monte Carlo simulation method provided the best improvement in uncertainty analysis and provided more useful outputs than other methods.

A study was performed by Chang et al. (1993) by using the Latin hypercubic sampling technique and the linear regression procedure to identify the sensitivity and uncertainty of the sediment transport model. The sediment transport model was selected to implement uncertainty analysis due to the randomness of sediment input data in nature. HEC2-SR (US Army Corps of Engineers, 1990) was preferred to obtain and review the analysis results. Manning's roughness coefficient (for left, right, and main channels), contraction and expansion coefficients, porosity, and grain sizes were selected as input. The study was conducted by assuming that the only feature affecting the uncertainty is the input parameters. The Uniform distribution was assigned as the Probability Density Function (PDF) for all inputs. After conducting the analyses, it was recorded that the major input parameter that caused uncertainty was the main channel Manning's roughness coefficient. As a consequence of the study, conducting uncertainty analysis to input parameters improved the precision of model results. According to the authors, the stochastic input values were enhanced with uncertainty and sensitivity analysis, leading engineers to study more efficient and reliable models. Lastly, the authors suggested that different types of non-normal distributions should be considered to show the model's response.

Altarejos-García et al. (2012) carried out a study to be an option for Monte Carlo simulation by applying Rosenblueth's Point-Estimate Method (PEM) in a stream that is part of the Turia River in Spain. The velocity and flow depth were selected to visualize the uncertainty effect on inundation risk assessment via flow modeling. In

the uncertainty analysis, Manning's roughness coefficients (main channel and both over banks) were considered as the origin of uncertainty to obtain the mean and standard deviation for the flow depth and velocity. For Manning's roughness coefficient, three types of distribution were assigned which are Uniform, Normal, and Triangular. Analyzes were performed for three different flow rates, 200, 300 and 500 m^3/s. The Uniform Flow model, 1D HEC-RAS model, and 2-D Shallow Water Equations model were used to monitor the results. To compare the productivity of the PEM and Monte Carlo methods, both of them were implemented via a 1D model. As a result, the Log-normal distribution is found to be suitable to estimate only flow depth according to the PEM method. Since the output variables were parallel with the Monte Carlo simulation, the 1D HEC-RAS model study was successful with the PEM method. It was stated that the method lost accuracy as the complexity and number of iterations rise while performing uncertainty studies on 2D models. Lastly, it was noted that the Monte Carlo method is proposed as an effective tool in uncertainty analysis.

The uncertainty of annual sediment deposition and sediment accumulation over a long period in the reservoir was studied by Salas and Shin (1999) in Kenny Reservoir in Colorado. Since the prediction of reservoir sedimentation depends on some variables, such as sediment load, it is subject to uncertainty. In this study, the uncertainty of the main factors which are flow rate, sediment load, the grain size of sediment, and trap efficiency was investigated. The analysis of the reservoir sedimentation study to evaluate the uncertainty was done with Latin hypercube sampling and Monte Carlo simulation methods. The results demonstrated that the most critical uncertainty resources for reservoir sedimentation are annual flow rate and sediment inflow.

Bozzi et al. (2015) conducted research based on roughness coefficient and flow rate uncertainty through a 1D model and visualized the effects with flow depth. The steady flow was used for this study for the rectangular cross-section for two rivers in

Italy and France. In the first step, by using the derived distribution method, PDFs of the flow depths were examined. In the second step, the Monte Carlo simulation was used to obtain output PDFs. It was stated that the coefficient of variation (COV) of output (flow depth) was lower than the COVs of inputs (roughness coefficient and flow rate). Moreover, despite the assigned symmetrical distributions for input parameters, the output provided asymmetrical distributions. For the flow depth PDFs, the left-skewed PDFs and the right-skewed flow depth PDFs were observed from the flow rate and roughness coefficient, respectively. As a result of this study, uncertainty analysis on the input roughness coefficient and flow rate should not be ignored when implementing flow depth analysis from a model.

The model and parameter study for the sediment transportation model was performed by Beckers et al. (2018). To conduct uncertainty analyses, the first-order second-moment method was selected because of computational ease. For model uncertainty, the Shield's parameter and Meyer-Peter Müller factor caused higher uncertainty in the sediment transportation model. For parameter uncertainty, river channel roughness and grain roughness were more uncertain relative to the others. In addition, it was stated in the study that although the first-order second-moment method used was successful, if the input and output values are not linear, different methods, such as Monte Carlo simulation, should be adopted.

As observed in many studies, the most fundamental step based on reliability and uncertainty analysis is selecting the most suitable COV and PDF for the governing variables. If these two variables are not selected appropriately, it may lead to errors in the analysis results (Johnson, 1996). In the uncertainty studies conducted in hydrology and water resources, COV and PDF selections were made in different values and distributions (Cesare, 1991; Johnson, 1999, 1996, 1995, 1992; Kentel and Yanmaz, 2008; Liao et al., 2015; Mays and Tung, 2002; Tung and Member, 1990; Wang, 2004; Yanmaz, 2003; Yeh et al., 1993). Therefore, the variables used in the uncertainty analyses reported in the literature are reviewed to identify the proposed

COVs and PDFs in this study. The summary information is presented in Table 1.1, and the selection of the relevant variables in this study is based on this table.

Table 1.1 The summary table for proposed COV and PDF for hydraulic variables

VARIABLE	***PROPOSED PDF***	***PROPOSED COV***	***REFERENCES***
Geometric mean size of bed material, D_g	Uniform distribution	0.05	(Yanmaz, 2003)
Fall velocity of bed material, W_f	Symmetrical Triangular distribution	0.2	(Yanmaz, 2003)
Flow Depth	Symmetrical Triangular distribution	0.2	(Johnson, 1999)
Flow Depth	Normal distribution	0.23	(Liao et al., 2015)
Flow Velocity	Triangular distribution	0.008	(Johnson, 1996)
Flow Velocity	Uniform distribution	0.012	(Johnson, 1996)
Flow Velocity	Symmetrical Triangular distribution	0.2	(Johnson, 1999)
Flow Velocity	NA	0.329	(Johnson, 1992)
Flow Velocity	NA	0.51	(Johnson, 1995)
Sediment particle size, D	Uniform distribution	0.02	(Yeh et al., 1993)
Sediment particle size, D	Uniform distribution	0.05	(Johnson, 1996)
Friction slope	Uniform distribution	0.17	(Yeh et al., 1993)
Sediment specific weight, γ_s	Uniform distribution	0.12	(Yeh et al., 1993)
Drainage Area, A	Normal distribution	0.1	(Kentel and Yanmaz, 2008)

NA*: Not Available

Table 1.1 (continued)

VARIABLE	***PROPOSED PDF***	***PROPOSED COV***	***REFERENCES***
Initial water level, h_0	Normal distribution	0.4	(Kentel and Yanmaz, 2008)
Runoff coefficient, C	Normal distribution	0.3	(Kentel and Yanmaz, 2008)
Rainfall intensity, i	Normal distribution	0.1	(Kentel and Yanmaz, 2008)
Manning roughness, n	Normal distribution	0.1, 0.15	(Cesare, 1991)
Manning roughness, n	Uniform distribution	0.28 , 0.18	(Johnson, 1996)
Manning roughness, n	Normal distribution	0.2, 0.053	(Mays and Tung, 2002)
Manning roughness, n	Triangular distribution	0.08	(Yeh et al., 1993)
Manning roughness, n	Log-normal distribution	0.20 - 0.35	(Yeh et al., 1993)
Manning roughness, n	Triangular & Gamma distribution	0.10, 0.055	(Tung and Member, 1990)
Discharge rate	Log-normal distribution	0.21 - 0.25	(Wang, 2004)
Channel slope	Normal distribution	0.3, 0.068	(Mays and Tung, 2002)
Channel slope	Triangular distribution	0.12, 0164	(Tung and Member, 1990)
Channel slope	Log-normal distribution	0.25	(Johnson, 1996)
Depth of tailwater	Symmetrical Triangular distribution	0.2	(Yanmaz, 2003)
Jet flow velocity	Symmetrical Triangular distribution	0.2	(Yanmaz, 2003)

NA*: Not Available

1.4 The Aim and Scope of the Study

The goal of this thesis is to implement uncertainty analysis based on hydraulic parameters and input variables in the computation of bed load rates and water surface profiles. Besides the deterministic approach, the stochastic approach is applied along with the Monte Carlo simulation based on the assigned PDFs and COVs. After the simulations, the results are investigated based on the Goodness of Fit (GOF) tests.

The study is carried out in two parts. In the first part, sediment bed load transport rate and Manning's roughness coefficient variables are used as sources of uncertainty in the Miliç Basin within the borders of Çarşamba Plain. Since Manning's roughness coefficient is influenced by the rate of bed load transportation in view of material accumulating and scouring, the investigation of the stochastic nature of bed load transportation gives valuable insight into the randomness of bed resistance.

With this awareness, in the second part, Manning's roughness coefficient and flow rate are selected to implement the uncertainty analysis through the HEC-RAS (US Army Corps of Engineers, 2016) in Taşlıdere Creek in Rize. The flow depth is received as an output parameter to interpret the results. The data obtained at the end of the study are investigated based on the PDFs and COVs. The general flowchart of the conducted study can be seen in Figure 1.1.

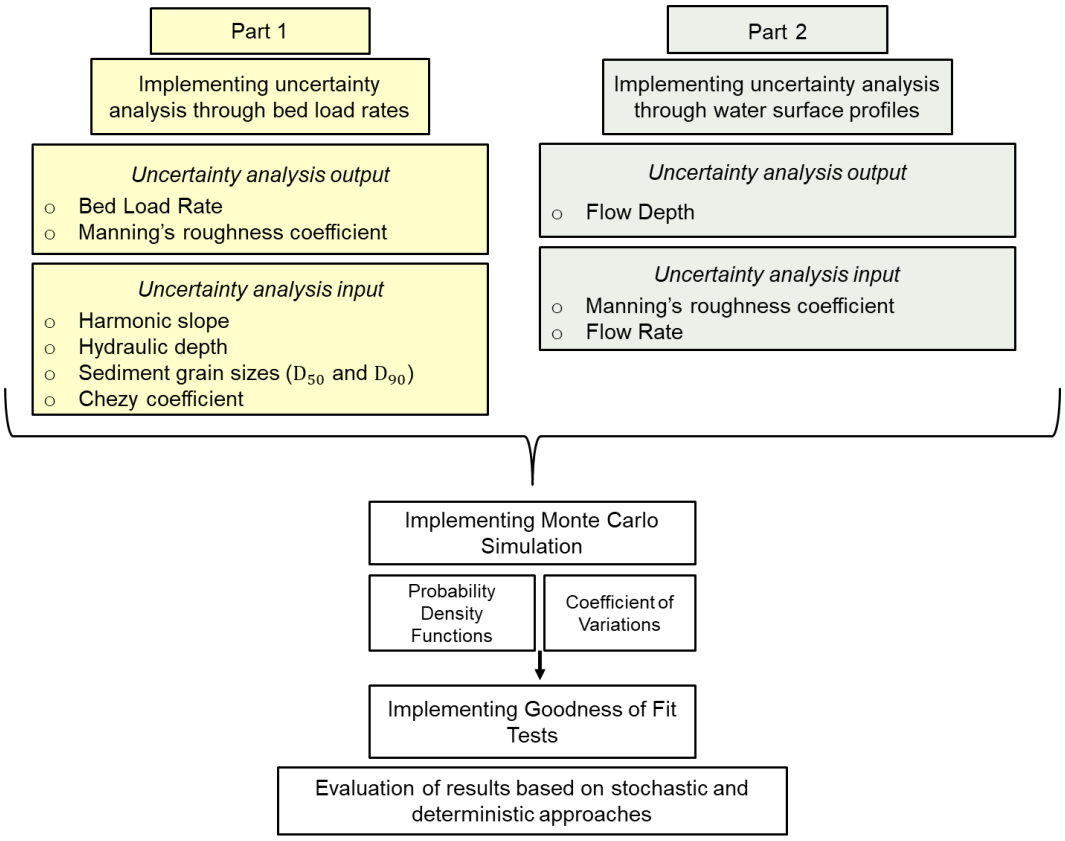

Figure 1.1 General flowchart of the study

Chapter 1 gives general information and a brief literature review together with the aim of the thesis. The definitions and mathematical representations of the methods, software, and variables are explained briefly in Chapter 2. Chapter 3 includes the analysis results and their discussions. Finally, a brief summary and conclusions are presented in Chapter 4.

CHAPTER 2

METHODOLOGY

2.1 Introduction

Problems related to hydrology and water resources are of inherent nature. For this reason, the systems are always subject to randomness and uncertainty. In this study, the probabilistic performance assessments based on uncertainty analyses involved in bed load transport rate and water surface profile computations are implemented with the Monte Carlo simulation to understand the uncertainty phenomena. The GOF tests are conducted to determine the best fittings to the governing variables. This study is conducted in two separate parts with different hydraulic variables. While in the first part an uncertainty study is carried out for bed load rate computation and Manning's roughness coefficient, in the second part another uncertainty study is carried out through the HEC-RAS (US Army Corps of Engineers, 2016) for studying the effect of the randomness of Manning's roughness coefficient and water surface elevation.

2.2 Monte Carlo Simulation Method

When working with mathematical models, input parameters rely on several outer factors and these factors are liable to some risks and uncertain situations. Generally, modeling is conducted using the deterministic approach and this is named the base case. In this case, the deterministic approach does not review all situations that contain risks. As a result, the evaluation is subject to providing uncertain outputs (Renard et al., 2013). Consequently, the stochastic approach is involved and the effect of sampling of variables throughout uncertainty analyses is investigated.

The Monte Carlo simulation is selected to apply uncertainty analysis in this study. The Monte Carlo simulation is a kind of statistical method which uses a set of random samples and defined probability distributions to understand the uncertainty underlying each variable that is part of a physical procedure (Raychaudhuri, 2008; Singh, 2010).

The following steps describe the process of the Monte Carlo simulation method (Dantan and Qureshi, 2009; Raychaudhuri, 2008):

1. The parameters to which the Monte Carlo simulation will be implemented are determined.
2. The statistical features are defined. The applicable PDF and COV are assigned to each parameter.
3. To generate the random samples the mean value of each input parameter is introduced to the system.
4. The simulation is run via a preferred software. By simulating as many times as required, an output set is obtained.
5. Each output value is the result of a scenario in the simulation. To conclude the simulation and the uncertainty analysis, statistical analyzes are accomplished on the output parameters. The study can be concluded by reaching certain conclusions as a result of this statistical analysis.

Inherently, the Monte Carlo simulation method has some advantages and drawbacks. One of the advantageous features is that the working mechanism and algorithm of the method are simple. Each computation is independent and it is not affected by the previous and next calculations (Sobol, 1994). The complicated systems can be modeled with Monte Carlo simulation as it takes into account a large number of input covariances and relations impulsively (Smid et al., 2010). Moreover, while it can deal with both minor and major uncertainties, it also does not need partial derivatives during this operation (Papadopoulos and Yeung, 2001). Despite these advantages, the simulation is variable according to the number of trials and size of the parameter.

Although the number of trials is high, endless trials give the most accurate analysis result (Shui-Tuang Cheng, 1982).

Many uncertainty analyzes have shown that Monte Carlo simulation gives effective results when it is not possible to use an analytical model. For example, Kopmann and Schmidt (2010) compared the Scatter Analysis method with the Monte Carlo simulation method in the study. As a result, although the Monte Carlo application time was longer than the Scatter Analysis method, Monte Carlo simulation was recommended because of its effect in computing the tolerance values for non-linear values correctly. In another study, three different uncertainty methods were compared (Iskra and Droste, 2008). These methods were Response surfaces, the method of moments, and the Monte Carlo simulations. As a consequence of the study, the high uncertainty was calculated with Monte Carlo simulation. Additionally, considering that the Monte Carlo simulation needed fewer assumptions, the recommended method was the Monte Carlo simulation.

As a result, the Monte Carlo simulation is selected to apply uncertainty analysis in this study.

Determining the number of simulations is an essential criterion for Monte Carlo simulation. Each repetition of the governing variable provides different values for the mean. In this study, the standard error is used to determine the number of simulations. The standard error is the standard deviation of the population mean. It is shown in Equation 2.1. The simulation is run with different simulation cycles and the results are compared based on standard error values. The selection is completed by choosing the number of simulations that provide the lowest error (Andrade, 2020).

$$\text{Standard Error} = \frac{\sigma}{\sqrt{n}} \tag{2.1}$$

where, σ: Standard Deviation

n: Number of samples

2.3 The Goodness of Fit Test

Model calibration and validation procedures must be applied to be considered successful in the methods and models used in simulating environmental values and processes (Ritter and Munoz-Carpena, 2013). To make statistical calculations more applicable, the obtained graphical result should be represented by an appropriate PDF. After the statistical data are represented graphically, a suitable density function for the distribution of this graph can be proposed. However, the suitability of this process needs to be tested (Yanmaz, 2022b). For this reason, the GOF tests should be applied after conducting an uncertainty analysis.

In this study, the most common two types of GOF tests are used. One of them is the Chi-square test, the other one is Kolmogorov-Smirnov Test.

2.3.1 The Chi-Square Test

The Chi-square test (χ^2) is a GOF test based on whether the difference between observed frequencies and expected frequencies is statistically significant. The Chi-square test is used to test the relevance argument for a population generated based on a random sample and it is applied to test whether a sample of data comes from a population with a certain distribution (Ugoni and Walker, 1995). There are some assumptions for applying the Chi-square test. As long as these assumptions are applied, the test is applicable. These assumptions are as follows (McHugh, 2013):

1. The frequencies or the number of variables should be tested.
2. Each variable promotes data only once and affects another variable only for one subject.
3. The result obtained for each individual does not affect or depend on others.
4. The 80% of the expected frequencies should be greater than five.

The observed frequency in the Chi-square test (f_i) and the estimated PDF frequency (P_i) which is also named estimated frequency are compared with each other. For this

purpose, Equation 2.2 with m being the number of class intervals giving the Chi-square results is calculated (Yanmaz, 2022b).

$$\chi^2 = \sum_{i=1}^{m} \frac{(f_i - P_i)^2}{P_i} < c_{1-\alpha,f} \tag{2.2}$$

It is checked whether the Chi-square value calculated with this equation is less than the limit value. The limit value of the Chi-square distribution is ($c_{1-\alpha,f}$), the significance level is α, the degree of freedom is $f = k - 1$, and the number of parameters is k. The significance levels are selected which are equal to any value between 0 and 1. The limit values of the Chi-square distribution, which should be selected depending on f and $1 - \alpha$, are shown in Table 2.1.

While the null hypothesis (H_0) indicates that the observed distribution follows the expected distribution, and the alternative hypothesis (H_a) indicates that variables do not follow the expected distribution. If the condition in Equation 2.2 is satisfied, the null hypothesis is accepted. Otherwise, the null hypothesis is rejected (Teegavarapu, 2019).

Table 2.1 The limit values for the Chi-square test distribution (Ang and Tang, 1975)

	$1-\alpha$								
f	**0.005**	**0.025**	**0.050**	**0.900**	**0.950**	**0.975**	**0.99**	**0.995**	**0.999**
1	0.04393	0.03982	0.02393	2.71	3.84	5.02	6.63	7.88	10.8
2	0.01	0.0506	0.103	4.61	5.99	7.38	9.21	10.6	13.8
3	0.0717	0.216	0.352	6.25	7.81	9.35	11.3	12.8	16.3
4	0.207	0.484	0.711	7.78	9.49	11.1	13.3	14.9	18.5
5	0.412	0.831	1.15	9.24	11.1	12.8	15.1	16.7	20.5
6	0.676	1.24	1.64	10.6	12.6	14.4	16.8	18.5	22.5
7	0.989	1.69	2.17	12	14.1	16	18.5	20.3	24.3
8	1.34	2.18	2.73	13.4	15.5	17.34	20.1	22	26.1
9	1.73	2.7	3.33	14.7	16.9	19	21.7	23.6	27.9
10	2.16	3.25	3.94	16	18.3	20.5	23.2	25.2	29.6

The Chi-Square test is a strong statistical test that allows the testing of the hypotheses of variables. Inherently, the outcomes are more certain with random samples and with wide sample sizes (McHugh, 2013).

2.3.2 The Kolmogorov-Smirnov Test

The Kolmogorov-Smirnov test is a GOF test. It provides information on whether two distributions have the same distribution by comparing them. One distribution is the distribution of the data set to be tested, while the other one is a known distribution. The null hypothesis (H_0) argues that the distribution tested and the known distribution are the same, while the alternative hypothesis (H_a) argues that there are different distributions (Teegavarapu, 2019). The Kolmogorov-Smirnov test has some limitations. It is necessary to use continuous distributions to perform the test, and the test is more critical in the center. Moreover, the distribution must be determined precisely by a simulation (Aslam, 2019).

In the Kolmogorov-Smirnov test, the variables are sorted from smallest to largest (x_1,x_2,...,x_n). Then $S_n(x)$ which is the empirical distribution function is calculated as follows:

- If $X < x_1$ then $S_n(x) = 0$
- If $x_k \leq X < x_{k+1}$ then $S_n(x) = k/n$
- If $X \geq x_n$ then $S_n(x) = 1$

The difference between the observed total frequencies, F(x), and the total frequencies of the PDF whose fit is investigated is calculated. The maximum value of this difference must be less than the limit value (Equation 2.3).

$$D_n = \max|F(x) - S_n(x)| < D_n^{\alpha} \quad (2.3)$$

In Equation 2.3, D_n^{α} is a critical value at the determined significance level which is shown in Table 2.2. In this table, n is the number of data (Yanmaz, 2022b).

Table 2.2 Kolmogorov-Smirnov test critical values, D_n^{α}, (Ang and Tang, 1975)

	α			
n	**0.20**	**0.10**	**0.05**	**0.01**
5	0.45	0.51	0.56	0.67
10	0.32	0.37	0.41	0.49
15	0.27	0.3	0.34	0.4
20	0.23	0.26	0.29	0.36
25	0.21	0.24	0.27	0.32
30	0.19	0.22	0.24	0.29
35	0.18	0.2	0.23	0.27
40	0.17	0.19	0.21	0.25
45	0.16	0.18	0.2	0.24
50	0.15	0.17	0.19	0.23
>50	$1.07/\sqrt{n}$	$1.22/\sqrt{n}$	$1.36/\sqrt{n}$	$1.63/\sqrt{n}$

2.4 Part 1

To identify the uncertainty of hydraulic parameters to be handled through the course of the Part 1 phase, the Monte Carlo simulation method is implemented in parameters of bed load transport rate and Manning's roughness coefficient for a river separately. Different PDFs and COVs are defined according to the literature review for input variables. Based on the defined PDF and COV, a Monte Carlo simulation is implemented for each variable separately. Consequently, the bed load transport rate and Manning's roughness coefficient are calculated with these results and analyzed based on GOF tests.

2.4.1 Study Area

The area surveyed within the scope of this thesis is the Miliç Basin located in Çarşamba Plain, Turkey. The project site can be divided into three in terms of landforms. These can be listed as the mountainous part, the plateaus between the mountainous part, and the coastal plains between the plateaus and the Black Sea. Çarşamba Plain borders can be seen in Figure 2.1. The region, which has a mild

climate under the influence of the Black Sea, has plenty of rain in every season, and the rains are more effective in autumn and winter seasons. Depending on the climate, the natural vegetation in the project area is forest.

The Miliç Basin, selected as the study area, covers an area of approximately 22 766 hectares.

Six main creeks are selected for analyses in the Miliç Basin. These creeks are named Leylek, Sakarlı, Kışla, Evci, Kocaman, and Miliç from the east to the west, respectively, which can be seen in Figure 2.2.

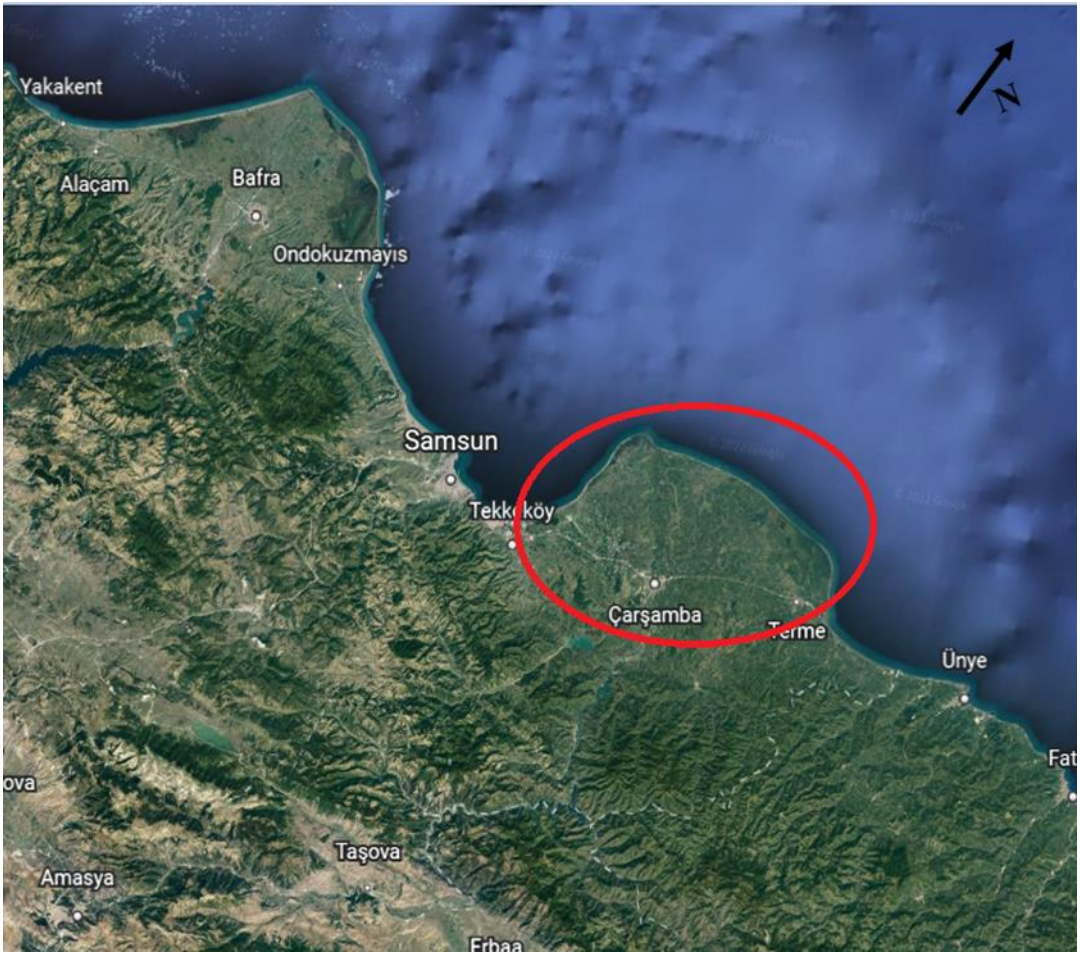

Figure 2.1 Satellite image of Çarşamba Plain (Google Earth February 27, 2022)

Figure 2.2 The six main creeks that are investigated in the Project (Google Earth February 27, 2022)

2.4.2 Bed Load Transport Analyses

Sediments are the particles that are dissolved or eroded from rocks and solid parts of the earth by water, wind, or gravity. The transportation or accumulation of these particles is called sediment transportation. Particle size, particle shape, fall velocity, or bulk properties of particles are the governing properties of sediment and sediment transportation (Yanmaz, 2022a). Sediment load can be computed based on the transport mechanism type, such as bed load transport and suspended load transport. The rolling, sliding, or saltation are the modes at the bed or near the bed leading to sediment transport, called bed load transport (Thorne, 2000). In river engineering, estimating and calculating sediment bed load play a critical role in the design and operation of various types of hydraulic structures. Many formulas have been developed for bed load transport rate. Some commonly used bed load transport formulas are listed below with characteristic grain size ranges (Haddadchi et al., 2013):

- Meyer-Peter and Müller (D_{50}: 0.4 mm – 28.6 mm)
- Schoklitsch (D_{40}: 0.3 mm – 5 mm)
- Einstein-Brown (D_{35}: 0.25 mm – 32 mm)

- Yalın (D_{50}: 0.315 mm – 28.65 mm)
- Engelund and Hansen (D_{50}: 0.15 mm – 5 mm)
- Ackers and White (D_{50}: 0.4 mm – 28.65 mm)
- Van Rijn (D_{90}: 0.6 mm – 2 mm)

Among these equations, two approaches are selected specifically to conduct the uncertainty analysis for the bed load rate calculations. These are the Meyer-Peter and Müller (MPM) and the Einstein-Brown (E-B) approaches. Considering the applicability conditions, these approaches are found to be compatible with the conditions of the study area. Normally MPM approach gives smaller values but the E-B approach gives greater results than actual transport rates (Yanmaz, 2022a). Although Yalın and Ackers and White's approaches are also applicable based on gravel sizes in the case of the study area, these approaches are based on highly complex sequential mathematical formulations. Therefore, the precision of stochastic analyses of these approaches may weaken due to many independent variables to be sampled via Monte Carlo analyses. Hence, only MPM and E-B approaches are accepted to be suitable for stochastic analyses in the study area.

Meyer-Peter and Müller (1949) Approach

In 1948-1949, a sediment load formula was developed based on sediments that have a distinctive specific gravity. MPM approach was enhanced based on uninterrupted dataset experiments for sediment load transportation (Sidiropoulos et al., 2021). This approach is one of the most preferred approaches (Huang, 2010). There are some restrictions to applying this approach. Uniform sediments with a specific gravity ranging from 1.25 to 4 were considered in this approach (Haddadchi et al., 2013). The bed load transport rate formula for the MPM approach is shown in Equation 2.4, while the intermediate steps are shown in Equations 2.5 and 2.6 (Yanmaz, 2022a).

$$\frac{q_B}{D_{50}^{3/2}\sqrt{g\,\Delta}} = 13.3\left(\frac{\mu\, y\, S_h}{\Delta\, D_{50}} - 0.047\right)^{3/2} \quad (2.4)$$

q_B: Bed load transport rate ($m^3/s/m$)

D_{50}: Median grain size (m)

g: Acceleration of gravity (m/s^2)

y: Average hydraulic depth (m)

S_h: Harmonic slope (%)

Δ: Relative density (1.65 for quartz sand)

μ: Bed shape factor

$$\mu = \left(\frac{C}{C'}\right)^{3/2} \quad (2.5)$$

C: Chezy coefficient

C': Chezy coefficient for the skin friction effect

$$C' = 18\ \log\left(\frac{12\, y}{D_{90}}\right) \quad (2.6)$$

D_{90}: Diameter at which 90% of the particle size distribution is less than it (m)

Einstein-Brown (1950) Approach

The Einstein-Brown (Brown, 1950), which is an approach obtained by performing one-directional flow flume tests using well-sorted sediment, is applied by replacement of shear stress with shear velocity (Li and Amos, 1995). There are some limitations for applying this approach. The bed load transport rate formula for the E-B approach is shown in Equation 2.7, while the bed shape factor equation is shown in Equation 2.8 (Yanmaz, 2022a).

$$\frac{q_B}{D_{50}^{3/2}\sqrt{g\,\Delta}} = 100\left(\frac{\Delta\, D_{50}}{\mu\, y\, S_h}\right)^{-1/3} \tag{2.7}$$

$$\mu = \left(\sqrt{\frac{2}{3} + \frac{36\, v^2}{\Delta\, g\, D_{50}^3}} - \sqrt{\frac{36\, v^2}{\Delta\, g\, D_{50}^3}}\right)^3 \tag{2.8}$$

where v: Kinematic viscosity (m^2/s)

Bed load transport rate is variable due to its nature. Since it is very time-consuming, imprecise, and costly to directly measure the bed load, the above-mentioned empirical methods are practical in use. Inherently, these approaches always contain some uncertainties. Considering the engineering studies, such as channel design, flood control systems, etc., identifying the most accurate sediment load is critical and it is important to apply uncertainty analysis to them (Eidsvik, 2004; Riahi-Madvar and Seifi, 2018; Schmelter et al., 2012). For this reason, in this study, uncertainty analysis for bed load rate is conducted through the aforementioned approaches, and each variable which is shown in Table 2.3 is evaluated separately.

Table 2.3 Input variables, which are used in Monte Carlo simulation, for bed load transport rate

Variable	Symbol	Unit
Harmonic slope	S_h	%
Hydraulic depth	y	m
Median grain size	D_{50}	m
Grain size	D_{90}	m
Chezy coefficient	C	-

2.4.3 Manning's Roughness Coefficient

One of the most important equations used in open-channel hydraulic calculations is the Manning formula by Robert Manning in 1889 which is widely used in uniform flow computations (Yen, 1992). The most important problem exposed in the use of the Manning equation is determining the suitable roughness coefficient for open

channels. Choosing an appropriate coefficient depends on a good evaluation since the roughness coefficient depends on several factors, such as accumulation and scouring, geometric features of the channel, type of bed material, and seasonal characteristics. For this reason, this coefficient is corrected according to Equations 2.9 and 2.10 based on cross-section geometry, channel dimension, vegetation and roughness in the flow area, and rate of curvature. These correction factors are given in Table 2.4 (Lagasse et al., 2001) in which sinuosity is the ratio of the length of channel reach to the Euclidean distance between both ends of the channel reach.

$$n = (n_b + n_1 + n_2 + n_3 + n_4)\, m \tag{2.9}$$

$$n_b = 0.0152\, D_{50}^{1/6} \tag{2.10}$$

n_b: Basic value for the straight, uniform, smooth channel in the natural materials involved

n_1: Correction factor for effect of surface irregularities

n_2: Correction factor for variations in shape and size of the channel cross − section

n_3: Correction factor for value of obstructions

n_4: Correction factor for vegetation and flow conditions

m: Correction factor for meandering of channel

D_{50}: Median grain size of definite area (mm)

Table 2.4 Correction factors for Manning's roughness coefficient (Lagasse et al., 2001)

n_i	Conditions	Values	Notes
n_1	Smooth	0	Very smooth channel
	Minor rough	0.001-0.005	Slopes with little erosion
	Moderate Rough	0.006-0.010	Rough base and slope
	Severe rough	0.011-0.020	-
n_2	Small variation	0	Gradual cross-section change
	Medium variation	0.001-0.005	Local section narrowing
	Large variation	0.010-0.015	Frequent section changes
n_3	Low rough	0-0.004	Obstructions occupy < %5 of the cross-sectional area
	Middle rough	0.005-0.015	Obstructions occupy < %15 of the cross-sectional area
	Rough	0.020-0.030	Obstructions occupy = (%15 - %50) of the cross-sectional area
	High rough	0.040-0.060	Obstructions occupy > %50 of the cross-sectional area
n_4	Small vegetation	0.002-0.01	y > 2 vegetation height
	Medium vegetation	0.025-0.050	y > vegetation height
	Large vegetation	0.050-0.1	y < vegetation height
	Extreme vegetation	0.040-0.060	y < 0.5 vegetation height
m	Low curvature	1.00	Sinuosity < 1.2
	Medium curvature	1.15	1.2≤ Sinuosity ≤1.5
	High curvature	1.30	Sinuosity >1.5

The most sensitive and important parameter in determining the flow properties in hydraulic analysis and modeling is Manning's roughness coefficient (Chang et al., 1993; Pappenberger et al., 2005). However, the reliable determination of Manning's roughness coefficient is difficult due to the limited available data (Kumar, 2019). For this reason, the assigned Manning's roughness coefficient values are selected from a wide parameter scale and this value is generally unrealistic according to environmental conditions (Savage et al., 2016). This causes an uncertainty in

Manning's roughness coefficient for conducted studies. For this reason, in this study, uncertainty analysis is performed for Manning's roughness coefficient. For each component of Manning's roughness coefficient, the mean of the minimum and maximum values given in Table 2.4 is calculated and are used as the mean value for n_1, n_2, n_3 and n_4 (see Table 2.5).

Table 2.5 Manning's roughness coefficient correction factors used in this study

$\mathbf{n_1}$	$\mathbf{n_2}$	$\mathbf{n_3}$	$\mathbf{n_4}$
0.0105	0.008	0.0305	0.006

2.4.4 Dataset

The data to be used in the analyses are taken from the Samsun-Terme Kocaman Group basin sediment transport study report (Karagöz and Erkmen, 2009). This study was conducted under the supervision of Prof. Yanmaz. It covers a wide range of sediment, channel geometry, and flow rate data. Since intensive information is available in this study, this basin is specifically selected in this study for the realistic evaluation of uncertainties based on field data. Flow rates of six main creeks in the Miliç Basin are given for 2-year, 5-year, 10-year, 25-year, 50-year, 100-year, and 500-year return periods in Table 2.6 for each creek.

Table 2.6 Flow rate values of Miliç Basin for different return periods

Creek Name	**Return Period**						
	2	**5**	**10**	**25**	**50**	**100**	**500**
	Flow Rate (m^3/s)						
Leylek	14.33	29.85	41.93	58.72	72.07	86.03	120.64
Sakarlı	10.98	22.97	32.29	45.25	55.56	66.34	93.06
Kışla	8.02	16.71	23.47	32.86	40.33	48.15	67.51
Evci	19.46	40.45	56.79	79.49	97.54	116.43	163.23
Kocaman	39.52	80.70	112.67	157.00	192.21	229.01	320.12
Miliç	41.74	85.17	118.87	165.61	202.73	241.54	337.6

The sediment bed load transport rates and the inputs used to calculate these values are shown in Table 2.7 and Table 2.8, in which u is the average flow velocity based on hydraulic depth.

Table 2.7 Bed load calculation according to 50-year return period flow rate

Name of stream	**S_h (%)**	**y (m)**	**D_{50} (mm)**	**D_{90} (mm)**	**u (m/s)**	**μ (MPM)**	**μ (EB)**	**q_B (m^3/s/m) (MPM)**	**q_B (m^3/s/m) (E-B)**
Leylek	0.15	1.65	0.38	21.00	0.69	0.135	0.26	0.0001	0.0030
Sakarlı	0.11	0.83	0.27	5.00	1.21	0.564	0.16	0.0003	0.0012
Kısla	0.66	0.61	19.00	42.00	1.69	0.536	0.54	0.0005	0.4338
Evci	0.30	1.73	26.00	60.00	2.28	0.603	0.54	0.0009	0.6808
Kocaman	0.18	2.02	18.00	45.00	2.22	0.66	0.54	0.0008	0.3936
Milic 1	1.24	1.39	16.00	64.00	3.52	0.498	0.54	0.0159	0.5762
Milic 2	0.03	1.52	0.08	0.1	1.39	0.561	0.003	0.00010	0.00006

Table 2.8 Bed load calculation according to 500-year return period flow rate

Name of stream	**S_h (%)**	**y (m)**	**D_{50} (mm)**	**D_{90} (mm)**	**u (m/s)**	**μ (MPM)**	**μ (EB)**	**q_B (m^3/s/m) (MPM)**	**q_B (m^3/s/m) (E-B)**
Leylek	0.15	1.84	0.38	21.00	0.82	0.158	0.26	0.0002	0.0031
Sakarlı	0.11	1.07	0.27	5.00	1.10	0.383	0.16	0.0002	0.0014
Kısla	0.66	0.67	19.00	42.00	2.00	0.627	0.54	0.0012	0.4475
Evci	0.30	2.09	26.00	60.00	2.70	0.642	0.54	0.0023	0.7251
Kocaman	0.18	2.40	18.00	45.00	2.54	0.684	0.54	0.0016	0.4169
Milic 1	1.24	1.45	16.00	64.00	4.03	0.583	0.54	0.0224	0.5844
Milic 2	0.03	1.93	0.08	0.1	1.61	0.571	0.003	0.00015	0.000016

2.4.5 Software

In this study, R programming is used to implement Monte Carlo simulation as part of the uncertainty analysis in Part 1. R programming is a continuously improved and updated programming language that analyzes and manipulates data, works with arrays and matrices, and provides visualization for analysis (Chan, 2018). It provides a high capacity for both statistical analysis and visualization. The working mechanism of Monte Carlo simulation in R programming is based on the probability of generating several random variables as much as required for known or newly assigned distributions (Robert et al., 2010). While visualizing simulation results in R programming, the histograms are created for each simulation. In the histogram, each column gives information about the density and frequency distributions of the outputs. The total area of the histogram must be equal to unity. Subsequently, the frequency or density axes (corresponding to the y-axis) are unitless and their decimals are automatically determined to have a total area of unity according to the decimals of the value on the x-axis (Li et al., 2019). Moreover, while determining the number of class intervals of the histograms for applying the GOF test, Sturges' Rule, which is shown in Equation 2.11, is taken into account in R programming (Sarkar and Rashid, 2016). In this study, some R programming codes are developed by the author by importing the required "triangle", "fitdistrplus", "dplyr", "readxl", and "stats" packages.

$$m = \log_2 n + 1 \tag{2.11}$$

n: The total number of observations in the dataset.

2.5 Part 2

In order to narrow the scope of uncertainty analysis for computing water surface profiles, a single waterway is taken into consideration in Part 2. To implement uncertainty analysis through HEC-RAS (US Army Corps of Engineers, 2016), the

Monte Carlo simulation is implemented to the Manning's roughness coefficient and flow rate for a creek. Firstly, the simulation is applied only to Manning's roughness coefficient, then it is applied to Manning's roughness coefficient and flow rate jointly. This study is conducted by assuming that Manning's roughness coefficient and flow rate are independent variables as also considered by Bozzi et al., (2015). Different PDFs and COVs are defined for them according to the reviewed past studies. Based on the defined PDF and COV, the Monte Carlo simulation is implemented with 10000 runs for each variable. Consequently, flow depth is calculated through HEC-RAS (US Army Corps of Engineers, 2016) to visualize and analyze the results based on GOF tests. The results of the analyses will be presented in Chapter 3.

2.5.1 Study Area

In this part, Taşlıdere Creek located in Rize is used to apply the uncertainty analysis to water surface elevation. There is a bridge in the study reach of the creek. The creek is in the Eastern Black Sea region of northern Turkey. The satellite image of Taşlıdere Creek is shown in Figure 2.3.

Figure 2.3 The study area, Taslıdere Creek in Rize. (Google Earth September 16, 2022)

2.5.2 Dataset

In many uncertainty analyses conducted for hydraulic estimations, it has been observed that the main channel roughness coefficient is the most effective variable regarding channel resistance (Chang et al., 1993; Hieu et al., 2015). Besides, it is highly recommended to perform an uncertainty analysis for the flow rate (Bozzi et al., 2015; Salas and Shin, 1999). This study conducts uncertainty analysis for the flow rate and Manning's roughness coefficient. Consequently, flow depth is used as the output variable to observe and analyze the applied study.

For the required inputs, the study that is carried out by Yıldırım (2013) is used with 12 cross-sections over the Taşlıdere Creek in Rize. The locations of 12 cross-sections in the region are shown in Figure 2.4.

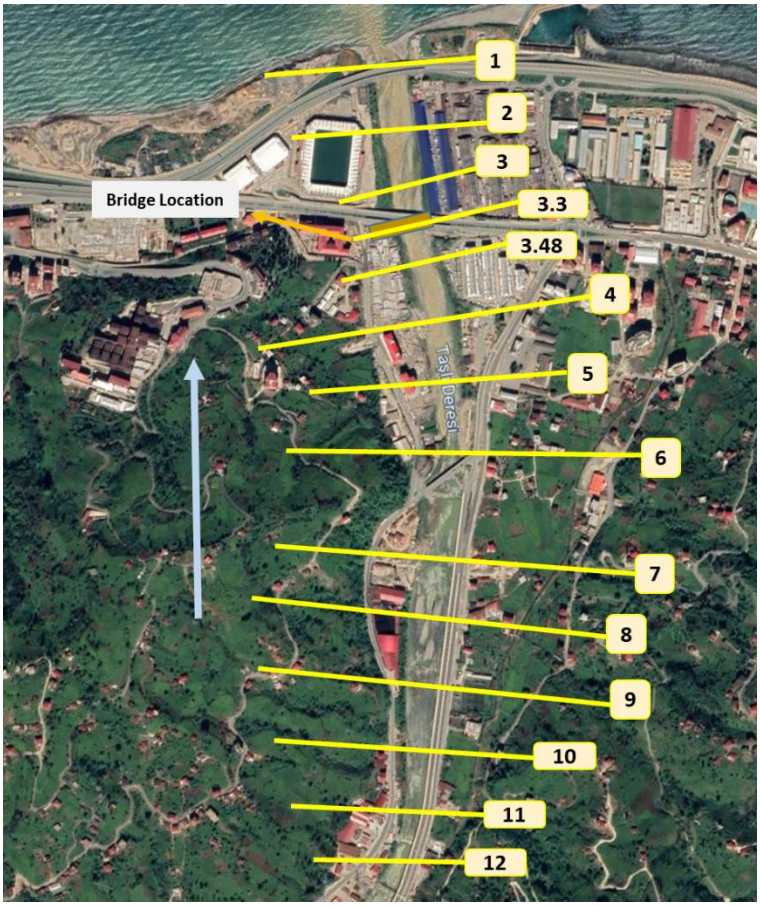

Figure 2.4 Cross Section and Bridge Location (Google Earth September 16, 2022)

According to the regional characteristics, Manning's roughness coefficient is assigned as 0.07 for the left and right riverbanks and 0.065 for the main channel. Based on the sieve analysis results for the bed materials, D_{50} is 0.52 mm, D_{60} is 0.65 mm and D_{90} is 1.65 mm. The discharge values according to the return periods are given in Table 2.9. In this study, 100-year return period discharge (Q_{100}) is used to conduct the uncertainty analysis. The main channel flow profile of Q_{100} flow (in subcritical regime) for Taşlıdere Creek can be seen in Figure 2.5.

Table 2.9 Peak discharge values based on return periods (Yıldırım, 2013)

Return period (year)	**Flow Rate, Q (m^3/s)**
5	356.5
10	432.6
25	545.2
50	642.2
100	750.3
500	970.1
1000	1064

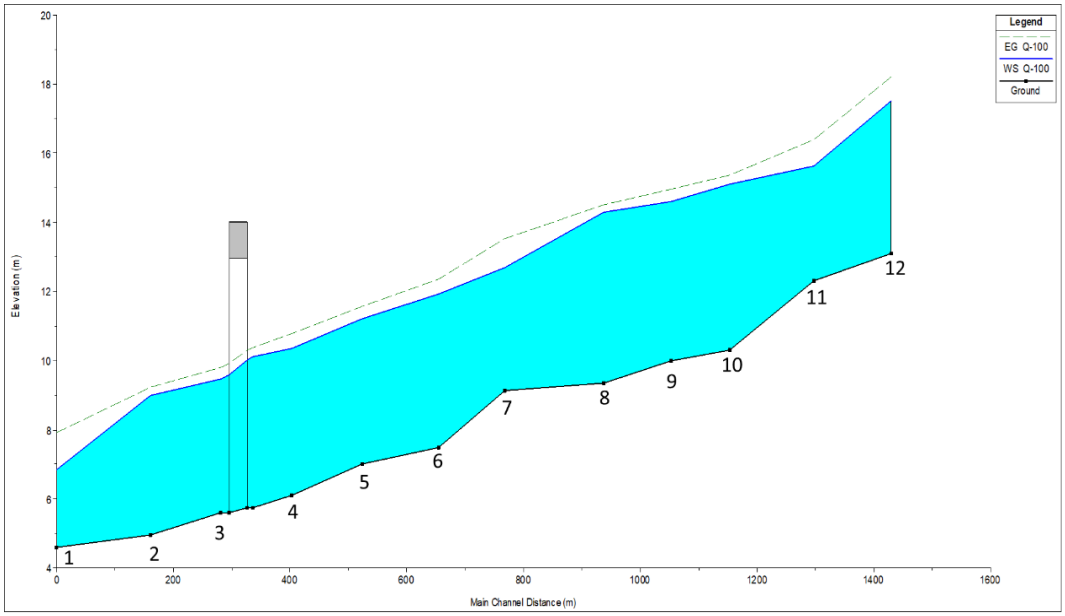

Figure 2.5 The main channel flow profile of Q_{100} flow for Taşlıdere Creek

2.5.3 Software

As explained in Part 1, the R programming is used to implement the Monte Carlo simulation in Part 2 as well. Subsequently, Manning's roughness coefficient and flow rate are examined by implementing 1D HEC-RAS steady flow. HEC-RAS is the river analysis system that carries out 1D steady flow and 1D/2D unsteady flow calculations, sediment transport analysis, bed modeling, and water quality analysis (US Army Corps of Engineers, 2016).

CHAPTER 3

ANALYSIS AND RESULTS

Since the study is conducted in separate parts, the analyses and results are discussed for Part 1 and Part 2 separately. The variables simulated in both parts are considered to be of independent nature. For this reason, the Monte Carlo analysis can be handled properly.

3.1 Analysis of the Results of Part 1

In Part 1, a stochastic approach is utilized for computing bed load rate using two commonly applied approaches and for Manning's roughness coefficient. Uncertainty analysis is performed for bed load transport rate (q_B) and Manning's roughness coefficient (n) through Monte Carlo simulation. These results are evaluated with the GOF test and the results are assessed based on randomness and probabilistic approaches.

Conducting the study for all creeks and return periods is unnecessary since some creeks contain similar hydrologic inputs. It is preferable to use variables of different sizes characterizing bed material and creek properties to analyze the results accurately. Therefore, based on the elimination of similar variables to a single set, a data selection is performed for the creeks and return periods. The data selection is based on maximum and minimum flow rate, harmonic slope, and median grain size. Values are ordered in ascending order, and maximum, minimum, and medium-sized values are selected. Four main creeks are chosen for analysis in the Miliç Basin. These creeks are Leylek, Sakarlı, Evci, and Miliç from the east to the west, respectively. The selected creeks and input values are shown in Table 3.1 and Figure 3.1. For Miliç Creek, which consists of two parts Miliç 1 and Miliç 2, 50-year return

period values for Miliç 1 and 500-year return period values for Miliç 2 are selected. Sediment grain size distribution is accepted to be uniform for Miliç Creek.

Table 3.1 Selected values to be used in this study

Name of Creek	Return Period (year)	Flow Rate, Q (m^3/s)	Harmonic slope, S_h (%)	Hydraulic Depth, y (m)	D_{50} (mm)	D_{90} (mm)
Leylek	50	72.07	0.15	1.65	0.38	21.00
Miliç 1	50	202.73	1.24	1.39	16.00	64.00
Evci	50	97.54	0.30	1.73	26.00	60.00
Sakarlı	500	93.06	0.11	1.07	0.27	5.00
Miliç 2	500	337.6	0.03	1.93	0.08	0.1

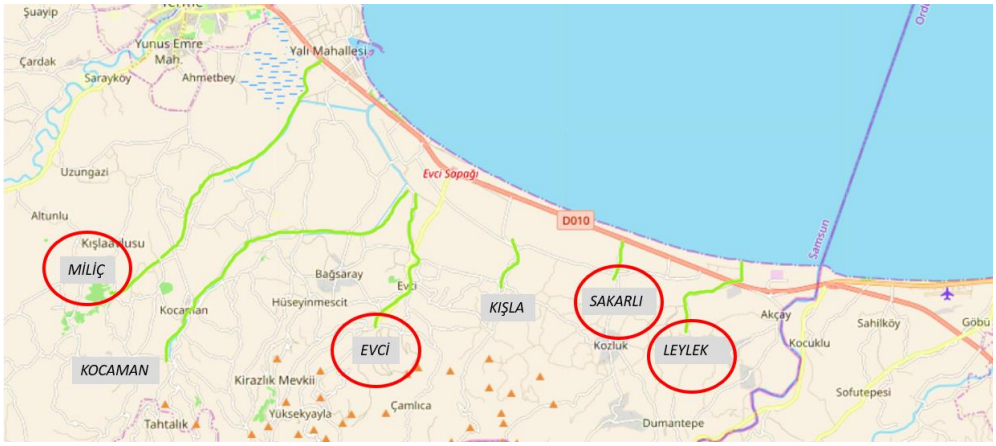

Figure 3.1 Selected main Creeks for analysis (Google Earth February 27, 2022)

In this study several PDFs are tested, i.e. Normal Distribution (N), Log-normal distribution (LN), Gamma distribution (G), Beta distribution (B), Triangular distribution (T), and Uniform distribution (U).

The PDF and COV values are assigned based on the literature review for the hydraulic parameters and inputs determined to carry out the Monte Carlo simulation analysis. In this study, for the bed load rate, the Monte Carlo simulation is applied based on the recommended COVs and half of these COVs (0.5COV) to observe the effect of sampling ranges. Moreover, since more than one PDF and COV values are recommended for Manning's roughness coefficient, three different arrangements are

used to search the effect of these choices outlined in Table 3.3. These assigned values are shown for q_B and n in Table 3.2 and Table 3.3, respectively.

Table 3.2 PDF and COV values defined for q_B analysis

Variables	**Harmonic slope**	**Hydraulic Depth**	**D_{50}**	**D_{90}**	**Chezy Coefficient, C**
COV	0.3	0.23	0.05	0.02	0.25
PDF	Normal distribution	Normal distribution	Uniform distribution	Uniform distribution	Normal distribution

Table 3.3 PDF and COV values defined for n analysis

Set of PDF & COV		**D_{50}**	**n_1**	**n_2**	**n_3**	**n_4**
1	**COV**	0.05	0.1	0.18	0.08	0.2
	PDF	Uniform distribution	Normal distribution	Uniform distribution	Triangular distribution	Normal distribution
2	**COV**	0.02	0.28	0.15	0.18	0.08
	PDF	Uniform distribution	Uniform distribution	Normal distribution	Uniform distribution	Triangular distribution
3	**COV**	0.05	0.08	0.053	0.1	0.28
	PDF	Uniform distribution	Triangular distribution	Normal distribution	Normal distribution	Uniform distribution

The determination of the number of simulation cycles for the Monte Carlo simulation is required before performing the study. For this reason, Leylek Creek with 50 year return period is selected to determine the simulation cycle. This study is implemented only for q_B with the MPM approach through R programming. However, the result obtained is also used in the analysis for n. Since the PDF and COV should be defined to implement the simulation, the variables in Table 3.2 are used for this study. The study is carried out with 100, 500, 1000, 2500, 5000, 10000, and 20000 simulation cycles. The Monte Carlo simulation based on defined simulation cycles is performed for each hydraulic variable (harmonic slope, hydraulic depth, D_{50}, D_{90}, and Chezy coefficient). Moreover, each simulation cycle is repeated 10 times to obtain reliably the mean values and standard deviations. After carrying out each cycle, q_B is calculated with simulated variables. To obtain a standard error, the average and

standard deviation of q_B are calculated. The standard error results are shown in Figure 3.2. As expected, the standard error decreases as the number of simulation cycles increases. As the rate of decrease of the standard error is negligibly small after 10000 simulations, it is decided to run 10000 simulations in this study.

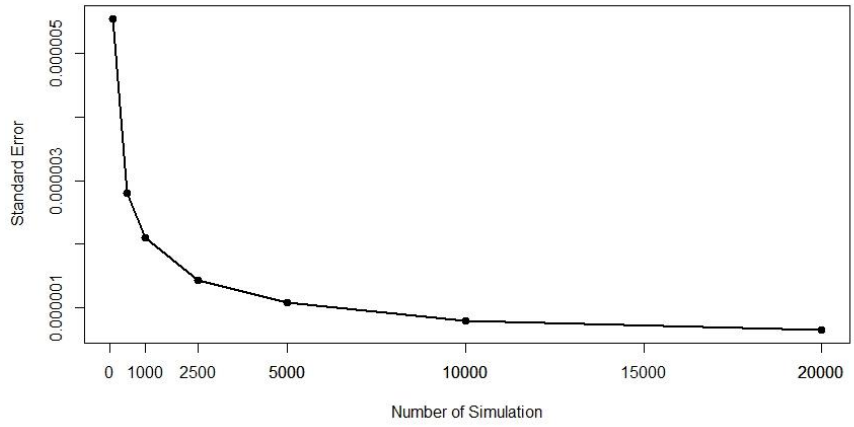

Figure 3.2 The standard error calculation with different simulation cycles

To observe the statistical distribution of the output, the graphical results (histograms) obtained with the Monte Carlo simulation can be represented by an appropriate PDF. For this reason, Chi-Square and Kolmogorov-Smirnov tests are applied to the Monte Carlo simulation results with R programming. The significance levels (**α**) are used as 0.05 and 0.1 for the Chi-square and Kolmogorov-Smirnov tests. If the test result is "Accepted" for any test, the overall decision is "Accepted", otherwise the decision is "Rejected". This approach is used to observe whether the output can be represented by commonly used PDFs.

3.1.1 Uncertainty Analysis of Sediment Bed load Transport Rate

The GOF test results for MPM and E-B approaches are shown in Tables 3.4 and 3.5, respectively. To observe the effect of COVs on samplings, the recommended COV values and 0.5COV values are tested and the output histograms for these cases are compared for both MPM and E-B approaches. The distributions fitted to the

simulation results for MPM and E-B approaches are shown in Appendix A and Appendix B, respectively.

Table 3.4 The GOF results for MPM

COVs	Creek	PDF	Chi-Square	Chi-Square	Kolmogorov-Smirnov	Kolmogorov-Smirnov	Final Decision
			α = 0.05	α = 0.1	α = 0.05	α = 0.1	
			Decision	Decision	Decision	Decision	
COV	Leylek (50-Y)	N	Rejected	Rejected	Rejected	Rejected	Rejected
		LN	Rejected	Rejected	Rejected	Rejected	Rejected
		G	Rejected	Rejected	Rejected	Rejected	Rejected
		B	Rejected	Rejected	**Accepted**	**Accepted**	**Accepted**
0.5COV	Leylek (50- Y)	N	Rejected	Rejected	Rejected	Rejected	Rejected
		LN	Rejected	Rejected	Rejected	Rejected	Rejected
		G	Rejected	Rejected	**Accepted**	**Accepted**	**Accepted**
		B	Rejected	Rejected	**Accepted**	**Accepted**	**Accepted**
COV	Miliç 1 (50- Y)	N	Rejected	Rejected	Rejected	Rejected	Rejected
		LN	Rejected	Rejected	Rejected	Rejected	Rejected
		G	Rejected	Rejected	Rejected	Rejected	Rejected
		B	**Accepted**	**Accepted**	**Accepted**	**Accepted**	**Accepted**
0.5COV	Miliç 1 (50- Y)	N	Rejected	Rejected	Rejected	Rejected	Rejected
		LN	Rejected	Rejected	Rejected	Rejected	Rejected
		G	**Accepted**	**Accepted**	**Accepted**	**Accepted**	**Accepted**
		B	**Accepted**	**Accepted**	**Accepted**	**Accepted**	**Accepted**
COV	Evci (50-Y)	N	Rejected	Rejected	Rejected	Rejected	Rejected
		LN	Rejected	Rejected	Rejected	Rejected	Rejected
0.5COV	Evci (50- Y)	N	Rejected	Rejected	Rejected	Rejected	Rejected
		LN	Rejected	Rejected	Rejected	Rejected	Rejected
		G	Rejected	Rejected	Rejected	Rejected	Rejected
		B	Rejected	Rejected	Rejected	Rejected	Rejected
COV	Sakarlı (500-Y)	N	Rejected	Rejected	Rejected	Rejected	Rejected
		LN	Rejected	Rejected	Rejected	Rejected	Rejected
		G	Rejected	Rejected	**Accepted**	**Accepted**	**Accepted**
		B	Rejected	Rejected	**Accepted**	**Accepted**	**Accepted**
0.5COV	Sakarlı (500-Y)	N	Rejected	Rejected	Rejected	Rejected	Rejected
		LN	Rejected	Rejected	Rejected	Rejected	Rejected
		G	Rejected	Rejected	**Accepted**	**Accepted**	**Accepted**
		B	**Accepted**	**Accepted**	**Accepted**	**Accepted**	**Accepted**
COV	Miliç 2 (500-Y)	N	Rejected	Rejected	Rejected	Rejected	Rejected
		LN	Rejected	Rejected	Rejected	Rejected	Rejected
		G	Rejected	Rejected	Rejected	Rejected	Rejected
		B	**Accepted**	**Accepted**	**Accepted**	**Accepted**	**Accepted**
0.5COV	Miliç 2 (500-Y)	N	Rejected	Rejected	Rejected	Rejected	Rejected
		LN	Rejected	Rejected	Rejected	Rejected	Rejected
		G	Rejected	Rejected	**Accepted**	**Accepted**	**Accepted**
		B	Rejected	Rejected	**Accepted**	**Accepted**	**Accepted**

Table 3.5 The GOF results for E-B

COVs	Creek	PDF	Chi-Square	Chi-Square	Kolmogorov-Smirnov	Kolmogorov-Smirnov	Final Decision
			α = 0.05	**α = 0.1**	**α = 0.05**	**α = 0.1**	
			Decision	**Decision**	**Decision**	**Decision**	
COV	Leylek (50-Y)	N	Rejected	Rejected	Rejected	Rejected	Rejected
		LN	Rejected	Rejected	Rejected	Rejected	Rejected
		G	Rejected	Rejected	Rejected	Rejected	Rejected
		B	**Accepted**	**Accepted**	**Accepted**	**Accepted**	**Accepted**
0.5COV	Leylek (50-Y)	N	Rejected	Rejected	Rejected	Rejected	Rejected
		LN	Rejected	Rejected	Rejected	Rejected	Rejected
		G	**Accepted**	**Accepted**	**Accepted**	**Accepted**	**Accepted**
		B	**Accepted**	**Accepted**	**Accepted**	**Accepted**	**Accepted**
COV	Miliç 1 (50-Y)	N	Rejected	Rejected	Rejected	Rejected	Rejected
		LN	Rejected	Rejected	Rejected	Rejected	Rejected
		G	Rejected	Rejected	Rejected	Rejected	Rejected
		B	Rejected	Rejected	Rejected	Rejected	Rejected
0.5COV	Miliç 1 (50-Y)	N	Rejected	Rejected	Rejected	Rejected	Rejected
		LN	Rejected	Rejected	Rejected	Rejected	Rejected
		G	Rejected	Rejected	Rejected	Rejected	Rejected
		B	**Accepted**	**Accepted**	**Accepted**	**Accepted**	**Accepted**
COV	Evci (50-Y)	N	Rejected	Rejected	Rejected	Rejected	Rejected
		LN	Rejected	Rejected	Rejected	Rejected	Rejected
		G	Rejected	Rejected	Rejected	Rejected	Rejected
		B	Rejected	Rejected	Rejected	Rejected	Rejected
0.5COV	Evci (50-Y)	N	Rejected	Rejected	Rejected	Rejected	Rejected
		LN	Rejected	Rejected	Rejected	Rejected	Rejected
		G	Rejected	Rejected	**Accepted**	**Accepted**	**Accepted**
		B	**Accepted**	**Accepted**	**Accepted**	**Accepted**	**Accepted**
COV	Sakarlı (500-Y)	N	Rejected	Rejected	Rejected	Rejected	Rejected
		LN	Rejected	Rejected	Rejected	Rejected	Rejected
		G	Rejected	Rejected	Rejected	Rejected	Rejected
		B	Rejected	Rejected	Rejected	Rejected	Rejected
0.5COV	Sakarlı (500-Y)	N	Rejected	Rejected	Rejected	Rejected	Rejected
		LN	Rejected	Rejected	Rejected	Rejected	Rejected
		G	Rejected	Rejected	Rejected	Rejected	Rejected
		B	Rejected	Rejected	**Accepted**	**Accepted**	**Accepted**
COV	Miliç 2 (500-Y)	N	Rejected	Rejected	Rejected	Rejected	Rejected
		LN	Rejected	Rejected	Rejected	Rejected	Rejected
		G	Rejected	Rejected	Rejected	Rejected	Rejected
		B	Rejected	Rejected	Rejected	Rejected	Rejected
0.5COV	Miliç 2 (500-Y)	N	Rejected	Rejected	Rejected	Rejected	Rejected
		LN	Rejected	Rejected	Rejected	Rejected	Rejected
		G	Rejected	Rejected	Rejected	Rejected	Rejected
		B	Rejected	Rejected	Rejected	Rejected	Rejected

3.1.2 Uncertainty Analysis of Manning's Roughness Coefficient

The GOF test results for n are shown in Table 3.6. The distributions fitted to the simulation results for n are shown in Appendix C. PDF and COV combinations as shown in column 1 of this table are formed according to Table 3.3.

Table 3.6 The GOF results for n

Set of PDF & COV	**Creek**	**PDF**	**Chi-Square**	**Chi-Square**	**Kolmogorov-Smirnov**	**Kolmogorov-Smirnov**	**Final Decision**
			α = 0.05	**α = 0.1**	**α = 0.05**	**α = 0.1**	
			Decision	**Decision**	**Decision**	**Decision**	
1	Leylek (50-Y)	N	Rejected	Rejected	Rejected	Rejected	Rejected
		LN	Rejected	Rejected	Rejected	Rejected	Rejected
		G	Rejected	Rejected	Rejected	Rejected	Rejected
		B	Rejected	Rejected	Rejected	Rejected	Rejected
		U	**Accepted**	Rejected	Rejected	Rejected	**Accepted**
2	Miliç 1 (50-Y)	N	**Accepted**	**Accepted**	Rejected	Rejected	**Accepted**
		LN	Rejected	Rejected	Rejected	Rejected	Rejected
		G	Rejected	Rejected	Rejected	Rejected	Rejected
		B	Rejected	Rejected	Rejected	Rejected	Rejected
3	Evci (50-Y)	N	**Accepted**	**Accepted**	**Accepted**	**Accepted**	**Accepted**
		LN	**Accepted**	**Accepted**	Rejected	Rejected	**Accepted**
		G	**Accepted**	**Accepted**	Rejected	Rejected	**Accepted**
		B	**Accepted**	**Accepted**	**Accepted**	**Accepted**	**Accepted**
1	Sakarlı (500-Y)	N	Rejected	Rejected	Rejected	Rejected	Rejected
		LN	Rejected	Rejected	Rejected	Rejected	Rejected
		G	Rejected	Rejected	Rejected	Rejected	Rejected
		B	Rejected	Rejected	Rejected	Rejected	Rejected
		U	Rejected	Rejected	Rejected	Rejected	Rejected
2	Miliç 2 (500-Y)	N	**Accepted**	**Accepted**	Rejected	Rejected	**Accepted**
		LN	Rejected	Rejected	Rejected	Rejected	Rejected
		G	**Accepted**	Rejected	Rejected	Rejected	**Accepted**
		B	**Accepted**	**Accepted**	Rejected	Rejected	**Accepted**

3.1.3 Results of Part 1

The output results are examined by using the COV and 0.5COV values for input variables. With 0.5COVs of the input variables, the baseline (ie, limiting the input values range to be generated for the data for output) is narrowed. Therefore, the output bed load rates are obtained closer to the mean values. The frequency distributions generated randomly for the inputs and the output can be seen in Figure 3.3 through Figure 3.6 for Leylek Creek. For the MPM method, output histograms resulted in different distributions, i.e. a right-skewed distribution is obtained for COV, whereas an almost asymmetrical distribution is generated for the case of 0.5COV. The reason may be attributed to the highly non-linear nature of the MPM approach. Small changes in the input values may result in pronounced changes due to the existence of big power of variables.

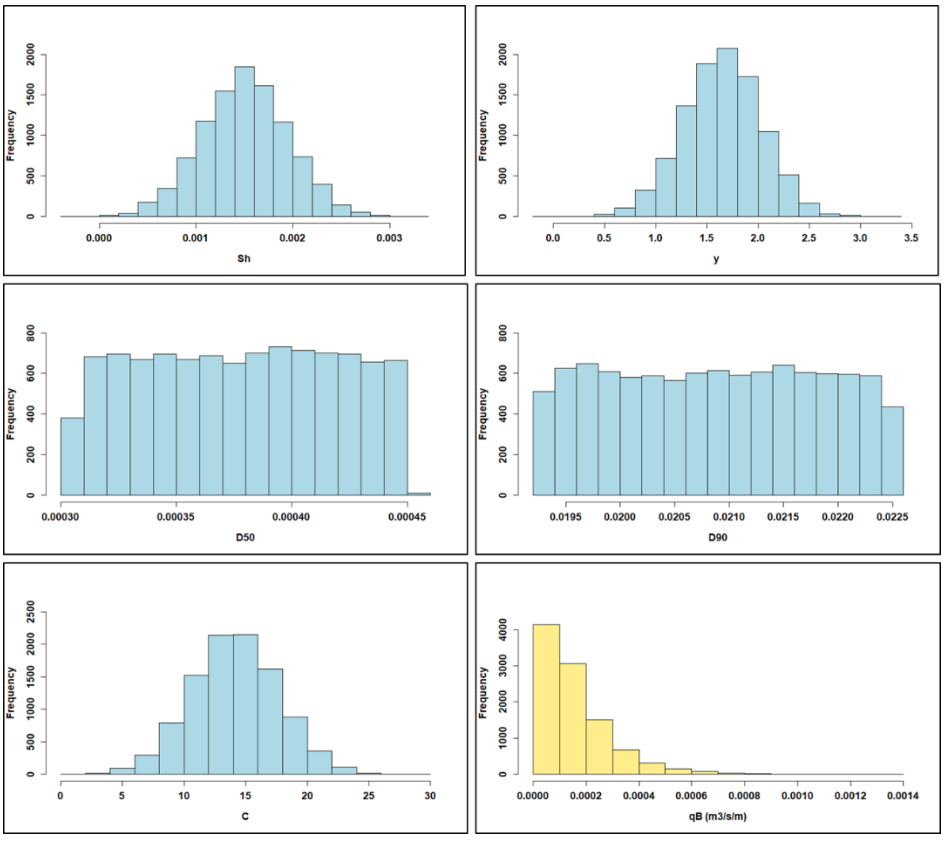

Figure 3.3 Input and output distributions for Leylek Creek with MPM based on assigned COV

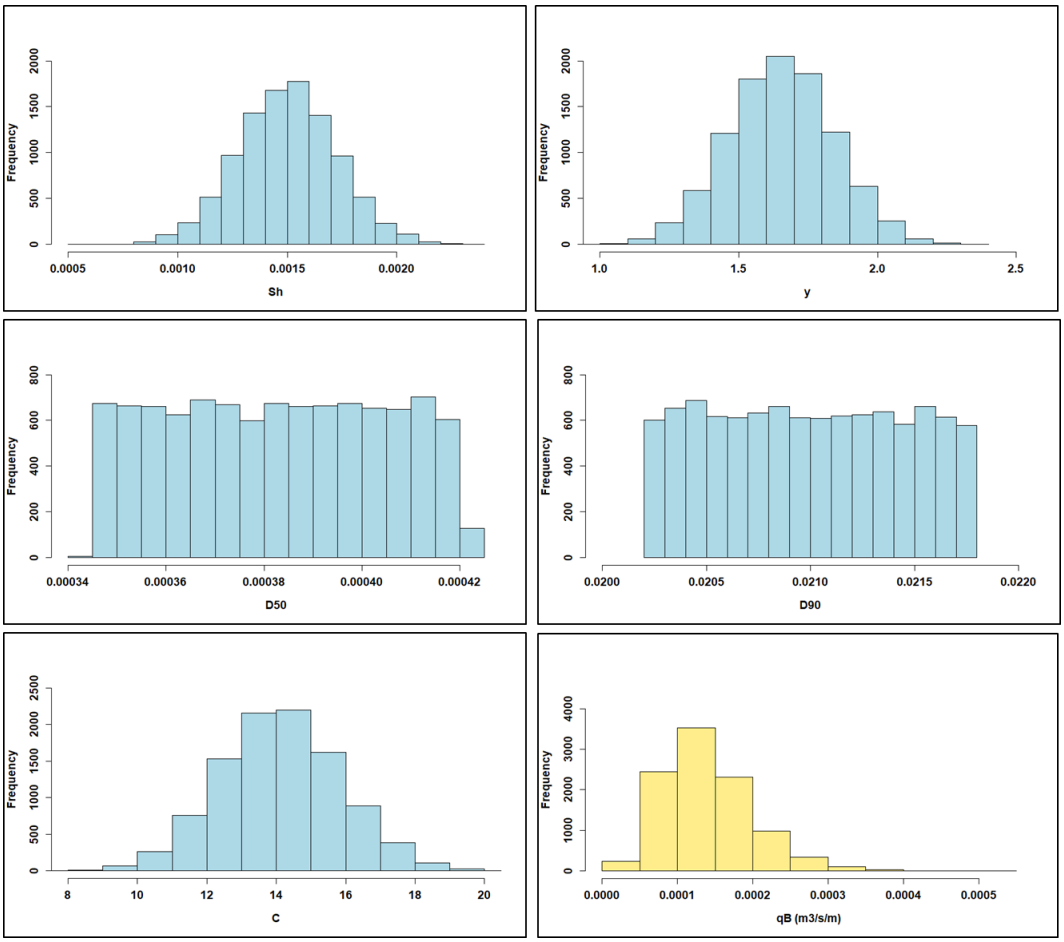

Figure 3.4 Input and output distributions for Leylek Creek with MPM based on assigned 0.5COV

When the E-B and MPM approaches are compared, the frequencies are observed to be concentrated around the mean with the E-B method, while a more left-skewed distribution is observed with the MPM method. Furthermore, output histograms under COV and 0.5COV are of similar-type distributions in the case of the E-B approach.

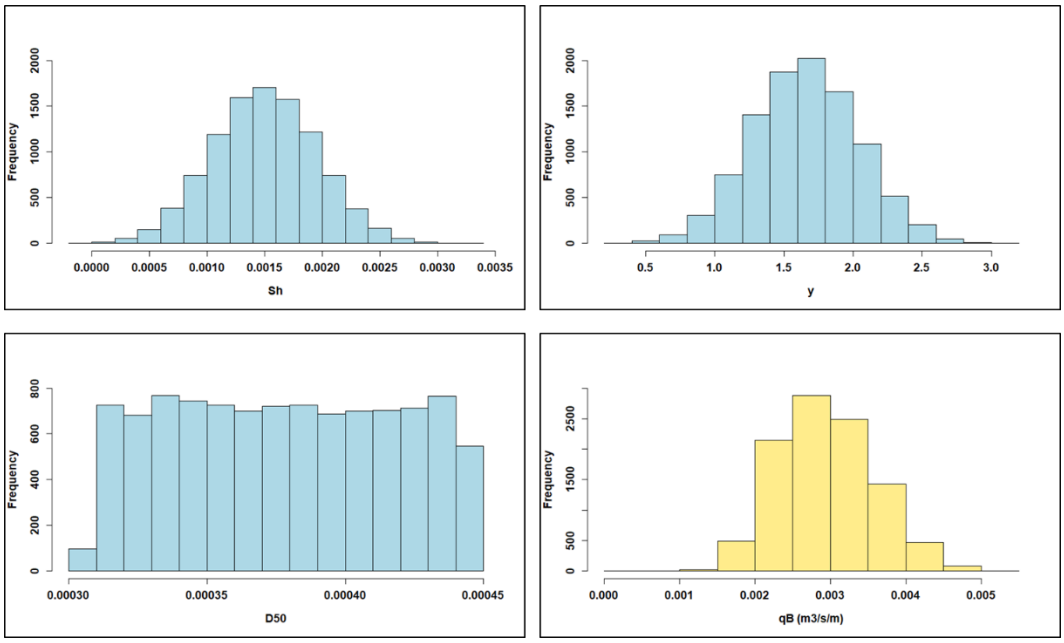

Figure 3.5 Input and output distributions for Leylek Creek with E-B based on assigned COV

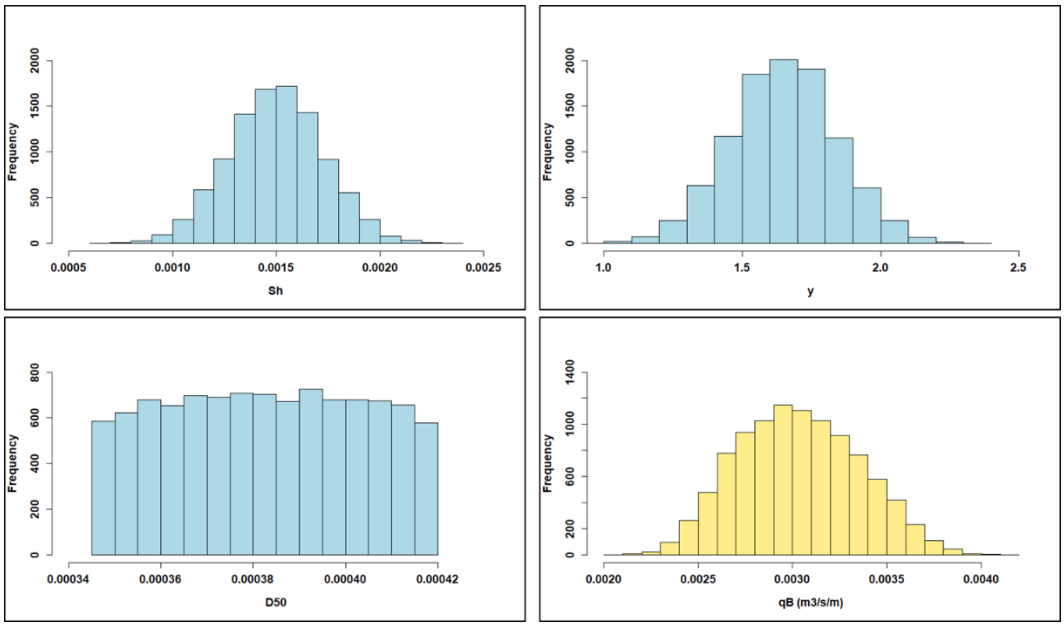

Figure 3.6 Input and output distributions for Leylek Creek with E-B based on assigned 0.5COV

The results of the uncertainty analysis conducted for q_B showed that Beta and Gamma distributions are observed for the analyses carried out by the MPM and E-B approaches based on this study area (Table 3.7).

The COV values obtained by dividing the standard deviation of a series by its mean are calculated for each analysis. As expected the series with small COV values are less variable according to others. In other words, the analyzed terms are distributed more homogeneously around the mean. Within the scope of the analysis results, the COVs obtained by the E-B approach are lower than the MPM approach (Table 3.7). Moreover, when the COV values are reduced by half, the output COV values also decreased.

When the obtained frequency distributions are examined, simulation results based on deterministic values are evaluated. The percentages are calculated over the frequency distributions for both smaller and larger values than the deterministic values. As a result of this evaluation, although the results vary regionally, generally 50% of the bed load rate values obtained by simulation are higher than the deterministic bed load rates.

In addition, it is seen that the rate of being greater than deterministic values increased from 50% to 72% for some of the results using 0.5COV values. This indicates the difference between the deterministic and the larger stochastic value even in a narrowed baseline (Table 3.7). The corresponding frequency histograms are also provided in Appendix A and Appendix B.

In light of these results for bed load rate, the stochastic approach provides crucial data for engineering design and knowledge for sediment transportation. Analyses and designs of hydraulic structures using deterministic bed load rates may underestimate the phenomenon. This may create some problems in view of the safety of foundations.

Table 3.7 Analysis results for q_B

Approach	Creek	COVs	Accepted PDF	COV	A percentage lower than the deterministic value	A percentage higher than the deterministic value
MPM	Leylek, 50	COV	B	0.426	42%	58%
MPM	Leylek, 50	0.5COV	B, G	0.429	28%	72%
E-B	Leylek, 50	COV	B	0.203	56%	44%
E-B	Leylek, 50	0.5COV	B, G	0.103	50%	50%
MPM	Milic 1, 50	COV	B	0.910	56%	44%
MPM	Milic 1, 50	0.5COV	B, G	0.446	53%	47%
E-B	Milic 1, 50	COV	-	0.190	54%	46%
E-B	Milic 1, 50	0.5COV	B	0.092	51%	48%
MPM	Evci, 50	COV	-	1.219	39%	61%
MPM	Evci, 50	0.5COV	-	0.882	49%	51%
E-B	Evci, 50	COV	-	0.192	49%	51%
E-B	Evci, 50	0.5COV	B, G	0.090	51%	49%
MPM	Sakarlı, 500	COV	B, G	0.841	50%	50%
MPM	Sakarlı, 500	0.5COV	B, G	0.415	41%	58%
E-B	Sakarlı, 500	COV	-	0.244	55%	45%
E-B	Sakarlı, 500	0.5COV	B	0.107	53%	47%
MPM	Milic 2, 500	COV	B	0.821	55%	45%
MPM	Milic 2, 500	0.5COV	B, G	0.408	52%	48%
E-B	Milic 2, 500	COV	-	0.299	31%	69%
E-B	Milic 2, 500	0.5COV	-	0.152	11%	89%

The results of the uncertainty analysis conducted for n demonstrated that the obtained distributions show a tendency to various types of PDFs (Table 3.8).

Table 3.8 The uncertainty analysis results of n

Name of Creek	Return Period (year)	Flow Rate,Q (m^3/s)	D_{50} (mm)	Observed PDF for n
Leylek	50	72.07	0.38	Uniform
Miliç 1	50	202.73	16	Normal
Evci	50	97.54	26	Gamma, Beta, Normal, Log-normal
Sakarlı	500	93.06	0.27	-
Miliç 2	500	337.6	0.08	Gama, Beta, Normal

In line with the obtained results, the COV values for n show parallelism with the distributions suggested in the literature (Table 3.9). The percentages are also calculated over the frequency distributions for both smaller and larger values than the deterministic values for n (Table 3.9). The corresponding frequency histograms are provided in Appendix C. Almost 50% of n values that come from the simulation are greater than the deterministic n values. This is an indication that the stochastic approach should be considered when making an analysis based on Manning's roughness coefficient.

Table 3.9 Analysis results for n

Creek	Set of PDF & COV	Accepted PDF	COV	A percentage lower than the deterministic value	A percentage higher than the deterministic value
Leylek, 50	1	U	0.32	54%	46%
Miliç 1, 50	2	N	0.27	48%	52%
Evci, 50	3	N,LN,G,B	0.15	50%	50%
Sakarlı, 500	1	-	0.29	49%	51%
Miliç 2, 500	2	N,B,G	0.28	60%	40%

3.2 Analysis of the Results of Part 2

In the second part of the uncertainty analysis, the effects of uncertainties of the HEC-RAS model input data are analyzed through output data by integrating Monte Carlo simulation. While main channel Manning's roughness coefficient (n) and flow rate (Q) are input data, the flow depth is selected as the output data. As stated before, Manning's roughness coefficient and flow rate are considered as independent variables.

The seven cross-sections are selected from a study conducted by (Yıldırım, 2013) to implement the uncertainty analysis. Instead of using all 12 cross-sections, seven different cross-sections are chosen to evaluate the results based on various hydraulic features and geometric characteristics. These cross-sections are 2, 3, 3.3 Bridge downstream, 3.3 Bridge upstream, 4, 7, and 11 (see Figure 2.4). The hydraulic features and cross-sections that are used to carry out the study are shown in Table 3.10.

Table 3.10 Hydraulic variables of selected river stations for Q_{100}

River Station	Q Total (m^3/s)	Water Surface Elevation (m)	Flow depth (m)	Main channel velocity (m/s)	Flow Area (m^2)	Main Channel Froude #
11	750.31	15.62	3.21	3.9	192.26	0.73
7	750.31	12.7	3.54	4.04	185.73	0.74
4	750.31	10.34	4.2	2.04	258.96	0.45
3.3 Bridge Upstream	750.31	10.01	4.31	2.38	315.23	0.41
3.3 Bridge Downstream	750.31	9.58	3.94	2.59	289.38	0.47
3	750.31	9.47	3.87	2.58	291.01	0.47
2	750.31	9	4.03	2.11	355.99	0.34

As the first step of the analysis, a Monte Carlo simulation is performed with PDF and COV values recommended in the literature (Table 3.11). Since many different PDF and COV values are suggested for n, three different distributions are selected.

As mean values, 0.065 for n and 750.31 m^3/s, which is the flow rate corresponding to a return period of 100 years, are used. Monte Carlo simulation is performed via R programming with 10000 simulation cycles. While selecting 10000 simulation cycles, as explained in Part 1, the n value is simulated 100, 500, 1000, 2500, 5000, 10000, and 20000 times. As the rate of decrease of the standard error is negligibly small after 10000 simulations, it is decided to run 10000 simulations in this study (Figure 3.7).

Table 3.11 Assigned PDF and COV values for Monte Carlo simulation

	Manning's roughness Coefficient (n)	**Flow Rate, Q (m^3/s)**
PDF	Normal Distribution	Log-normal Distribution
COV	0.2	0.25
PDF	Triangular Distribution	Log-normal Distribution
COV	0.1	0.25
PDF	Uniform Distribution	Log-normal Distribution
COV	0.28	0.25

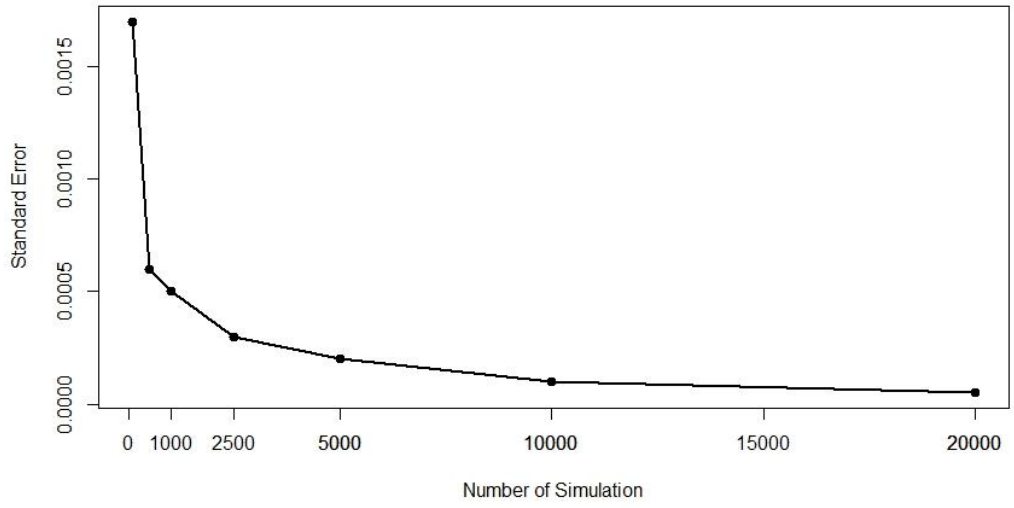

Figure 3.7 The standard error calculation with different simulation cycles with n

The values obtained by Monte Carlo simulation are implemented one by one to HEC-RAS (US Army Corps of Engineers, 2016). Firstly, the n value is presented to the model as a single uncertain variable. Then n and Q values are presented to the model as multiple uncertain variables to observe the effects of n and Q values. The method

recommended by Goodell (2014) is used to run 10000 values one by one over HEC-RAS. The simulated values are recorded on a sheet in MS Excel and are tested one by one with a code running on Visual Basic with HEC-RAS. As a result of this study, flow depth values as output are received and printed on another excel sheet. Then, the flow depths are converted into a dataset using R programming. The Chi-Square and Kolmogorov-Smirnov tests are applied to check the compatibility of the obtained flow depth results with any known distribution. As in Part 1, the significance levels (**α**) are used as 0.05 and 0.1 for both tests. The flowchart that summarizes the analysis is displayed in Figure 3.8.

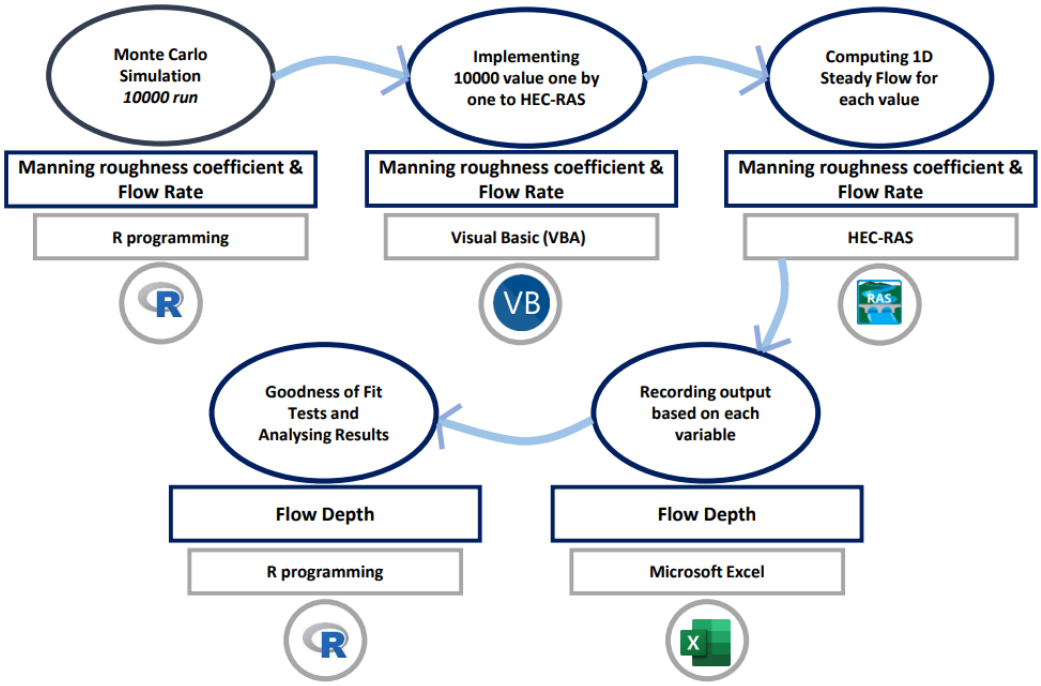

Figure 3.8 Flowchart of Part 2 with Software

3.2.1 Successive Analyses According to Cross-Sections

The geometric details of cross-section 2 are indicated in Figure 3.9.

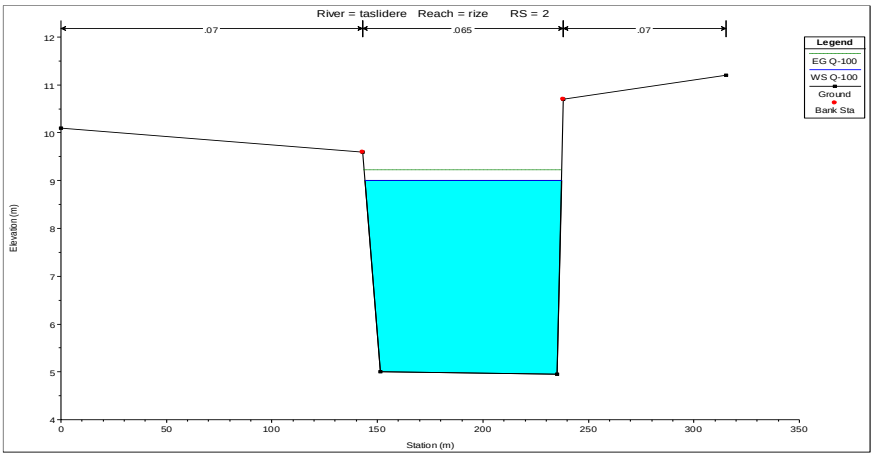

Figure 3.9 Geometric features of cross-section 2 in the HEC-RAS model

The GOF test results of cross-section 2 for flow depth are shown in Table 3.12.

Table 3.12 The GOF test results for cross-section 2

Variable	Variable PDF	PDF	Chi-Square	Chi-Square	Kolmogorov-Smirnov	Kolmogorov-Smirnov	Final Decision
			α = 0.05	α = 0.1	α = 0.05	α = 0.1	
			Decision	Decision	Decision	Decision	
n	**N**	**N**	Rejected	Rejected	Rejected	Rejected	Rejected
n	**N**	**LN**	Rejected	Rejected	Rejected	Rejected	Rejected
n	**N**	**G**	Rejected	Rejected	Rejected	Rejected	Rejected
n, Q	**N, LN**	**N**	Rejected	Rejected	Rejected	Rejected	Rejected
n, Q	**N, LN**	**LN**	Rejected	Rejected	**Accepted**	**Accepted**	**Accepted**
n, Q	**N, LN**	**G**	Rejected	Rejected	Rejected	Rejected	Rejected
n	**T**	**N**	Rejected	Rejected	Rejected	Rejected	Rejected
n	**T**	**LN**	Rejected	Rejected	Rejected	Rejected	Rejected
n	**T**	**G**	Rejected	Rejected	Rejected	Rejected	Rejected
n, Q	**T, LN**	**N**	Rejected	Rejected	Rejected	Rejected	Rejected
n, Q	**T, LN**	**LN**	**Accepted**	**Accepted**	**Accepted**	**Accepted**	**Accepted**
n, Q	**T, LN**	**G**	Rejected	Rejected	Rejected	Rejected	Rejected
n	**U**	**N**	Rejected	Rejected	Rejected	Rejected	Rejected
n	**U**	**LN**	Rejected	Rejected	Rejected	Rejected	Rejected
n	**U**	**G**	Rejected	Rejected	Rejected	Rejected	Rejected
n, Q	**U, LN**	**N**	Rejected	Rejected	Rejected	Rejected	Rejected
n, Q	**U, LN**	**LN**	Rejected	Rejected	Rejected	Rejected	Rejected
n, Q	**U, LN**	**G**	Rejected	Rejected	Rejected	Rejected	Rejected

The geometric details of cross-section 3 are indicated in Figure 3.10.

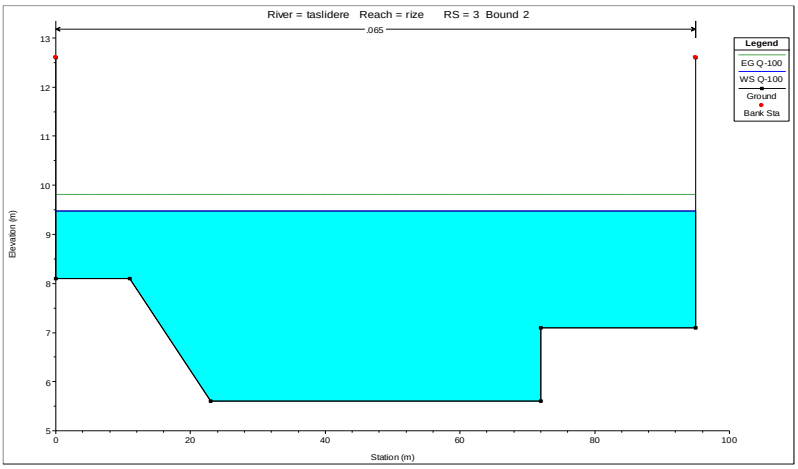

Figure 3.10 Geometric features of cross-section 3 in the HEC-RAS model

The GOF test results of cross-section 3 for flow depth are shown in Table 3.13.

Table 3.13 The GOF test results for cross-section 3

Variable	**Variable PDF**	**PDF**	**Chi-Square**	**Chi-Square**	**Kolmogorov-Smirnov**	**Kolmogorov-Smirnov**	**Final Decision**
			α = 0.05	**α = 0.1**	**α = 0.05**	**α = 0.1**	
			Decision	**Decision**	**Decision**	**Decision**	
n	**N**	**N**	Rejected	Rejected	Rejected	Rejected	Rejected
n	**N**	**LN**	Rejected	Rejected	Rejected	Rejected	Rejected
n	**N**	**G**	Rejected	Rejected	Rejected	Rejected	Rejected
n, Q	**N, LN**	**N**	Rejected	Rejected	Rejected	Rejected	Rejected
n, Q	**N, LN**	**LN**	Rejected	Rejected	Rejected	Rejected	Rejected
n, Q	**N, LN**	**G**	Rejected	Rejected	**Accepted**	Rejected	**Accepted**
n	**T**	**N**	Rejected	Rejected	Rejected	Rejected	Rejected
n	**T**	**LN**	Rejected	Rejected	Rejected	Rejected	Rejected
n	**T**	**G**	Rejected	Rejected	Rejected	Rejected	Rejected
n, Q	**T, LN**	**N**	Rejected	Rejected	Rejected	Rejected	Rejected
n, Q	**T, LN**	**LN**	Rejected	Rejected	Rejected	Rejected	Rejected
n, Q	**T, LN**	**G**	Rejected	Rejected	Rejected	Rejected	Rejected
n	**U**	**N**	Rejected	Rejected	Rejected	Rejected	Rejected
n	**U**	**LN**	Rejected	Rejected	Rejected	Rejected	Rejected
n	**U**	**G**	Rejected	Rejected	Rejected	Rejected	Rejected
n, Q	**U, LN**	**N**	Rejected	Rejected	Rejected	Rejected	Rejected
n, Q	**U, LN**	**LN**	Rejected	Rejected	Rejected	Rejected	Rejected
n, Q	**U, LN**	**G**	Rejected	Rejected	Rejected	Rejected	Rejected

The geometric details of the cross-section 3.3 bridge downstream (BD) are indicated in Figure 3.11.

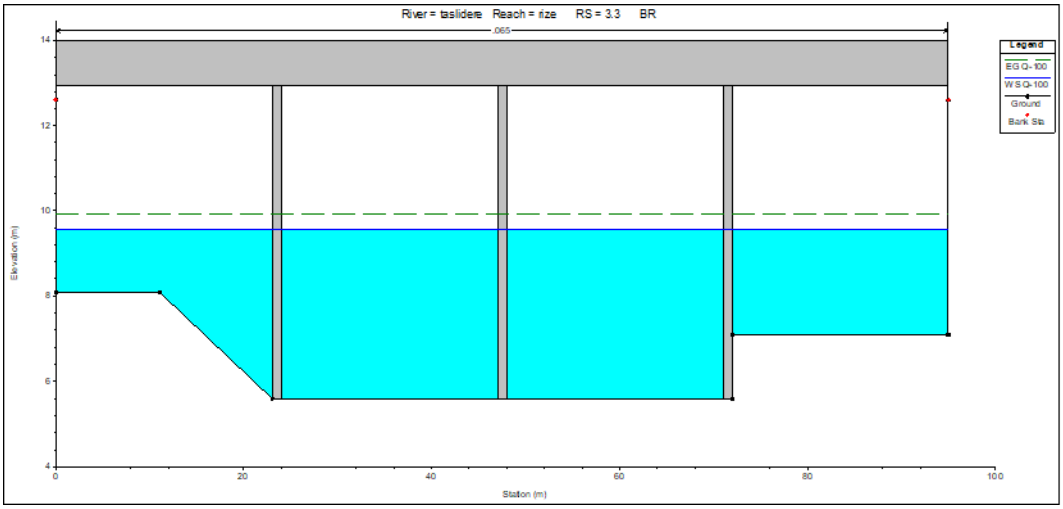

Figure 3.11 Geometric features of cross-section 3.3 BD in the HEC-RAS model

The GOF test results of cross-section 3.3 BD for flow depth are shown in Table 3.14.

Table 3.14 The GOF test results for cross-section 3.3 BD

Variable	Variable PDF	PDF	Chi-Square	Chi-Square	Kolmogorov-Smirnov	Kolmogorov-Smirnov	Final Decision
			α = 0.05	α = 0.1	α = 0.05	α = 0.1	
			Decision	Decision	Decision	Decision	
n	**N**	**N**	Rejected	Rejected	Rejected	Rejected	Rejected
n	**N**	**LN**	Rejected	Rejected	Rejected	Rejected	Rejected
n	**N**	**G**	Rejected	Rejected	Rejected	Rejected	Rejected
n, Q	**N, LN**	**N**	Rejected	Rejected	Rejected	Rejected	Rejected
n, Q	**N, LN**	**LN**	Rejected	Rejected	Rejected	Rejected	Rejected
n, Q	**N, LN**	**G**	Rejected	Rejected	Rejected	Rejected	Rejected
n	**T**	**N**	Rejected	Rejected	Rejected	Rejected	Rejected
n	**T**	**LN**	Rejected	Rejected	Rejected	Rejected	Rejected
n	**T**	**G**	Rejected	Rejected	Rejected	Rejected	Rejected
n, Q	**T, LN**	**N**	Rejected	Rejected	Rejected	Rejected	Rejected
n, Q	**T, LN**	**LN**	Rejected	Rejected	Rejected	Rejected	Rejected
n, Q	**T, LN**	**G**	Rejected	Rejected	Rejected	Rejected	Rejected
n	**U**	**N**	Rejected	Rejected	Rejected	Rejected	Rejected
n	**U**	**LN**	Rejected	Rejected	Rejected	Rejected	Rejected
n	**U**	**G**	Rejected	Rejected	Rejected	Rejected	Rejected
n, Q	**U, LN**	**N**	Rejected	Rejected	Rejected	Rejected	Rejected
n, Q	**U, LN**	**LN**	Rejected	Rejected	Rejected	Rejected	Rejected
n, Q	**U, LN**	**G**	Rejected	Rejected	Rejected	Rejected	Rejected

The geometric details of the cross-section 3.3 bridge upstream (BU) are indicated in Figure 3.12.

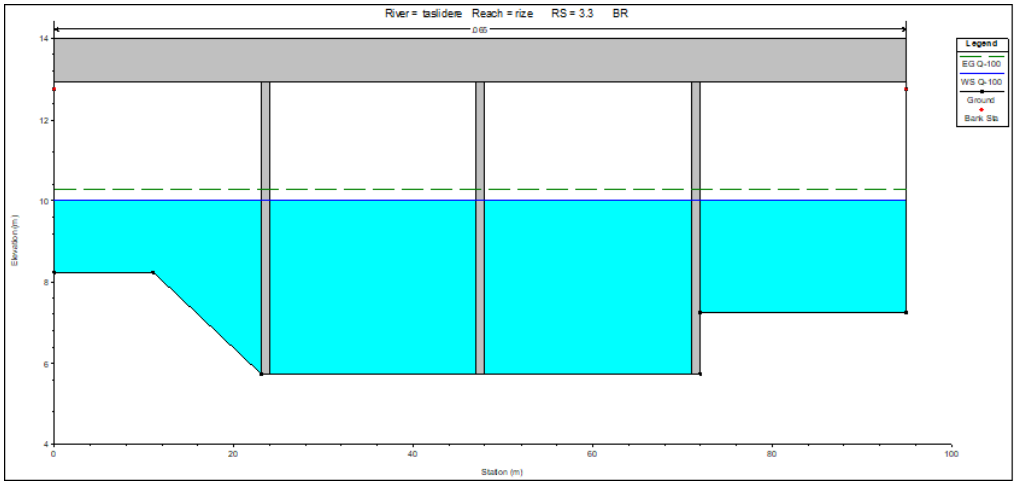

Figure 3.12 Geometric features of cross-section 3.3 BU in the HEC-RAS model

The GOF test results of cross-section 3.3 BU for flow depth are shown in Table 3.15.

Table 3.15 The GOF test results for cross-section 3.3 BU

Variable	Variable PDF	PDF	Chi-Square	Chi-Square	Kolmogorov-Smirnov	Kolmogorov-Smirnov	Final Decision
			α = 0.05	α = 0.1	α = 0.05	α = 0.1	
			Decision	Decision	Decision	Decision	
n	**N**	**N**	Rejected	Rejected	Rejected	Rejected	Rejected
n	**N**	**LN**	Rejected	Rejected	Rejected	Rejected	Rejected
n	**N**	**G**	Rejected	Rejected	Rejected	Rejected	Rejected
n, Q	**N, LN**	**N**	Rejected	Rejected	Rejected	Rejected	Rejected
n, Q	**N, LN**	**LN**	Rejected	Rejected	**Accepted**	**Accepted**	**Accepted**
n, Q	**N, LN**	**G**	Rejected	Rejected	Rejected	Rejected	Rejected
n	**T**	**N**	Rejected	Rejected	Rejected	Rejected	Rejected
n	**T**	**LN**	Rejected	Rejected	Rejected	Rejected	Rejected
n	**T**	**G**	Rejected	Rejected	Rejected	Rejected	Rejected
n, Q	**T, LN**	**N**	Rejected	Rejected	Rejected	Rejected	Rejected
n, Q	**T, LN**	**LN**	Rejected	Rejected	**Accepted**	**Accepted**	**Accepted**
n, Q	**T, LN**	**G**	Rejected	Rejected	Rejected	Rejected	Rejected
n	**U**	**N**	Rejected	Rejected	Rejected	Rejected	Rejected
n	**U**	**LN**	Rejected	Rejected	Rejected	Rejected	Rejected
n	**U**	**G**	Rejected	Rejected	Rejected	Rejected	Rejected
n, Q	**U, LN**	**N**	Rejected	Rejected	Rejected	Rejected	Rejected
n, Q	**U, LN**	**LN**	Rejected	Rejected	Rejected	Rejected	Rejected
n, Q	**U, LN**	**G**	Rejected	Rejected	Rejected	Rejected	Rejected

The geometric details of cross-section 4 are indicated in Figure 3.13.

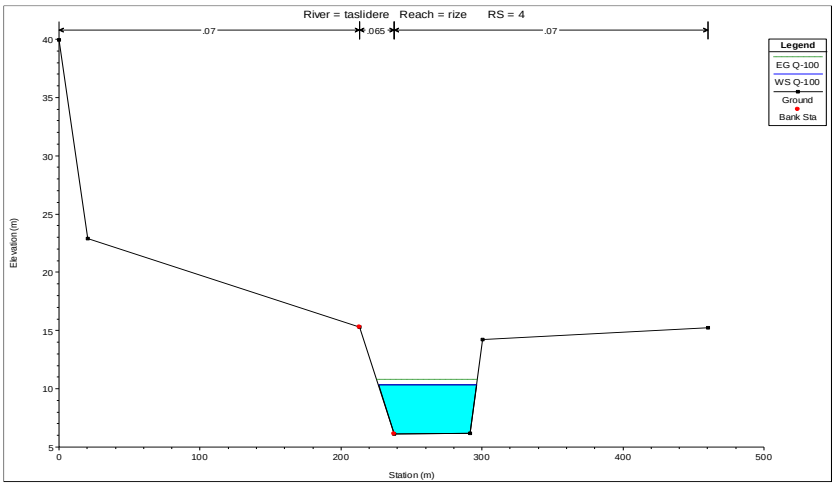

Figure 3.13 Geometric features of cross-section 4 in the HEC-RAS model

The GOF test results of cross-section 4 for flow depth are shown in Table 3.16.

Table 3.16 The GOF test results for cross-section 4

Variable	Variable PDF	PDF	Chi-Square	Chi-Square	Kolmogorov-Smirnov	Kolmogorov-Smirnov	Final Decision
			α = 0.05	α = 0.1	α = 0.05	α = 0.1	
			Decision	Decision	Decision	Decision	
n	**N**	**N**	Rejected	Rejected	Rejected	Rejected	Rejected
n	**N**	**LN**	Rejected	Rejected	Rejected	Rejected	Rejected
n	**N**	**G**	Rejected	Rejected	Rejected	Rejected	Rejected
n, Q	**N, LN**	**N**	Rejected	Rejected	Rejected	Rejected	Rejected
n, Q	**N, LN**	**LN**	**Accepted**	Rejected	**Accepted**	**Accepted**	**Accepted**
n, Q	**N, LN**	**G**	Rejected	Rejected	Rejected	Rejected	Rejected
n	**T**	**N**	Rejected	Rejected	Rejected	Rejected	Rejected
n	**T**	**LN**	Rejected	Rejected	Rejected	Rejected	Rejected
n	**T**	**G**	Rejected	Rejected	Rejected	Rejected	Rejected
n, Q	**T, LN**	**N**	Rejected	Rejected	Rejected	Rejected	Rejected
n, Q	**T, LN**	**LN**	**Accepted**	Rejected	**Accepted**	**Accepted**	**Accepted**
n, Q	**T, LN**	**G**	Rejected	Rejected	Rejected	Rejected	Rejected
n	**U**	**N**	Rejected	Rejected	Rejected	Rejected	Rejected
n	**U**	**LN**	Rejected	Rejected	Rejected	Rejected	Rejected
n	**U**	**G**	Rejected	Rejected	Rejected	Rejected	Rejected
n, Q	**U, LN**	**N**	Rejected	Rejected	Rejected	Rejected	Rejected
n, Q	**U, LN**	**LN**	Rejected	Rejected	Rejected	Rejected	Rejected
n, Q	**U, LN**	**G**	Rejected	Rejected	Rejected	Rejected	Rejected

The geometric details of cross-section 7 are indicated in Figure 3.14.

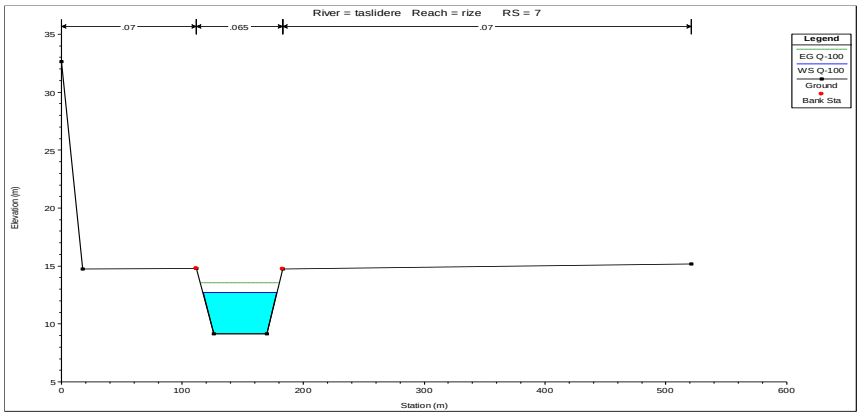

Figure 3.14 Geometric features of cross-section 7 in the HEC-RAS model

The GOF test results of cross-section 7 for flow depth are shown in Table 3.17.

Table 3.17 The GOF test results for cross-section 7

Variable	**Variable PDF**	**PDF**	**Chi-Square**	**Chi-Square**	**Kolmogorov-Smirnov**	**Kolmogorov-Smirnov**	**Final Decision**
			α = 0.05	**α = 0.1**	**α = 0.05**	**α = 0.1**	
			Decision	**Decision**	**Decision**	**Decision**	
n	**N**	**N**	Rejected	Rejected	Rejected	Rejected	Rejected
n	**N**	**LN**	Rejected	Rejected	Rejected	Rejected	Rejected
n	**N**	**G**	Rejected	Rejected	Rejected	Rejected	Rejected
n, Q	**N, LN**	**N**	Rejected	Rejected	Rejected	Rejected	Rejected
n, Q	**N, LN**	**LN**	Rejected	Rejected	Rejected	Rejected	Rejected
n, Q	**N, LN**	**G**	Rejected	Rejected	**Accepted**	Rejected	**Accepted**
n	**T**	**N**	Rejected	Rejected	Rejected	Rejected	Rejected
n	**T**	**LN**	Rejected	Rejected	Rejected	Rejected	Rejected
n	**T**	**G**	Rejected	Rejected	Rejected	Rejected	Rejected
n, Q	**T, LN**	**N**	Rejected	Rejected	Rejected	Rejected	Rejected
n, Q	**T, LN**	**LN**	Rejected	Rejected	Rejected	Rejected	Rejected
n, Q	**T, LN**	**G**	Rejected	Rejected	**Accepted**	**Accepted**	**Accepted**
n	**U**	**N**	Rejected	Rejected	Rejected	Rejected	Rejected
n	**U**	**LN**	Rejected	Rejected	Rejected	Rejected	Rejected
n	**U**	**G**	Rejected	Rejected	Rejected	Rejected	Rejected
n, Q	**U, LN**	**N**	Rejected	Rejected	Rejected	Rejected	Rejected
n, Q	**U, LN**	**LN**	Rejected	Rejected	Rejected	Rejected	Rejected
n, Q	**U, LN**	**G**	Rejected	Rejected	Rejected	Rejected	Rejected

The geometric details of cross-section 11 are indicated in Figure 3.15.

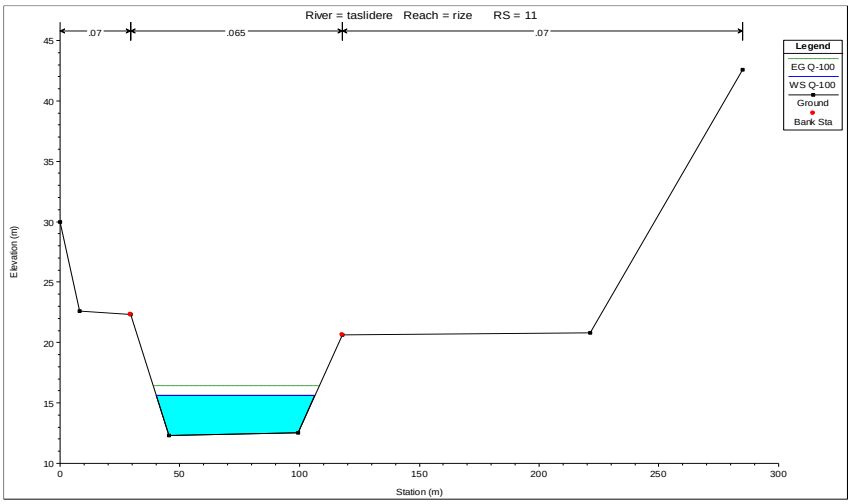

Figure 3.15 Geometric features of cross-section 11 in the HEC-RAS model

The GOF test results of cross-section 11 for flow depth are shown in Table 3.18.

Table 3.18 The GOF test results for cross-section 11

Variable	Variable PDF	PDF	Chi-Square	Chi-Square	Kolmogorov-Smirnov	Kolmogorov-Smirnov	Final Decision
			α = 0.05	α = 0.1	α = 0.05	α = 0.1	
			Decision	Decision	Decision	Decision	
n	**N**	**N**	Rejected	Rejected	Rejected	Rejected	Rejected
n	**N**	**LN**	Rejected	Rejected	Rejected	Rejected	Rejected
n	**N**	**G**	Rejected	Rejected	Rejected	Rejected	Rejected
n, Q	**N, LN**	**N**	Rejected	Rejected	Rejected	Rejected	Rejected
n, Q	**N, LN**	**LN**	Rejected	Rejected	Rejected	Rejected	Rejected
n, Q	**N, LN**	**G**	Rejected	Rejected	Rejected	Rejected	Rejected
n	**T**	**N**	Rejected	Rejected	Rejected	Rejected	Rejected
n	**T**	**LN**	Rejected	Rejected	Rejected	Rejected	Rejected
n	**T**	**G**	Rejected	Rejected	Rejected	Rejected	Rejected
n, Q	**T, LN**	**N**	Rejected	Rejected	Rejected	Rejected	Rejected
n, Q	**T, LN**	**LN**	Rejected	Rejected	Rejected	Rejected	Rejected
n, Q	**T, LN**	**G**	Rejected	Rejected	Rejected	Rejected	Rejected
n	**U**	**N**	Rejected	Rejected	Rejected	Rejected	Rejected
n	**U**	**LN**	Rejected	Rejected	Rejected	Rejected	Rejected
n	**U**	**G**	Rejected	Rejected	Rejected	Rejected	Rejected
n, Q	**U, LN**	**N**	Rejected	Rejected	Rejected	Rejected	Rejected
n, Q	**U, LN**	**LN**	Rejected	Rejected	Rejected	Rejected	Rejected
n, Q	**U, LN**	**G**	Rejected	Rejected	Rejected	Rejected	Rejected

The distributions fitted to the simulation results for flow depth are shown in Appendix D for all cross-sections.

3.2.2 Results of Part 2

The uncertainty analysis results carried out through the HEC-RAS model for n and Q are evaluated based on flow depth. The COV values are calculated for analysis results. The COV results in Table 3.19 represent values only when n is simulated, while the COV results in Table 3.20 represent values when n and Q are simulated jointly.

Table 3.19 COV results for flow depth for each cross-section (n is simulated)

n PDF	CS 2	CS 3	CS 3.3 BD	CS 3.3 BU	CS 4	CS 7	CS 11
Normal	0.076108	0.101944	0.097045	0.087004	0.084076	0.131007	0.152912
Triangle	0.058406	0.078092	0.075621	0.068513	0.065571	0.114251	0.131168
Uniform	0.327078	0.303185	0.291794	0.293745	0.225511	0.299445	0.380792

Table 3.20 COV results for flow depth for each cross-section (n and Q are simulated)

n PDF	CS 2	CS 3	CS 3.3 BD	CS 3.3 BU	CS 4	CS 7	CS 11
Normal	0.279721	0.286847	0.273731	0.26434	0.270651	0.349616	0.382695
Triangle	0.272055	0.276187	0.264941	0.257247	0.262579	0.340941	0.374475
Uniform	0.418275	0.397468	0.385301	0.398063	0.352257	0.421594	0.504305

The COV values from n analysis are lower than the COV values from n and Q analysis. Approximate values to the COV values suggested in the literature (Table 3.21) are observed when uncertainty analysis is applied for both Q and n jointly.

Table 3.21 Flow depth PDF and COV values based on literature

Variable	Proposed PDF	Proposed COV	References
Flow Depth	Symmetrical Triangular distribution	0.2	(Johnson, 1999)
Flow Depth	Normal distribution	0.23	(Liao et al., 2015)

All distributions are rejected when uncertainty analysis is applied only for n (Table 3.22). In contrast, Gamma and Log-normal distributions are accepted for flow depth when uncertainty analysis is performed jointly for both n and Q (Table 3.23).

Table 3.22 PDF results for flow depth for each cross-section (n is simulated)

n PDF	CS 2	CS 3	CS 3.3 BD	CS 3.3 BU	CS 4	CS 7	CS 11
Normal	Rejected	Rejected	Rejected	Rejected	Rejected	Rejected	Rejected
Triangle	Rejected	Rejected	Rejected	Rejected	Rejected	Rejected	Rejected
Uniform	Rejected	Rejected	Rejected	Rejected	Rejected	Rejected	Rejected

Table 3.23 PDF results for flow depth for each cross-section (n and Q are simulated)

n PDF	CS 2	CS 3	CS 3.3 BD	CS 3.3 BU	CS 4	CS 7	CS 11
Normal	Log-normal	Gamma	Rejected	Log-normal	Log-normal	Gamma	Rejected
Triangle	Log-normal	Rejected	Rejected	Log-normal	Log-normal	Gamma	Rejected
Uniform	Rejected	Rejected	Rejected	Rejected	Rejected	Rejected	Rejected

The percentages are calculated between the flow depth values obtained as a result of the simulation and the deterministic flow depth value (Table 3.24). This table presents percentages of higher and lower values than the deterministic value. The corresponding frequency histograms are provided in Appendix D. When the percentages are examined, it is seen that 50% of the flow depths obtained by simulation are generally higher than the deterministic flow depths. This situation is observed even when only n is simulated, n and Q are simulated jointly, in different

cross-sections, and when input has different PDFs. This may imply that some parameters to be dealt with in view of safety, such as freeboards computed using deterministic approaches would be underestimated according to the stochastic approach. Therefore, a more realistic decision can be made for hydraulic analysis and design by using a stochastic approach.

Table 3.24 Analysis results for flow depth

CS	Variable	Variable PDF	Accepted PDF	A percentage lower than the deterministic value	A percentage higher than the deterministic value
2	n	N	-	50%	50%
2	n	T	-	44%	56%
2	n	U	-	44%	56%
2	n, Q	N, LN	LN	50%	50%
2	n, Q	T, LN	LN	48%	52%
2	n, Q	U, LN	-	49%	51%
3	n	N	-	49%	51%
3	n	T	-	43%	57%
3	n	U	-	44%	56%
3	n, Q	N, LN	G	50%	50%
3	n, Q	T, LN	-	48%	52%
3	n, Q	U, LN	-	49%	51%
3.3 BD	n	N	-	46%	54%
3.3 BD	n	T	-	39%	61%
3.3 BD	n	U	-	43%	57%
3.3 BD	n, Q	N, LN	-	49%	51%
3.3 BD	n, Q	T, LN	-	46%	54%
3.3 BD	n, Q	U, LN	-	48%	52%
3.3 BU	n	N	-	55%	45%
3.3 BU	n	T	-	51%	49%
3.3 BU	n	U	-	45%	55%
3.3 BU	n, Q	N, LN	LN	52%	48%
3.3 BU	n, Q	T, LN	LN	50%	50%
3.3 BU	n, Q	U, LN	-	50%	50%
4	n	N	-	49%	51%
4	n	T	-	43%	57%
4	n	U	-	39%	61%
4	n, Q	N, LN	LN	51%	49%
4	n, Q	T, LN	LN	48%	52%
4	n, Q	U, LN	-	43%	57%
7	n	N	-	50%	50%

Table 3.24 Continued

CS	Variable	Variable PDF	Accepted PDF	A percentage lower than the deterministic value	A percentage higher than the deterministic value
7	n	T	-	44%	56%
7	n	U	-	42%	58%
7	n, Q	N, LN	G	50%	50%
7	n, Q	T, LN	G	48%	52%
7	n, Q	U, LN	-	42%	58%
11	n	N	-	50%	50%
11	n	T	-	44%	56%
11	n	U	-	43%	57%
11	n, Q	N, LN	-	50%	50%
11	n, Q	T, LN	-	48%	52%
11	n, Q	U, LN	-	47%	53%

As a concluding summary, generally, the analysis with mean n and Q values offers a deterministic approach, while a stochastic approach is implemented with the Monte Carlo simulation covering possible multiple combinations of variables and their mean values. Instead of obtaining a value uncertain with the deterministic approach, a wide range of results is presented by applying uncertainty analysis to each input with the stochastic approach. In this direction, variations from mean behavior are captured by filling the gaps with the stochastic approach. In addition to offering valuable insights into system performance, uncertainty analysis (stochastic approach) also provides crucial data for engineering design and knowledge.

CHAPTER 4

SUMMARY AND CONCLUSIONS

Dealing with certain hydraulic variables is required for engineers in decision-making, sediment transportation analysis, data processing, and cost-effective designs. At this point, a stochastic approach is required since it explains the randomness and distributions of variables. In this study, the probabilistic performance assessments based on uncertainty analysis are performed for the stochastic approach. Monte Carlo simulation is used to investigate the uncertainty underlying each variable for the stochastic approach. The required number of simulation cycles for each simulation is determined based on the standard error and time efficiency, and the study is carried out with 10000 simulation cycles accordingly. The PDF and COV assigned to each input in the simulation are defined in line with the literature review. R programming is used to operate the Monte Carlo simulation. The GOF tests are applied after conducting an uncertainty analysis. In this study, the Chi-Square test and Kolmogorov-Smirnov test with 0.05 and 0.1 significance levels are performed.

The study is conducted in two parts. In the first part, bed load transport rate and Manning's roughness coefficient are analyzed for the Miliç Basin, Turkey. The four branches of the river are used with 50-year and 500-year return period flow rates. Two methods are selected to conduct the uncertainty analysis for the bed load sediment rate calculation i.e. Meyer-Peter and Müller and Einstein-Brown approaches. The PDFs are assigned to the input variables together with a recommended COV. In the second part, the effects of the uncertainties of the HEC-RAS model input data are analyzed through output data by implementing Monte Carlo simulation. The main channel Manning's roughness coefficient and flow rate are evaluated as input data, while the flow depth is examined as output data. In this study, seven different river stations on Taşlıdere Creek, Turkey, are selected to

implement the uncertainty analysis for the second part. To perform the Monte Carlo simulation, the Normal, Triangular, and Uniform distributions are assigned for Manning's roughness coefficient, while the Log-normal distribution is assigned for the flow rate. To monitor the effects of Manning's roughness coefficient and flow rate separately, Manning's roughness coefficient is presented to the model as a single uncertain variable and then both of them are presented to the model as multiple uncertain variables.

The following results are obtained throughout the study:

- The results of the uncertainty analysis conducted for bed load rate showed that the Beta and Gamma distributions are observed with the analyses carried out by the MPM and E-B approaches for Miliç Basin.
- Although the results vary regionally, generally 50% of the stochastic bed load rate values are higher than the deterministic bed load rates for nearly all simulations with both approaches. Additionally, the rate of being greater than deterministic values is higher than 50% for some results by using 0.5COVs.
- The COVs for Manning's roughness coefficient show parallelism with the distributions suggested in the literature.
- The COVs for flow depth are in line with the recommended values suggested in the literature.
- All distributions are rejected for flow depth when uncertainty analysis is applied only for Manning's roughness coefficient, whereas Gamma and Log-normal distributions are accepted for flow depth when uncertainty analysis is performed for Manning's roughness coefficient and flow rate jointly for Taşlıdere Creek.
- The 50% of the flow depths obtained by simulation are generally higher than the deterministic flow depths. This is an important by-product of a stochastic approach in view of safety requirements in open channel design.

Conducting similar analyses with mainly fine sediments and using different bed load transport rate equations may be a topic for future research.

REFERENCES

Altarejos-García, L., Martínez-Chenoll, M.L., Escuder-Bueno, I., Serrano-Lombillo, A., 2012. Assessing the impact of uncertainty on flood risk estimates with reliability analysis using 1-D and 2-D hydraulic models. Hydrol. Earth Syst. Sci. 16, 1895–1914.

Andrade, C., 2020. Understanding the difference between standard deviation and standard error of the mean, and knowing when to use which. Indian J. Psychol. Med. 42, 409–410.

Ang, A.H.S., Tang, W.H., 1975. Probability concepts in engineering planning and design, basic principles. John Wiley & Sons Incorporated.

Aslam, M., 2019. Introducing Kolmogorov–Smirnov tests under uncertainty: an application to radioactive data. ACS omega 5, 914–917.

Beckers, F., Noack, M., Wieprecht, S., 2018. Uncertainty analysis of a 2D sediment transport model: an example of the Lower River Salzach. J. Soils Sediments 18, 3133–3144.

Bozzi, S., Passoni, G., Bernardara, P., Goutal, N., Arnaud, A., 2015. Roughness and Discharge Uncertainty in 1D Water Level Calculations. Environ. Model. Assess. 20, 343–353.

Brown, C.B., 1950. Sediment transportation. Eng. Hydraul. 12, 769–857.

Cesare, M.A., 1991. First-Order Analysis of Open-Channel Flow. J. Hydraul. Eng. 117, 242–247.

Chan, B.K.C., 2018. Data analysis using R programming, in: Biostatistics for Human Genetic Epidemiology. Springer, pp. 47–122.

Chang, C.-H., Yang, J.-C., Tung, Y.-K., 1993. Sensitivity and uncertainty analysis of a sediment transport model: a global approach. Stoch. Hydrol. Hydraul 7, 299–314.

Corotis, R.B., 2015. An overview of uncertainty concepts related to mechanical and civil engineering. ASCE-ASME J. Risk Uncertain. Eng. Syst. Part B Mech. Eng. 1, 40801.

Dantan, J.Y., Qureshi, A.J., 2009. Worst-case and statistical tolerance analysis based on quantified constraint satisfaction problems and Monte Carlo simulation. CAD Comput. Aided Des. 41, 1–12.

Eidsvik, K.J., 2004. Some contributions to the uncertainty of sediment transport predictions. Cont. Shelf Res. 24, 739–754.

Goodell, C., 2014. Breaking the HEC-RAS Code - A User's Guide to Automating HEC-RAS.

Google Earth., 2022. Google Inc.

Haddadchi, A., Omid, M.H., Dehghani, A.A., 2013. Bedload equation analysis using bed load-material grain size. J. Hydrol. Hydromechanics 61, 241–249.

Hieu, M.T., Nowak, W., Kopmann, R., 2015. Using algorithmic differentiation for uncertainty analysis. Conf. Pap. 52–58.

Huang, H.Q., 2010. Reformulation of the bed load equation ofMeyer-Peter and Müller in light of the linearity theory for alluvial channel flow. Water Resour. Res. 46, 1–11.

Iskra, I., Droste, R., 2008. Parameter Uncertainty of a Watershed Model. Can. Water Resour. J. 33, 5–22.

Jajarmizadeh, M., Harun, S., Salarpour, M., 2012. A review on theoretical consideration and types of models in hydrology. J. Environ. Sci. Technol. 5, 249–261.

Johnson, P.A., 1999. Fault Tree Analysis of Bridge Failure due to Scour and Channel Instability. J. Infrastruct. Syst. 5, 35–41.

Johnson, P.A., 1996. Uncertainty of Hydraulic Parameters. J. Hydraul. Eng. 122, 112–114.

Johnson, P.A., 1995. Comparison of Pier-Scour Equations Using Field Data. J. Hydraul. Eng. 121, 626–629.

Johnson, P.A., 1992. Reliability Based Pier Scour Engineering. J. Hydraul. Eng. 118, 1344–1358.

Karagöz, C., Erkmen, U., 2009. Samsun-Terme Kocaman Grubu (Miliç Irmağı Kolları) Havzası Taşkın ve Rüsubat Kontrolü Fizibilite Raporu - Sediment Taşınım Etüdü Raporu. Devlet Su İşleri Genel Müdürlüğü.

Kentel, E., Yanmaz, A.M., 2008. Impact of Hydrologic Uncertainties in Reservoir Routing. BALWOIS 2008 Conf. 1–10.

Kopmann, R.;, Schmidt, A., 2010. Comparison of different reliability analysis methods for a 2D morphodynamic numerical model of River Danube. Conf. Pap. 1615–1620.

Kumar, M., 2019. Sensitivity analysis of Manning's roughness coefficient in MIKE 11 model for Mahanadi delta region. Ann. Plant Soil Res. 21, 62–66.

Lagasse, P.F., Zevenbergen, L.W., Schall, J.D., Clopper, P.E., 2001. Bridge scour and stream instability countermeasures. experience, selection, and design guidance. United States. Federal Highway Administration. Office of Bridge Technology.

Li, M.Z., Amos, C.L., 1995. SEDTRANS92: A sediment transport model for continental shelves. Comput. Geosci. 21, 533–554.

Li, Y., Zhang, Y., Yu, M., Li, X., 2019. Drawing and studying on histogram. Cluster Comput. 22, 3999–4006.

Liao, K.W., Lu, H.J., Wang, C.Y., 2015. A probabilistic evaluation of pier-scour potential in the Gaoping River Basin of Taiwan. Vilnius Gedim. Tech. Univ. 21, 637–653.

Mays, L.W., Tung, Y.-K., 2002. Hydrosystems Engineering and Management.

McHugh, M.L., 2013. The chi-square test of independence. Biochem. medica 23, 143–149.

Montanari, A., Shoemaker, C.A., Van De Giesen, N., 2009. Introduction to special section on uncertainty assessment in surface and subsurface hydrology: An overview of issues and challenges. Water Resour. Res. 45.

Papadopoulos, C.E., Yeung, H., 2001. Uncertainty estimation and Monte Carlo simulation method. Flow Meas. Instrum. 12, 291–298.

Pappenberger, F., Beven, K., Horritt, M., Blazkova, S., 2005. Uncertainty in the calibration of effective roughness parameters in HEC-RAS using inundation and downstream level observations. J. Hydrol. 302, 46–69.

Raychaudhuri, S., 2008. Introduction to monte carlo simulation. Proc. - Winter Simul. Conf. 91–100.

Renard, P., Alcolea, A., Ginsbourger, D., 2013. Stochastic versus Deterministic Approaches. Environ. Model. Find. Simplicity Complex. Second Ed. 133–149.

Riahi-Madvar, H., Seifi, A., 2018. Uncertainty analysis in bed load transport prediction of gravel bed rivers by ANN and ANFIS. Arab. J. Geosci. 11, 1–20.

Ritter, A., Munoz-Carpena, R., 2013. Performance evaluation of hydrological models: Statistical significance for reducing subjectivity in goodness-of-fit assessments. J. Hydrol. 480, 33–45.

Robert, C.P., Casella, G., Casella, G., 2010. Introducing monte carlo methods with r. Springer.

Salas, J.D., Shin, H.-S., 1999. Uncertainty Analysis of Reservoir Sedimentation 339–350.

Sarkar, J., Rashid, M., 2016. A geometric view of the mean of a set of numbers. Teach. Stat. 38, 77–82.

Savage, T.S.J., Pianosi, F., Bates, P., Freer, J., Wagener, T., 2016. Quantifying the importance of spatial resolution and other factors through global sensitivity analysis of a flood inundation model. Water Resour. Res. 52, 9146–9163.

Schmelter, M.L., Erwin, S.O., Wilcock, P.R., 2012. Accounting for uncertainty in cumulative sediment transport using Bayesian statistics. Geomorphology 175, 1–13.

Shui-Tuang Cheng, 1982. Overtopping Risk Evaluation For an Existing Dam. Univeristy of Illinois at Urbana-Champaign.

Sidiropoulos, E., Vantas, K., Hrissanthouand, V., Papalaskaris, T., 2021. Extending the Applicability of the Meyer–Peter and Müller Bed Load Transport Formula Epaminondas. Water (Switzerland) 1–18.

Singh, V.P., 2010. Flow Routing in Open Channels: Some Recent Advances.

Smid, J.H., Verloo, D., Barker, G.C., Havelaar, A.H., 2010. Strengths and weaknesses of Monte Carlo simulation models and Bayesian belief networks in microbial risk assessment. Int. J. Food Microbiol. 139, S57–S63.

Sobol, I.M., 1994. A primer for the Monte Carlo method. CRC press.

Teegavarapu, R.S. V, 2019. Methods for analysis of trends and changes in hydroclimatological time-series, in: Trends and Changes in Hydroclimatic Variables. Elsevier, pp. 1–89.

Thorne, C.R., 2000. Sediment Transport in the Lower Mississippi River Final Report Principal Investigator : Colin R Thorne Research Associates : Oliver P Harmar and Nicholas Wallerstein School of Geography , University of Nottingham University Park Submitted to U . S . Army .

Tung, Y.-K., Member, A., 1990. Mellin Transform Applied to Uncertainty Analysis in Hydrology / Hydraulics. J. Hydraul. Eng. 116, 659–674.

Ugoni, A., Walker, B.F., 1995. The Chi square test: an introduction. COMSIG Rev. 4, 61.

US Army Corps of Engineers, 2016. HEC-RAS River Analysis System Hydraulic Reference Manual. Hydrol. Eng. Cent. 547.

US Army Corps of Engineers, 1990. HEC2-SR Water Surface Profiles.

Verhoeven, R., Banasiak, R., Okruszko, T., Chormanski, J., 2003. Hydraulic Modelling of River Flow - data collection and problem solving.

Wang, M.G. and J., 2004. Reliability Model for Bridge Scour Analysis.

Wilson, E.M., 1990. Engineering hydrology. Bloomsbury Publishing.

Yanmaz, A.M., 2022a. Applied Water Resources Engineering, 6th ed. Nobel Academic Publication, Ankara.

Yanmaz, A.M., 2022b. Bridge Hydraulics, 2nd ed. Nobel Academic Publications, Ankara (in Turkish).

Yanmaz, A.M., 2003. Reliability simulation of scouring downstream of outlet facilities. Turkish J. Eng. Environ. Sci. 27, 65–71.

Yeh, K.-C., Tung, Y.-K., Member, A., 1993. Uncertainty And Sensitivity Analyses of Pit-Migration Model. J. Hydraul. Eng. 119, 262–283.

Yen, B.C., 2010. System and component uncertainties in water resources. Risk, Reliab. Uncertainty, Robustness Water Resour. Syst. 133–142.

Yen, B.C., 1992. Channel flow resistance: centennial of Manning's formula. Water Resources Publication.

Yıldırım, M.S., 2013. Computer-Assisted Design Methodology for Armoring Type Bridge Scour Countermeasures. Master Thesis, Middle East Technical University.

APPENDICES

A. Distribution Fittings of Bed Load Rate (MPM)

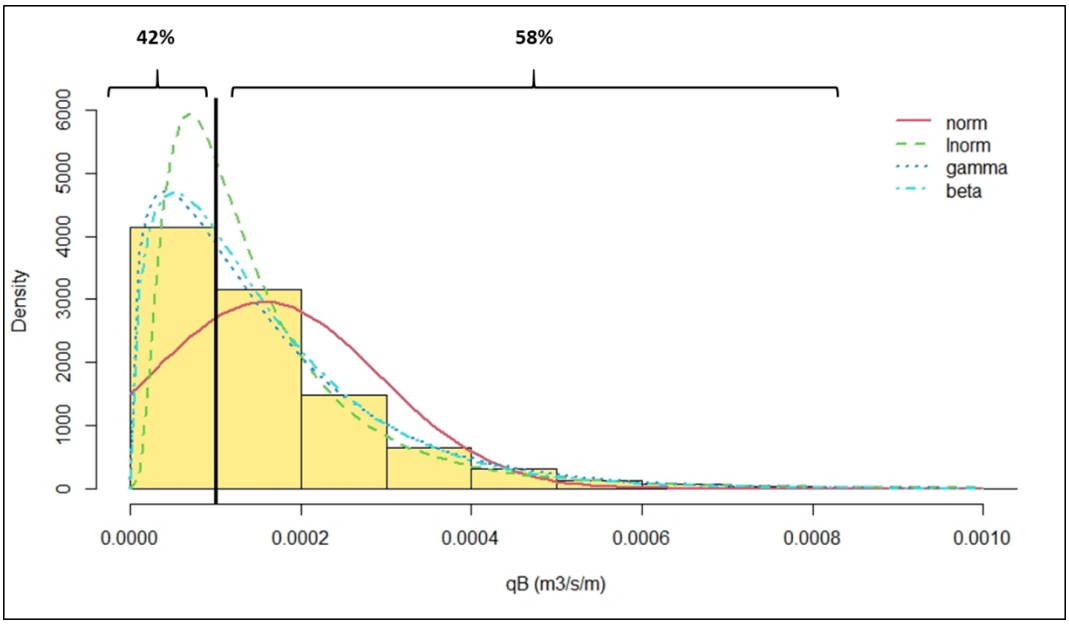

Figure A. 1 Distribution fitting (Leylek Creek, 50 years)

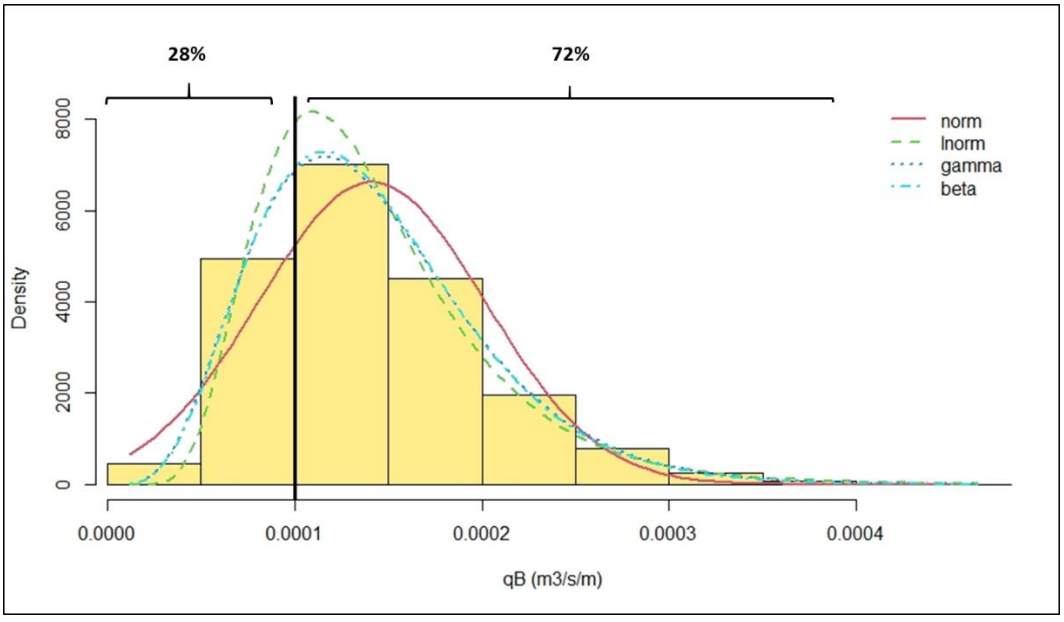

Figure A. 2 Distribution fitting (Leylek Creek, 50 years) with 0.5COV

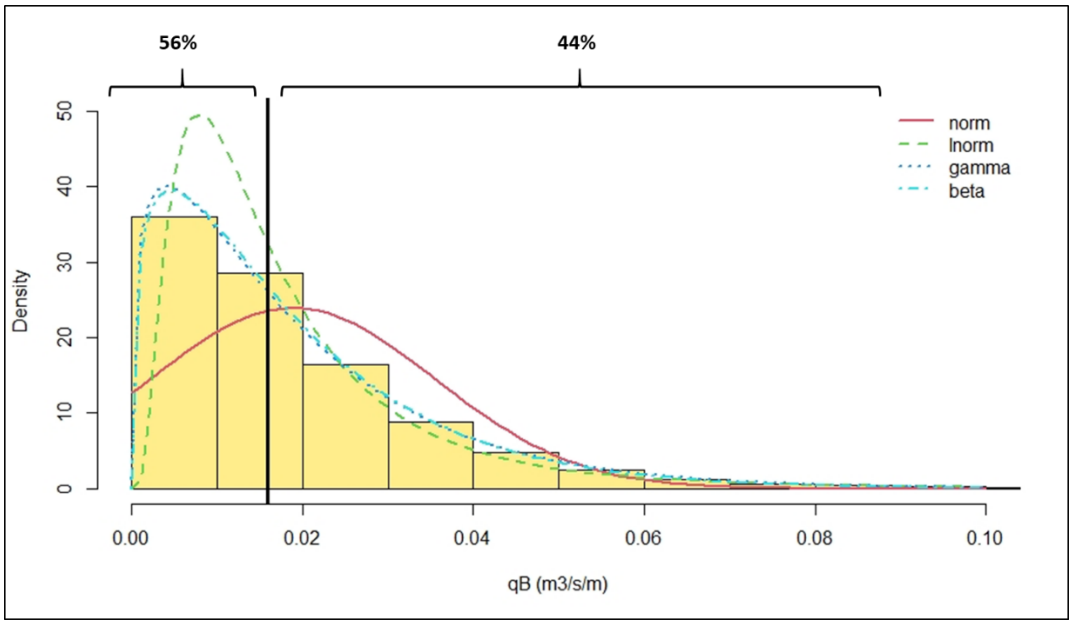

Figure A. 3 Distribution fitting (Miliç 1 Creek, 50 years)

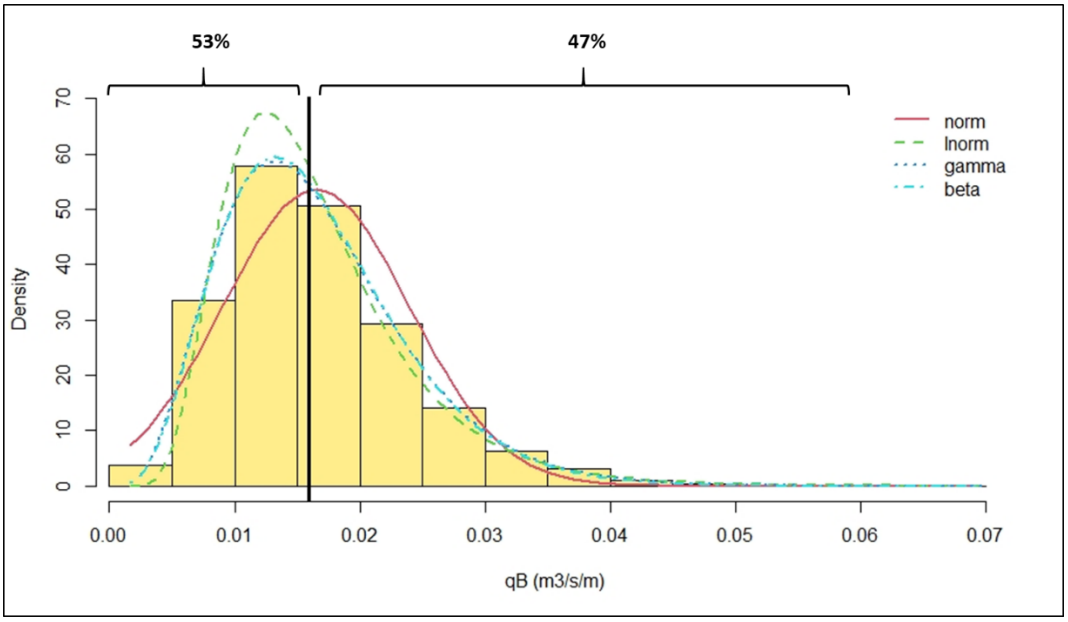

Figure A. 4 Distribution fitting (Miliç 1 Creek, 50 years) with 0.5COV

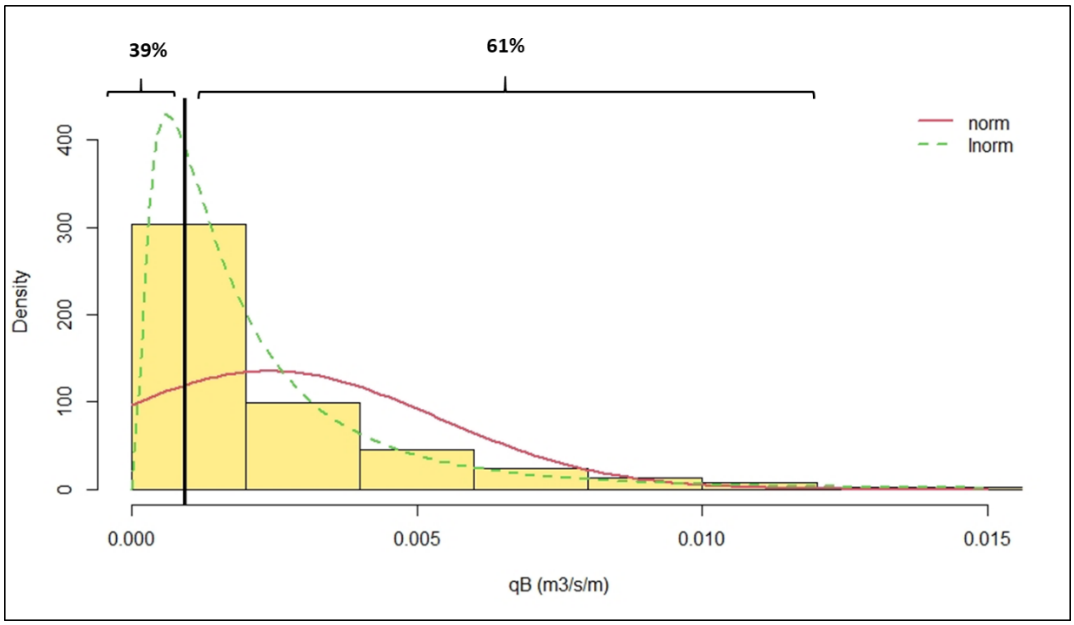

Figure A. 5 Distribution fitting (Evci Creek, 50 years)

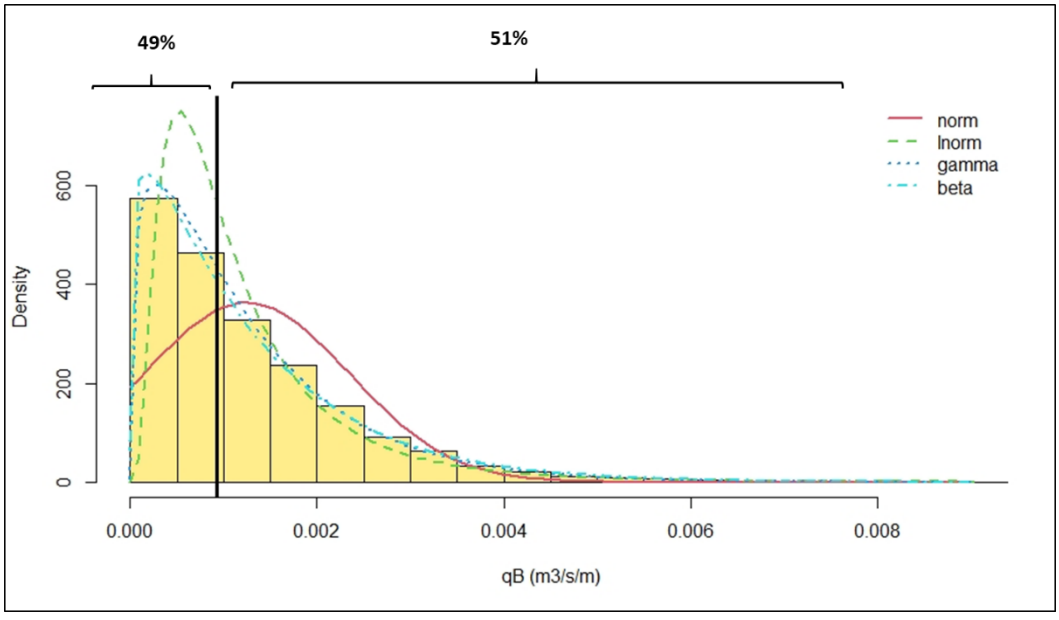

Figure A. 6 Distribution fitting (Evci Creek, 50 years) with 0.5COV

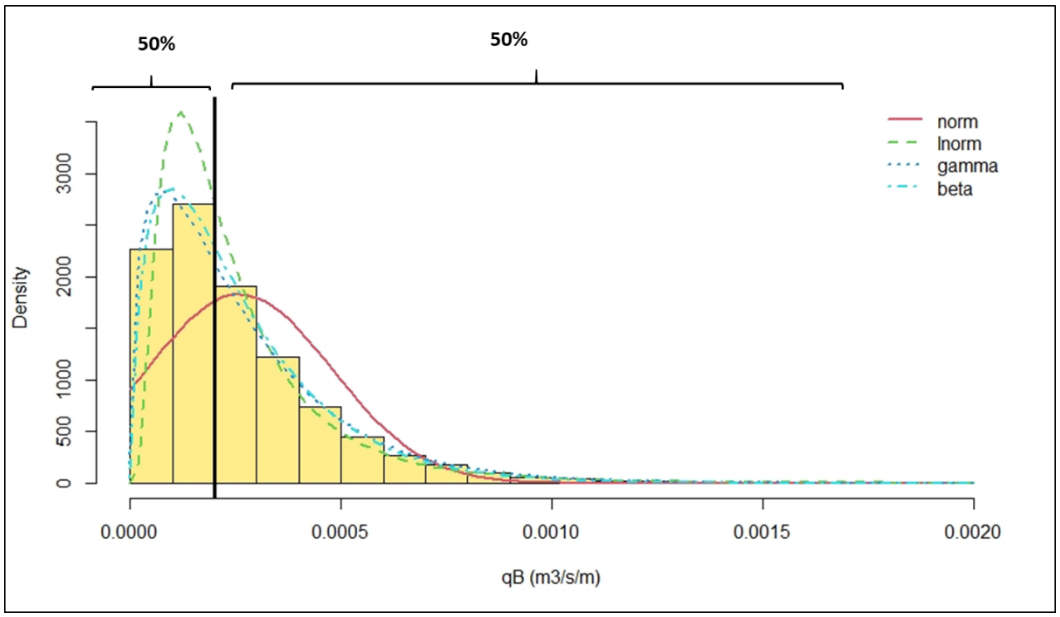

Figure A. 7 Distribution fitting (Sakarlı Creek, 500 years)

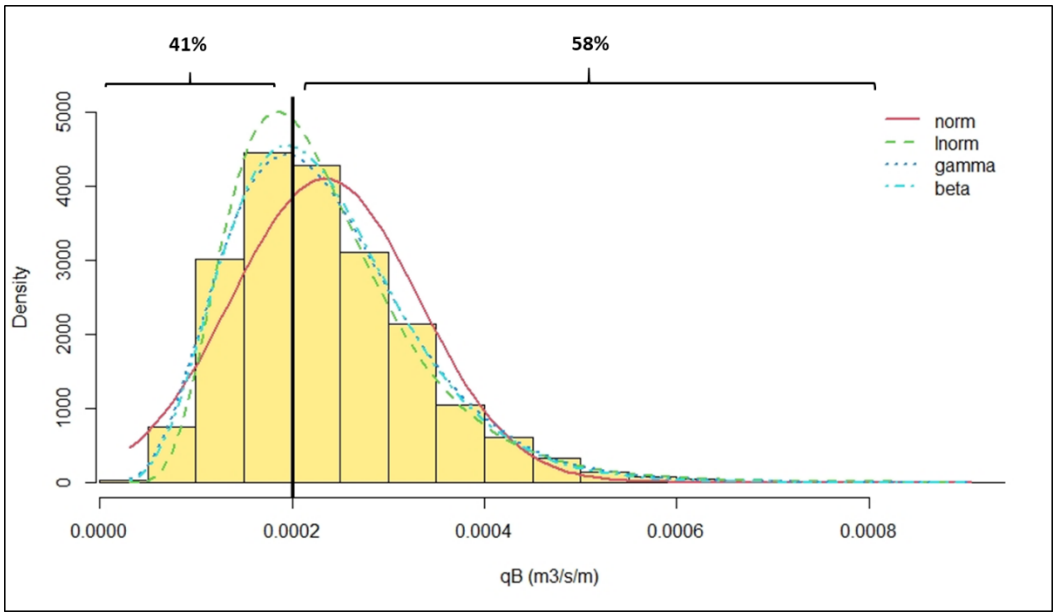

Figure A. 8 Distribution fitting (Sakarlı Creek, 500 years) with 0.5COV

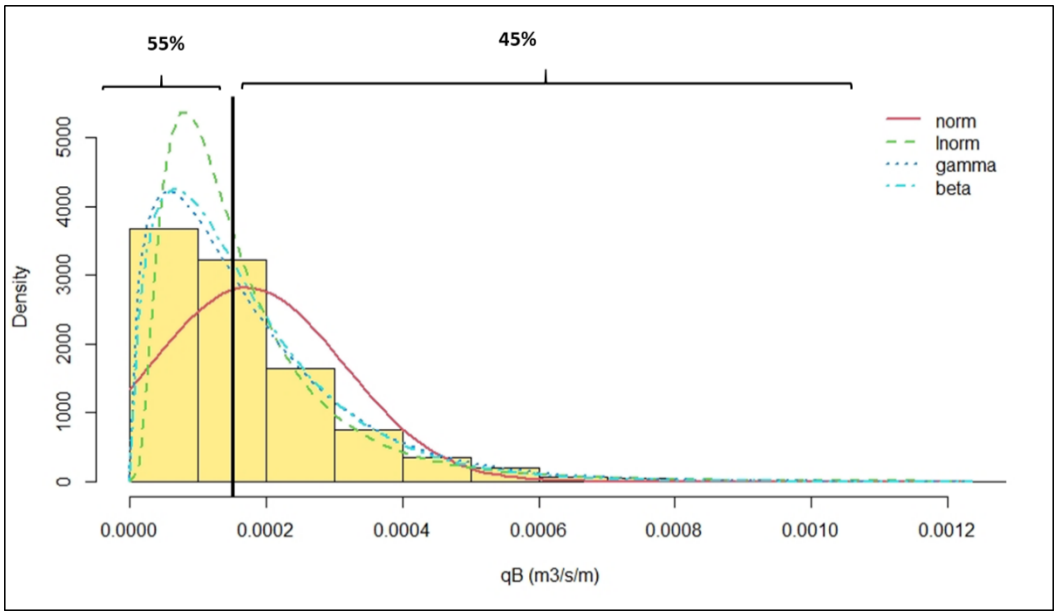

Figure A. 9 Distribution fitting (Miliç 2 Creek, 500 years)

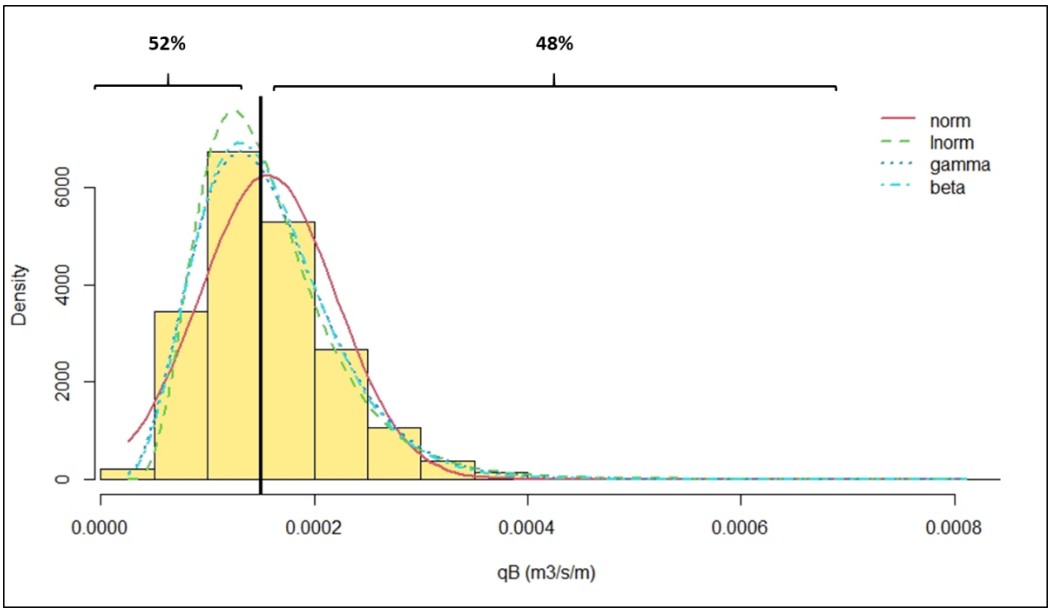

Figure A. 10 Distribution fitting (Miliç Creek, 500 years) with 0.5COV

B. Distribution Fittings of Bed Load Rate (E-B)

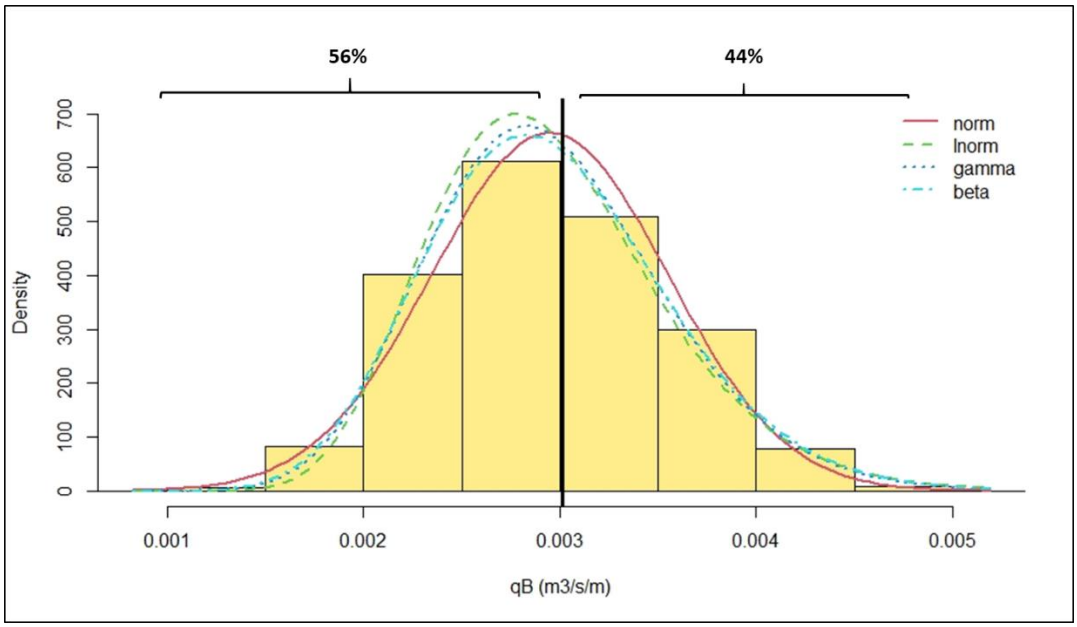

Figure B. 1 Distribution fitting (Leylek Creek, 50 years)

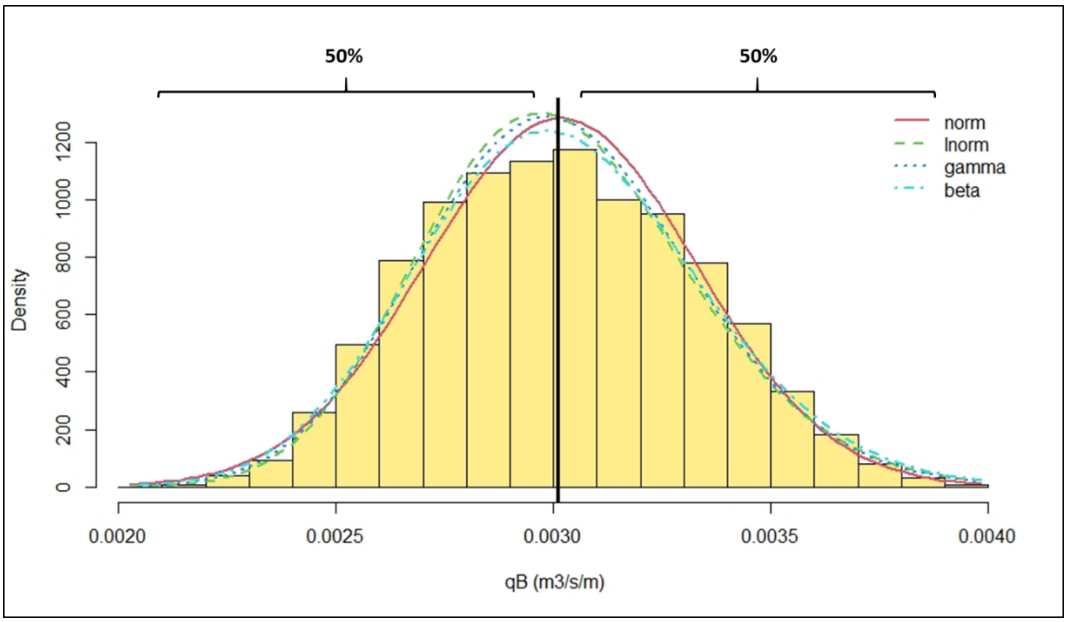

Figure B. 2 Distribution fitting (Leylek Creek, 50 years) with 0.5COV

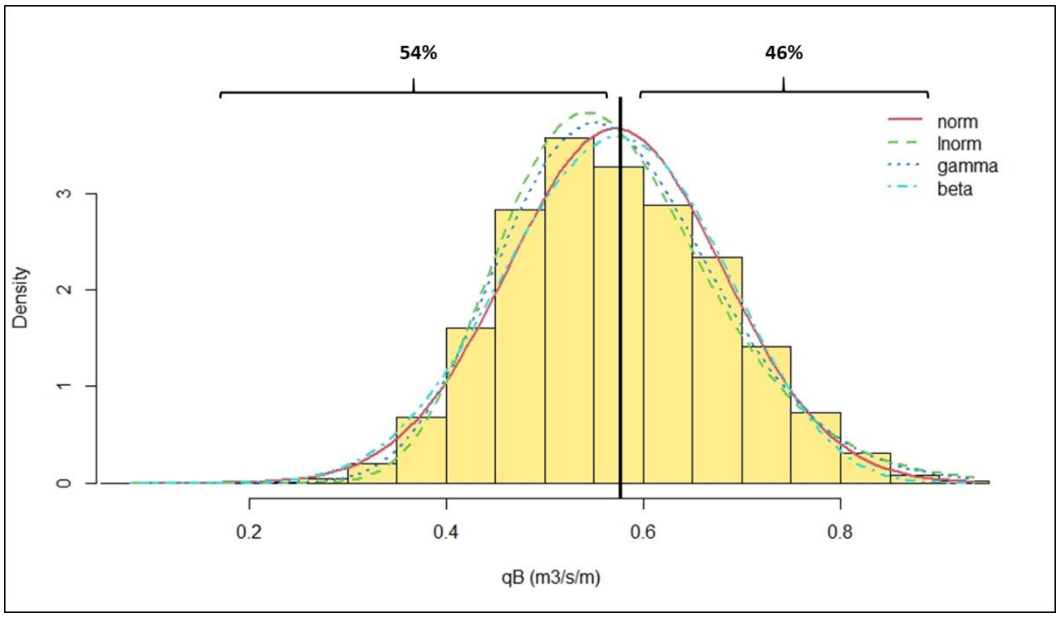

Figure B. 3 Distribution fitting (Miliç 1 Creek, 50 years)

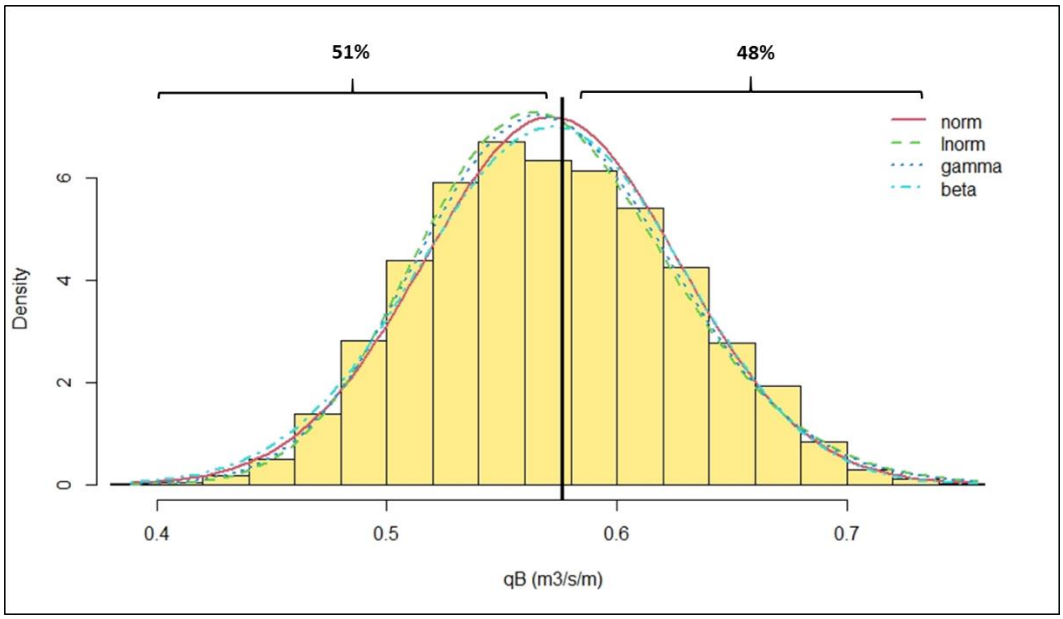

Figure B. 4 Distribution fitting (Miliç 1 Creek, 50 years) with 0.5COV

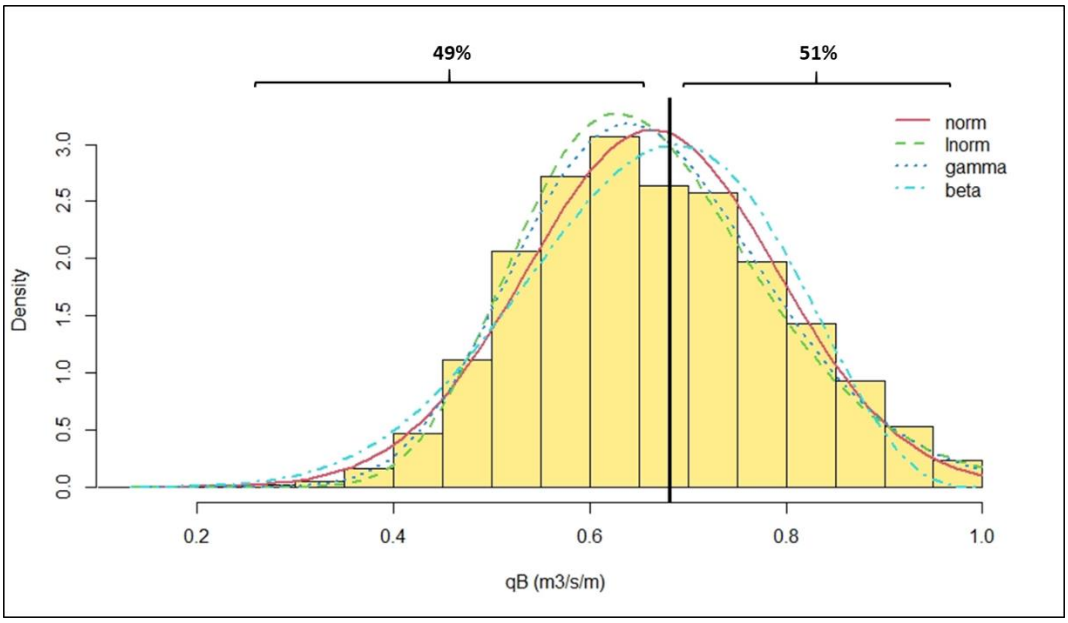

Figure B. 5 Distribution fitting (Evci Creek, 50 years)

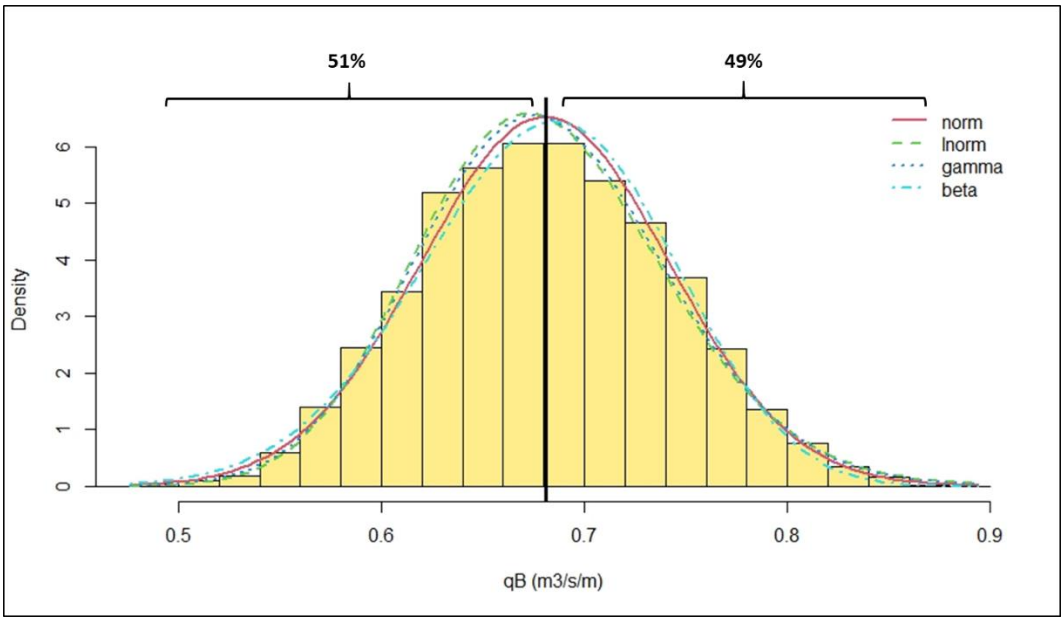

Figure B. 6 Distribution fitting (Evci Creek, 50 years) with 0.5COV

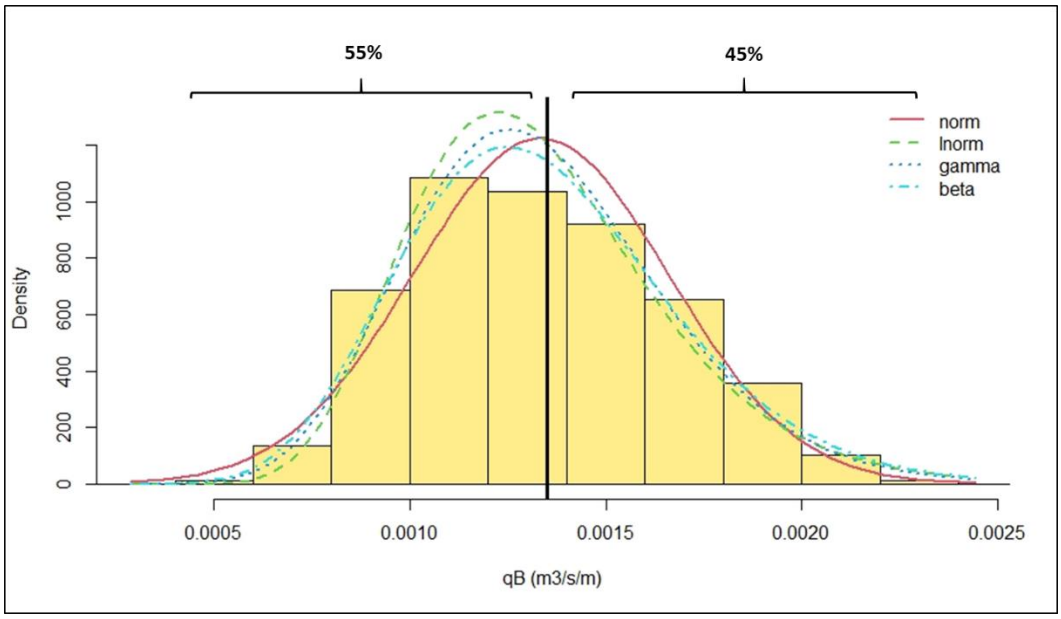

Figure B. 7 Distribution fitting (Sakarlı Creek, 500 years)

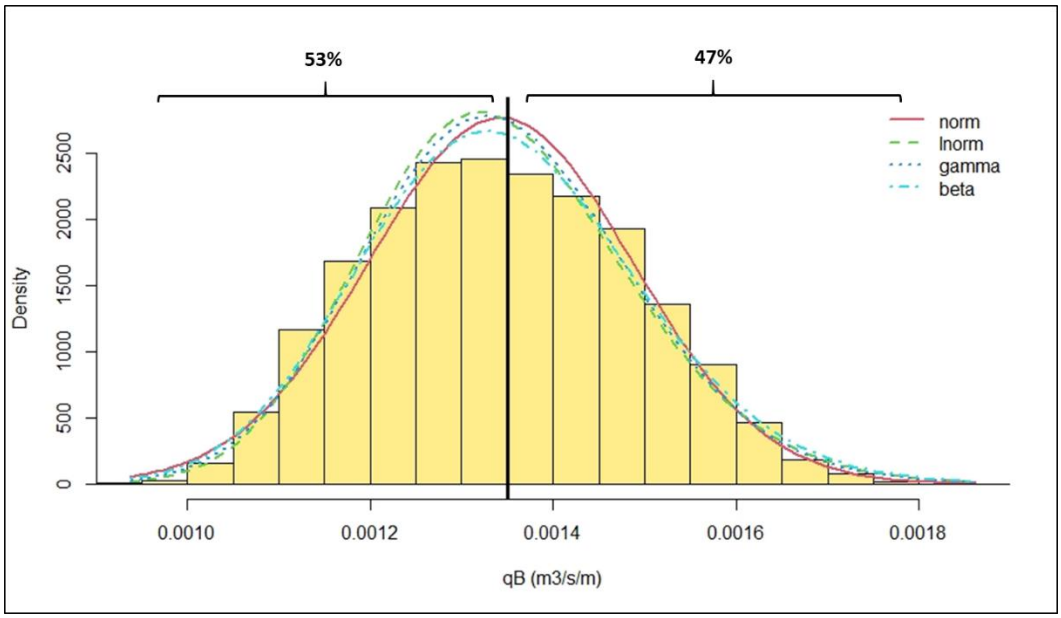

Figure B. 8 Distribution fitting (Sakarlı Creek, 500 years) with 0.5COV

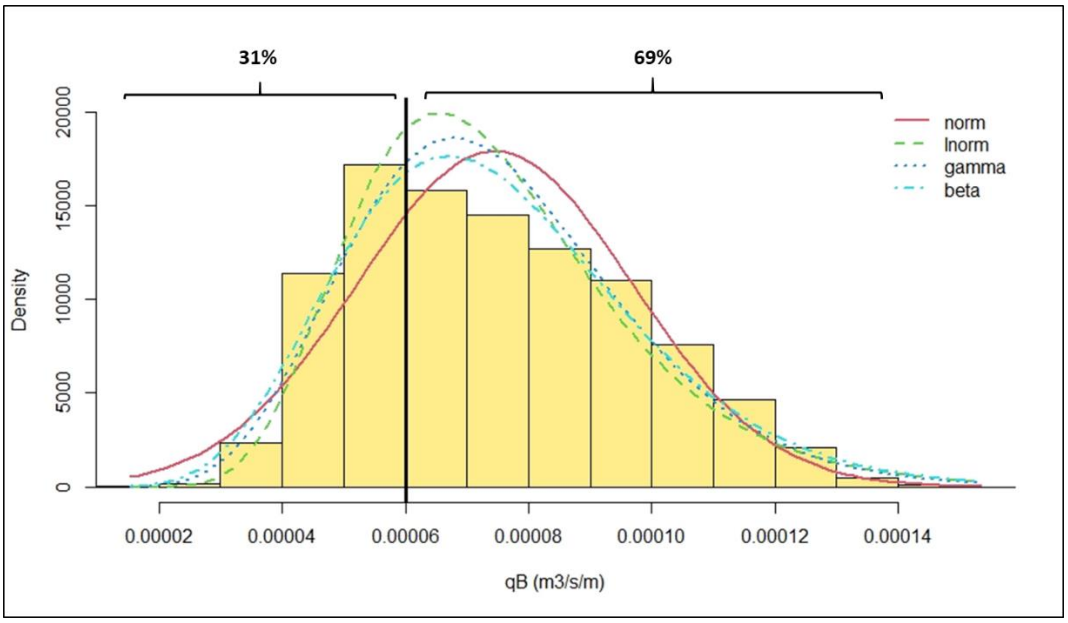

Figure B. 9 Distribution fitting (Miliç 2 Creek, 500 years)

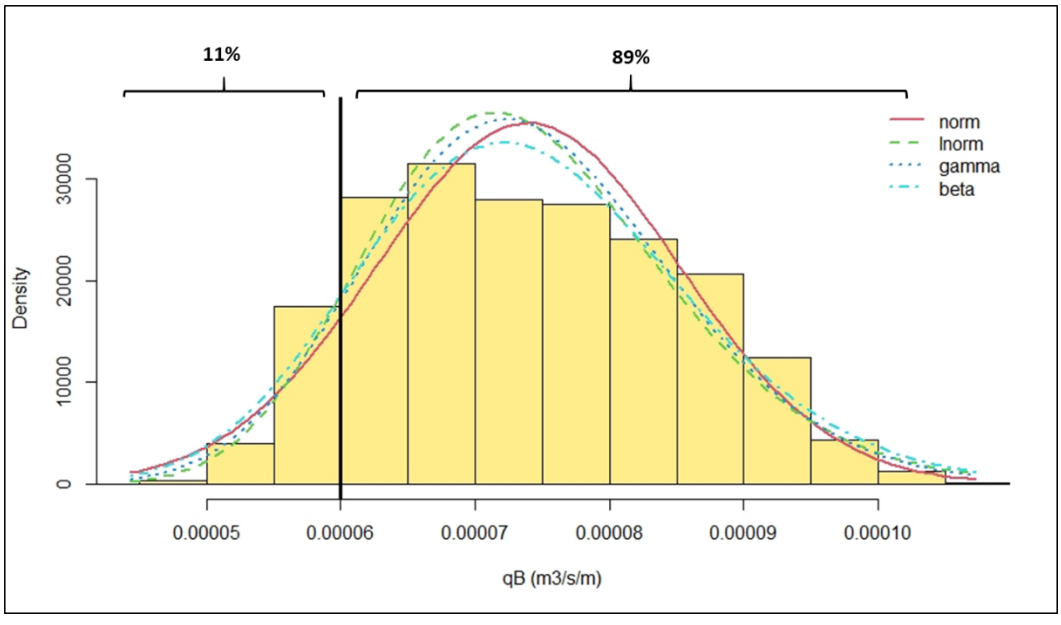

Figure B. 10 Distribution fitting (Miliç 2 Creek, 500 years) with 0.5COV

C. Distribution Fittings of Manning's Roughness Coefficient

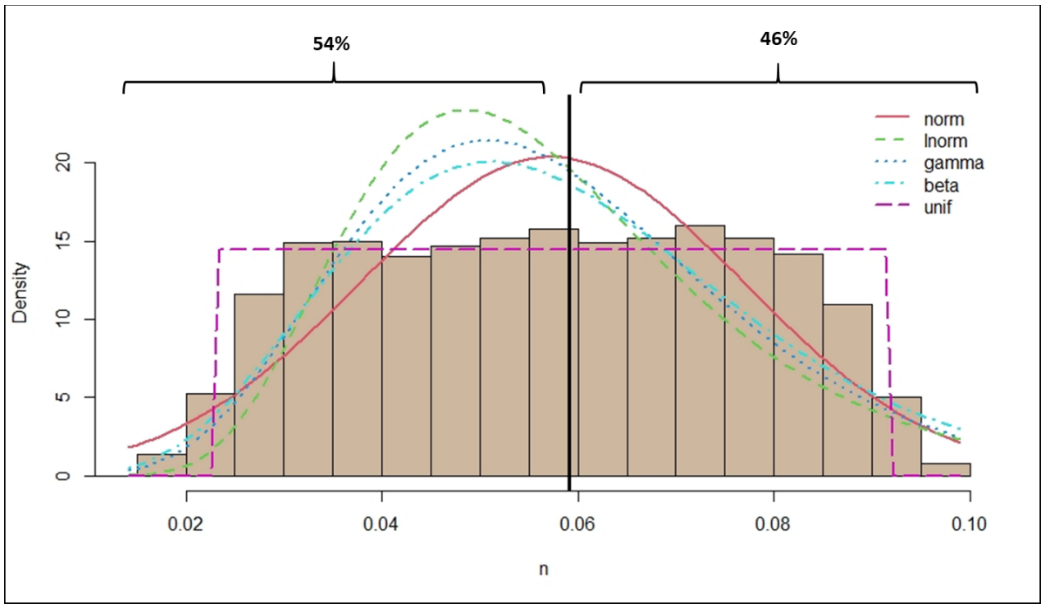

Figure C. 1 Distribution fitting (Leylek Creek, 50 years) for Set 1 PDF & COV

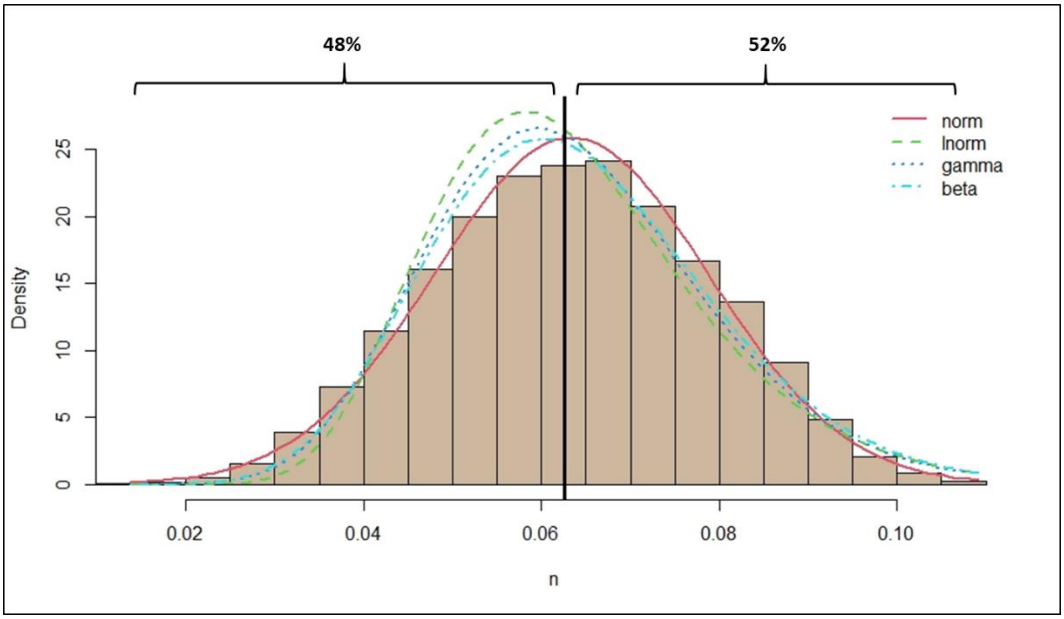

Figure C. 2 Distribution fitting (Miliç 1 Creek, 50 years) for Set 2 PDF & COV

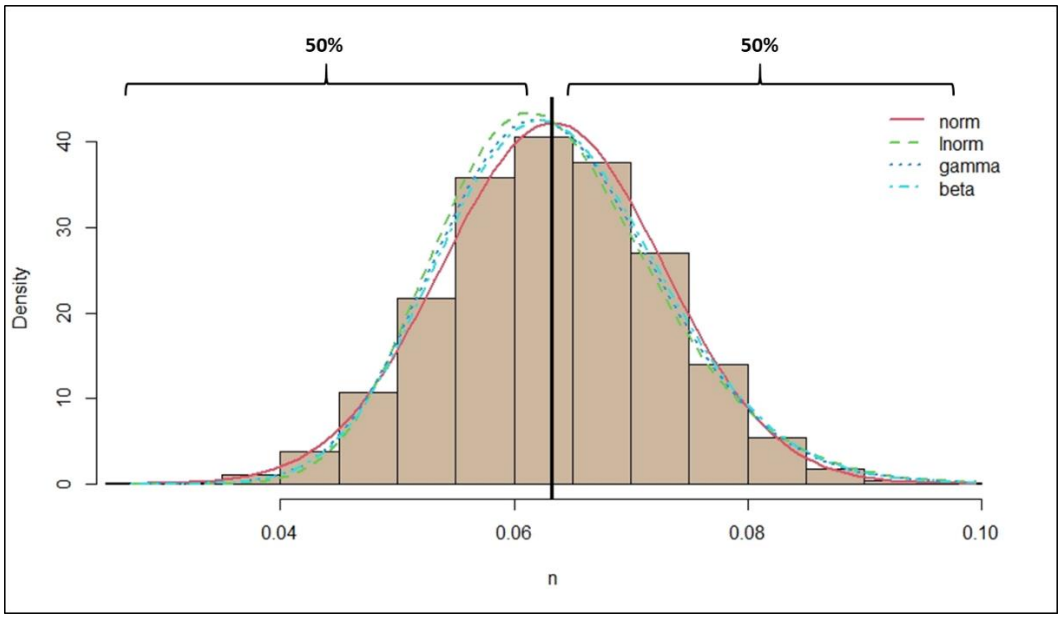

Figure C. 3 Distribution fitting (Evci Creek, 50 years) for Set 3 PDF & COV

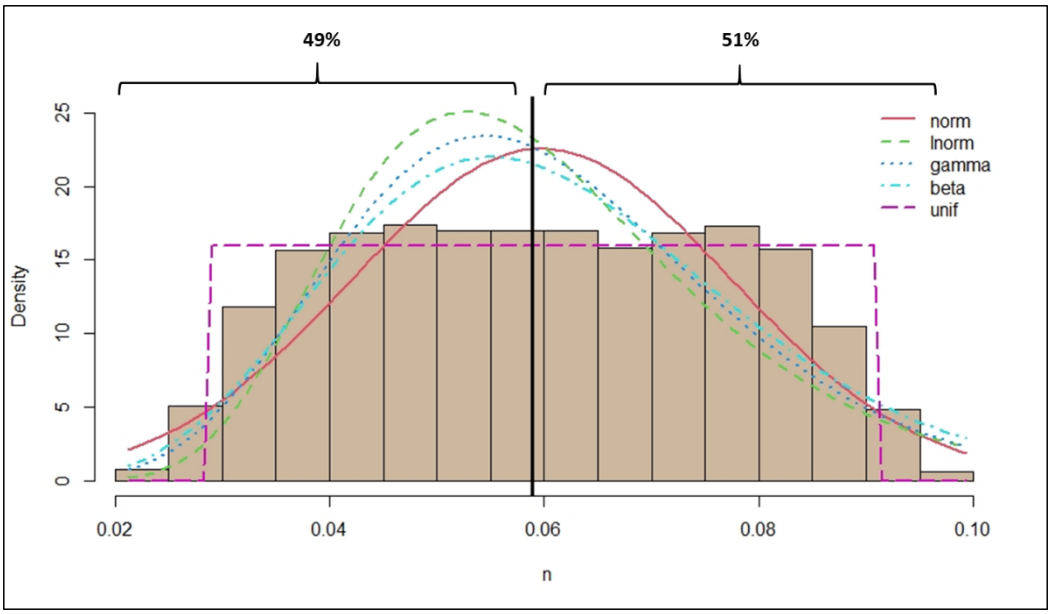

Figure C. 4 Distribution fitting (Sakarlı Creek, 500 years) for Set 1 PDF & COV

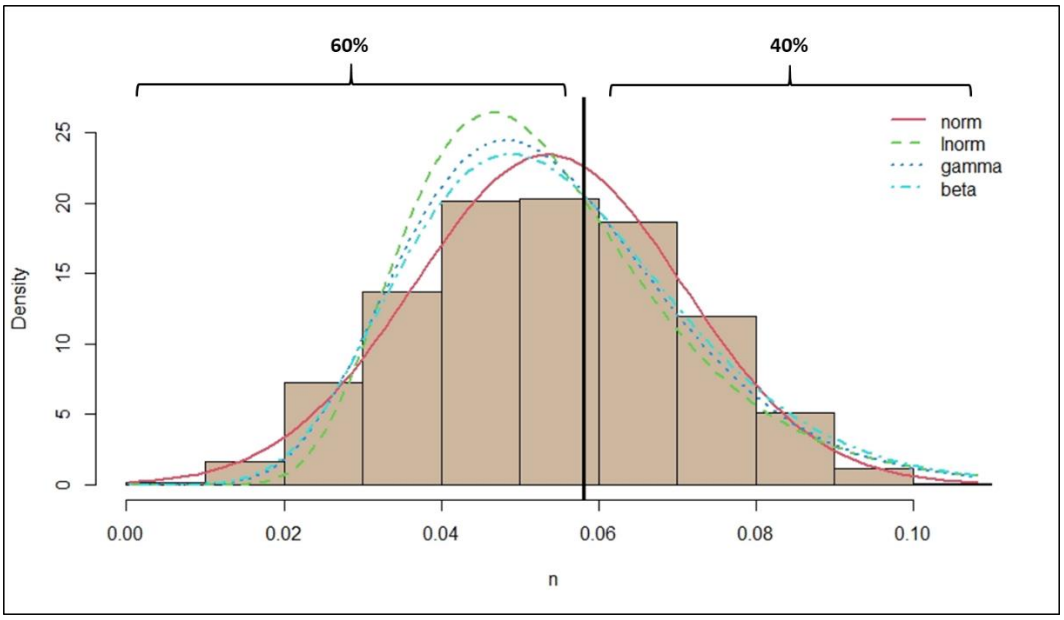

Figure C. 5 Distribution fitting (Miliç 2 Creek, 500 years) for Set 2 PDF & COV

D. Distribution Fittings of Flow Depth

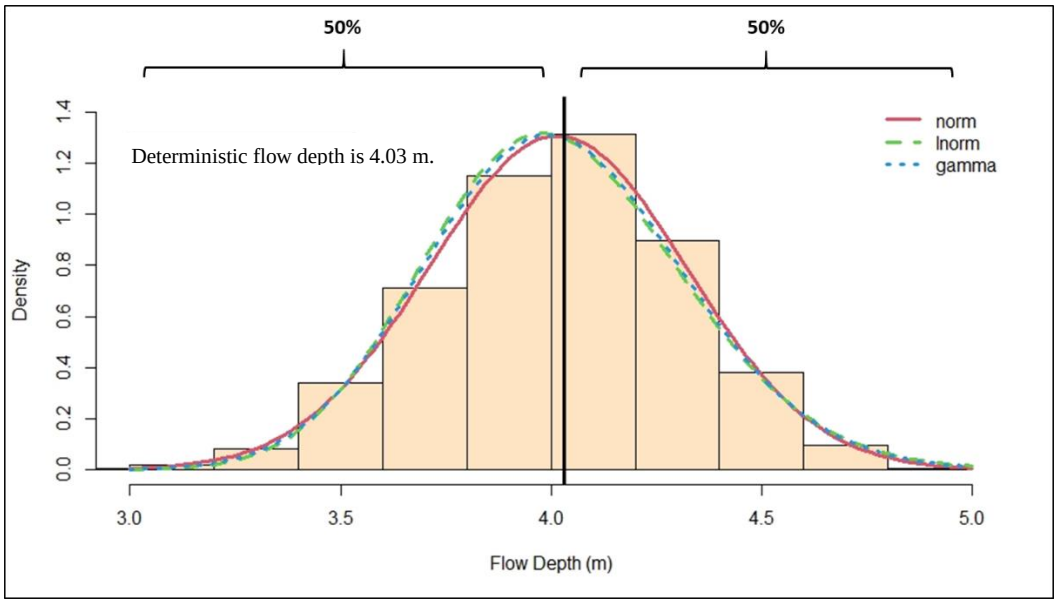

Figure D. 1 Distribution fitting for flow depth Cross-Section 2 (n: Normal distribution)

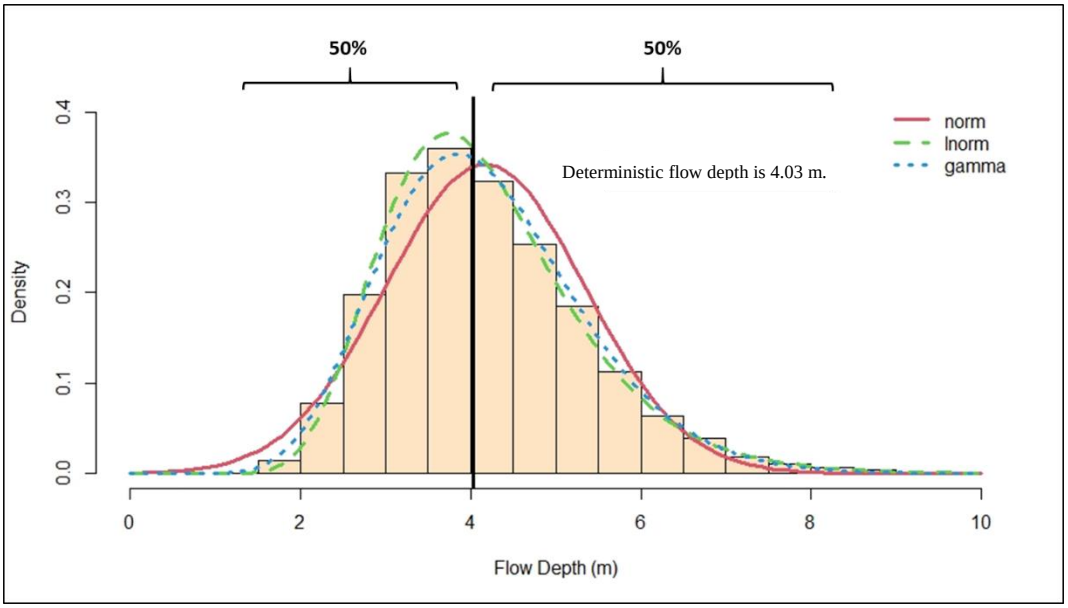

Figure D. 2 Distribution fitting for flow depth Cross-Section 2 (n: Normal distribution, Q: Log-Normal distribution)

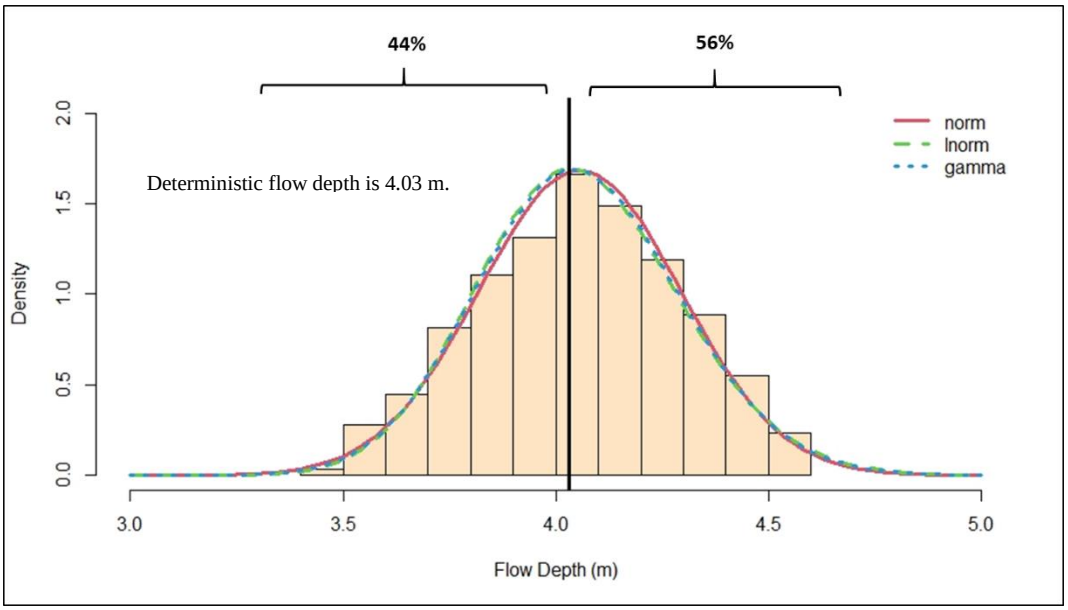

Figure D. 3 Distribution fitting for flow depth Cross-Section 2 (n: Triangular distribution)

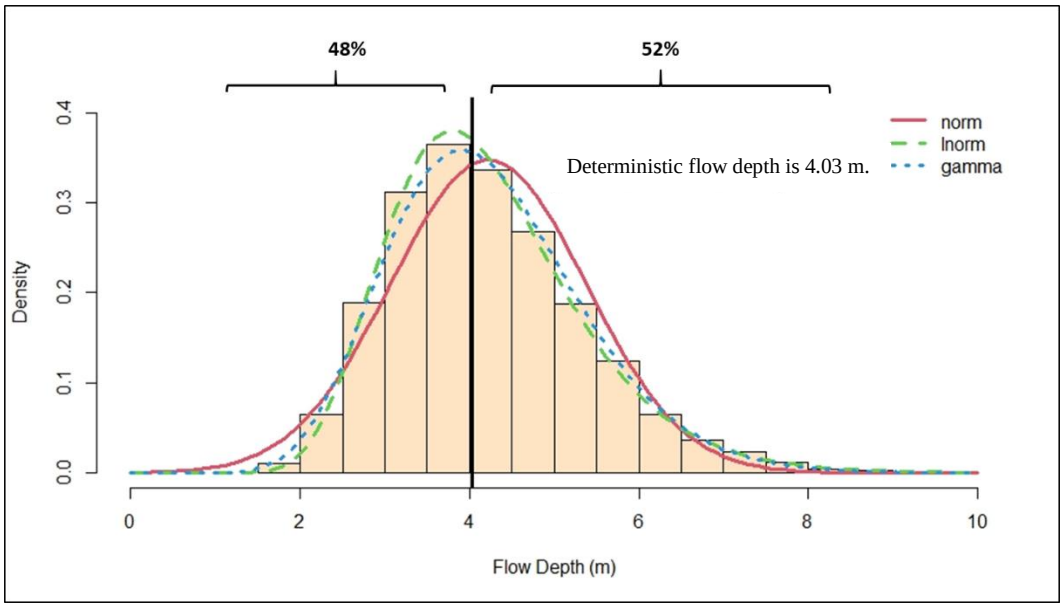

Figure D. 4 Distribution fitting for flow depth Cross-Section 2 (n: Triangular distribution, Q: Log-Normal distribution)

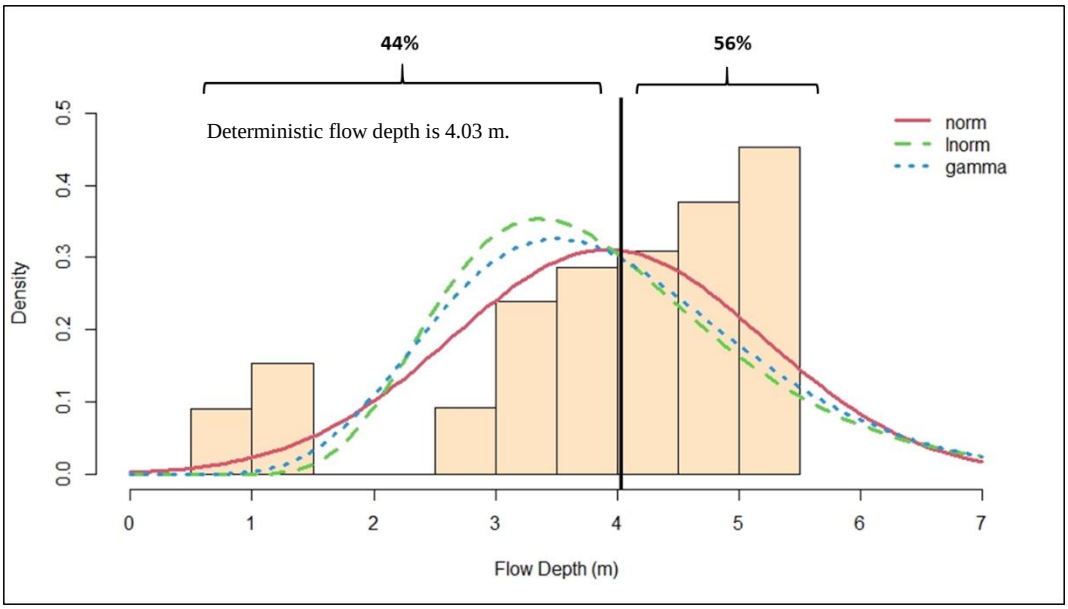

Figure D. 5 Distribution fitting for flow depth Cross-Section 2 (n: Uniform distribution)

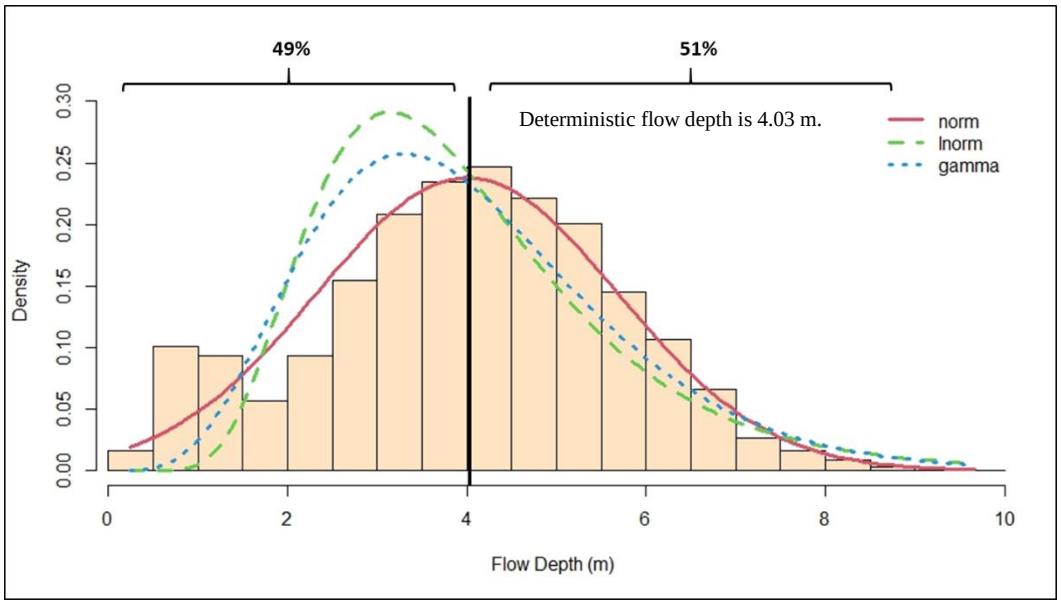

Figure D. 6 Distribution fitting for flow depth Cross-Section 2 (n: Uniform distribution, Q: Log-Normal distribution)

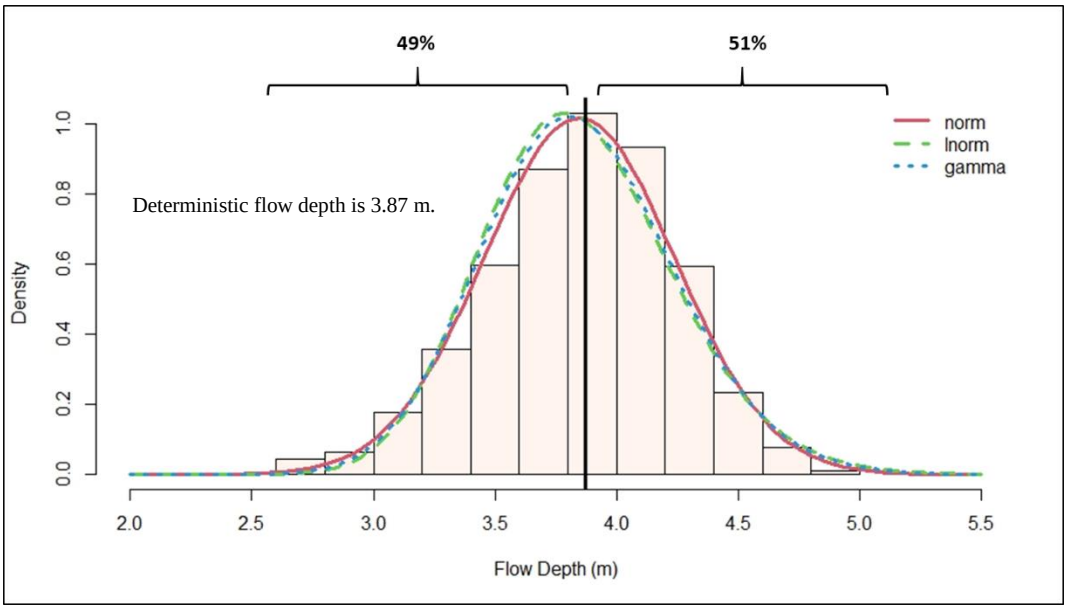

Figure D. 7 Distribution fitting for flow depth Cross-Section 3 (n: Normal distribution)

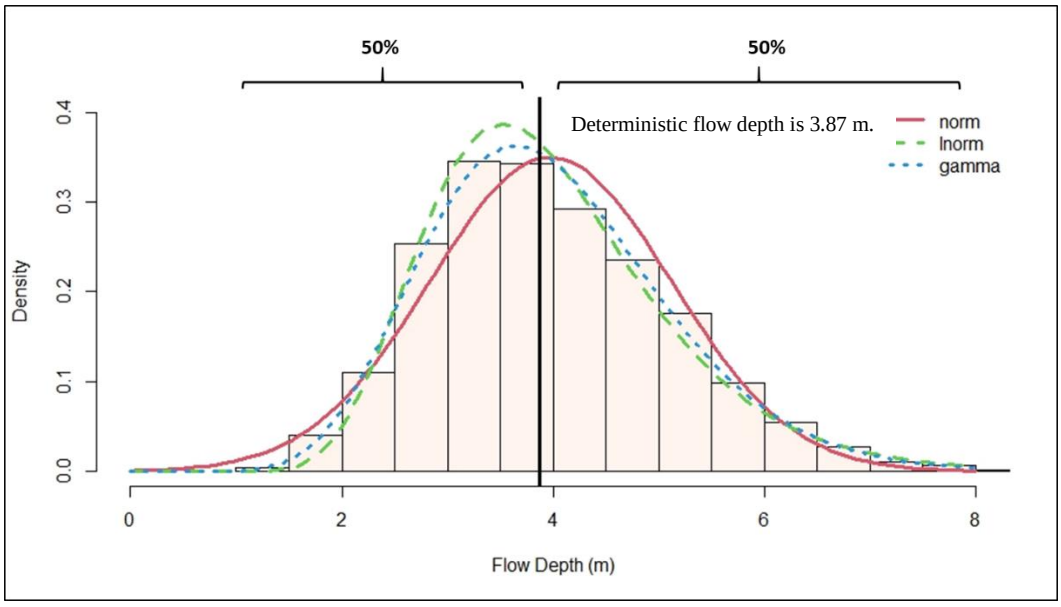

Figure D. 8 Distribution fitting for flow depth Cross-Section 3 (n: Normal distribution, Q: Log-Normal distribution)

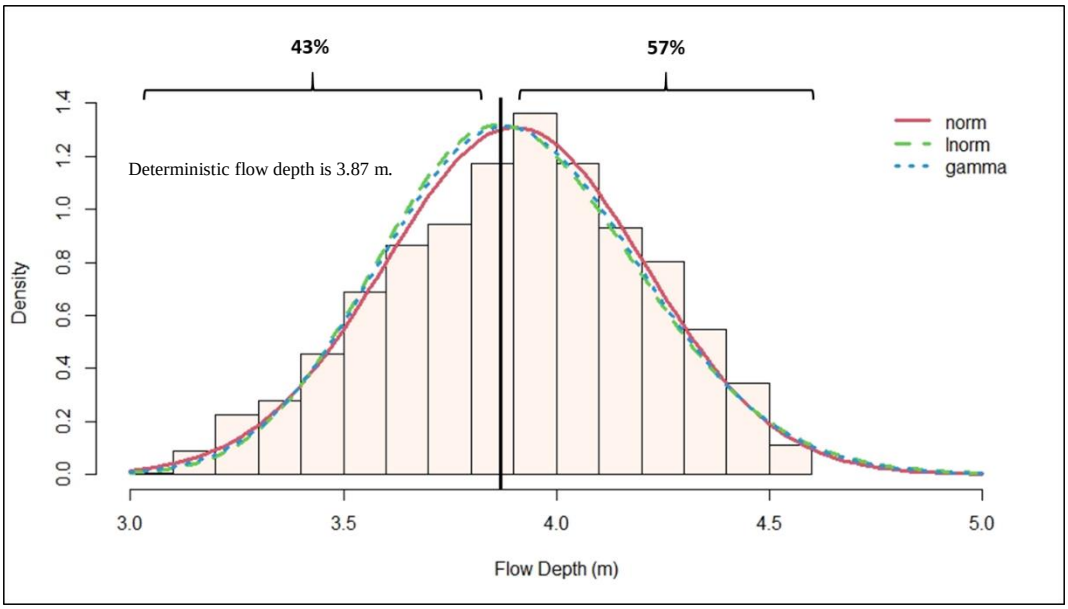

Figure D. 9 Distribution fitting for flow depth Cross-Section 3 (n: Triangular distribution)

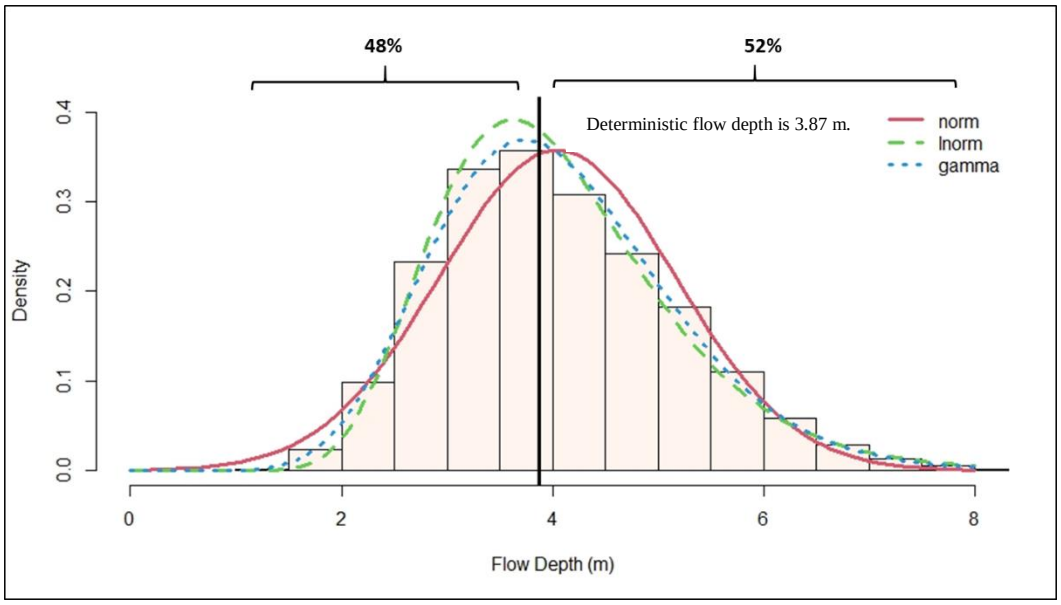

Figure D. 10 Distribution fitting for flow depth Cross-Section 3 (n: Triangular distribution, Q: Log-Normal distribution)

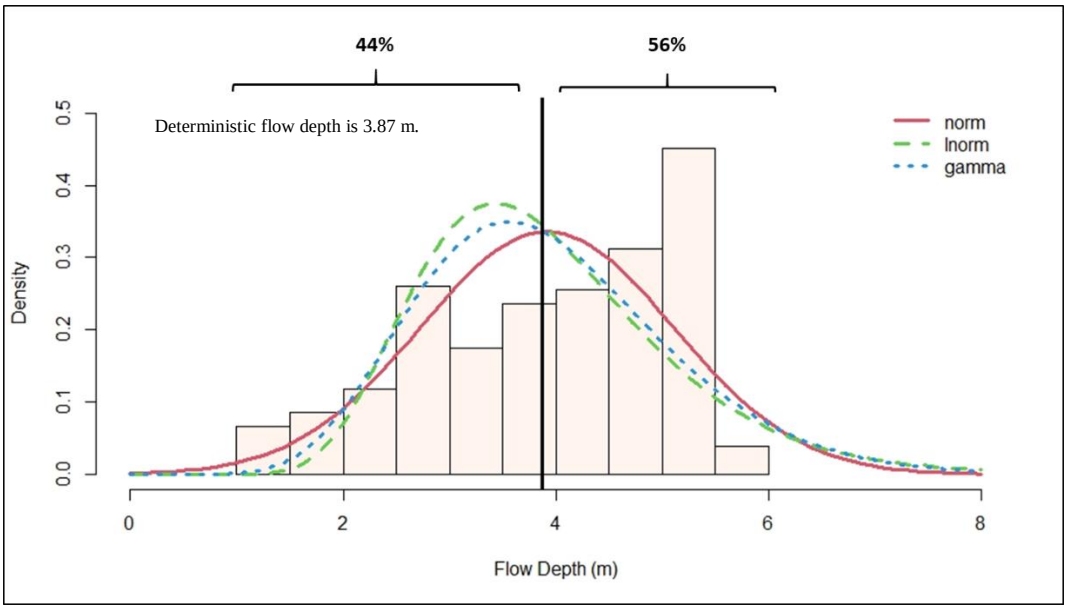

Figure D. 11 Distribution fitting for flow depth Cross-Section 3 (n: Uniform distribution)

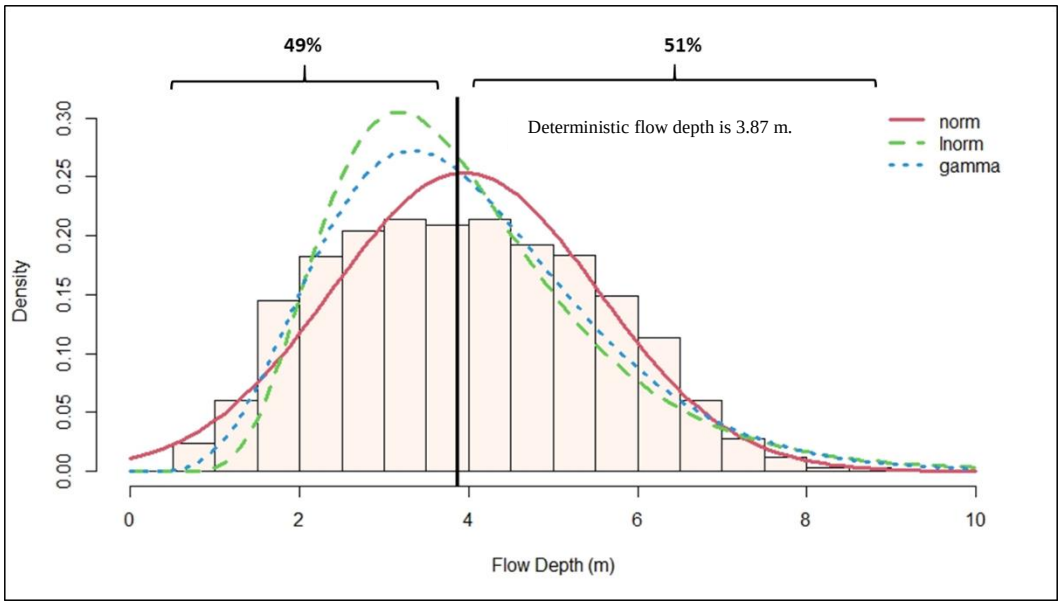

Figure D. 12 Distribution fitting for flow depth Cross-Section 3 (n: Uniform distribution, Q: Log-Normal distribution)

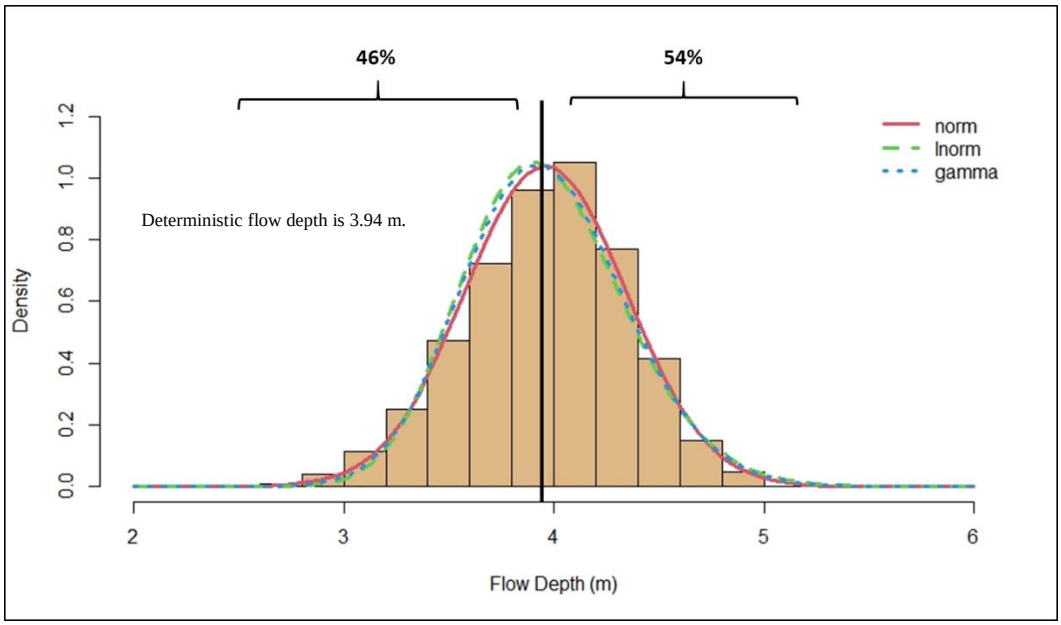

Figure D. 13 Distribution fitting for flow depth Cross-Section 3.3 BD (n: Normal distribution)

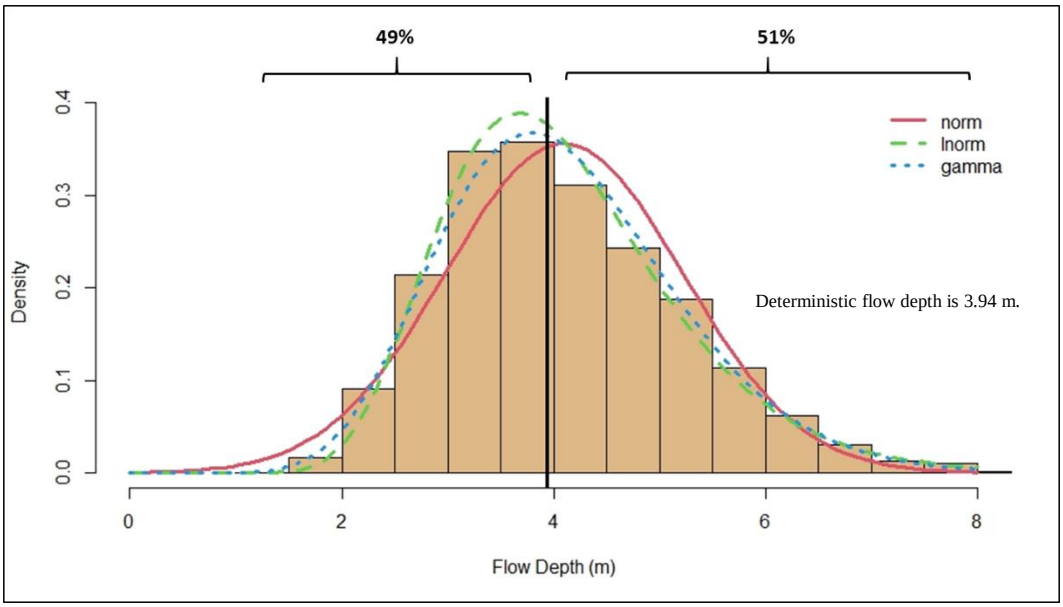

Figure D. 14 Distribution fitting for flow depth Cross-Section 3.3 BD (n: Normal distribution, Q: Log-Normal distribution)

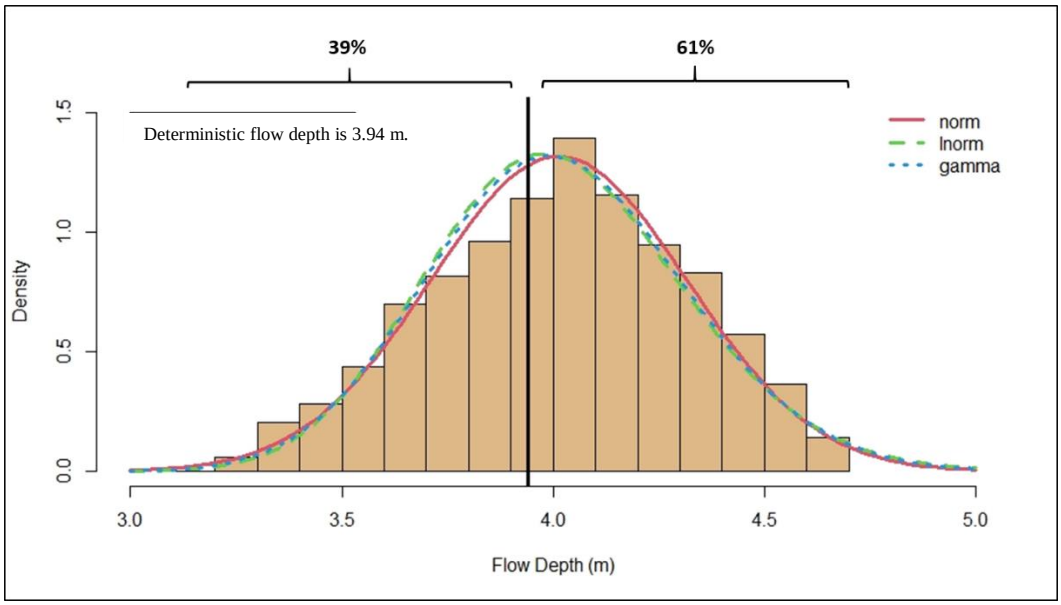

Figure D. 15 Distribution fitting for flow depth Cross-Section 3.3 BD (n: Triangular distribution)

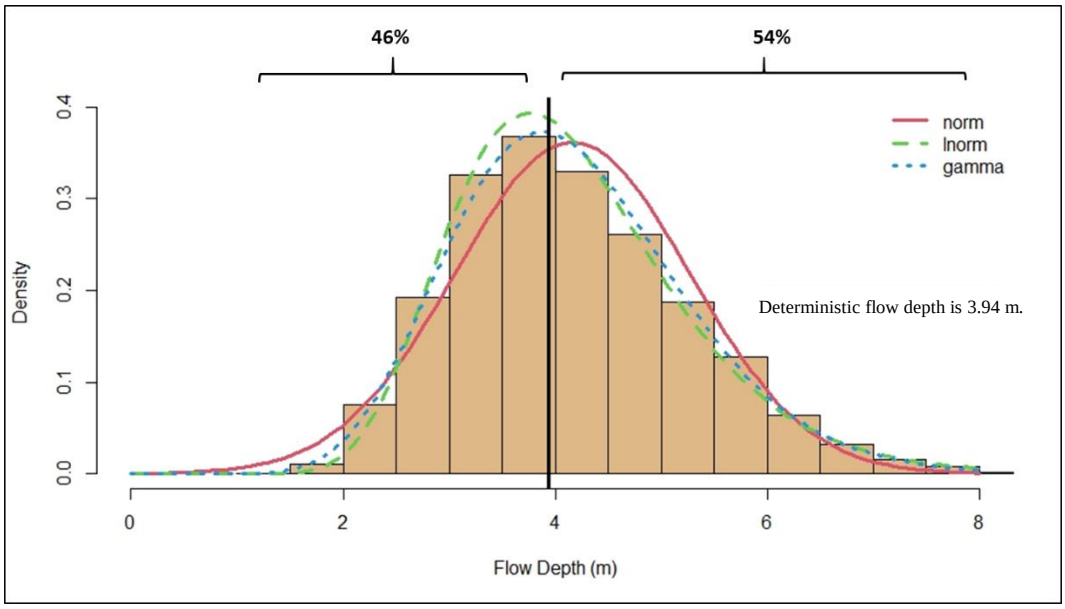

Figure D. 16 Distribution fitting for flow depth Cross-Section 3.3 BD (n: Triangular distribution, Q: Log-Normal distribution)

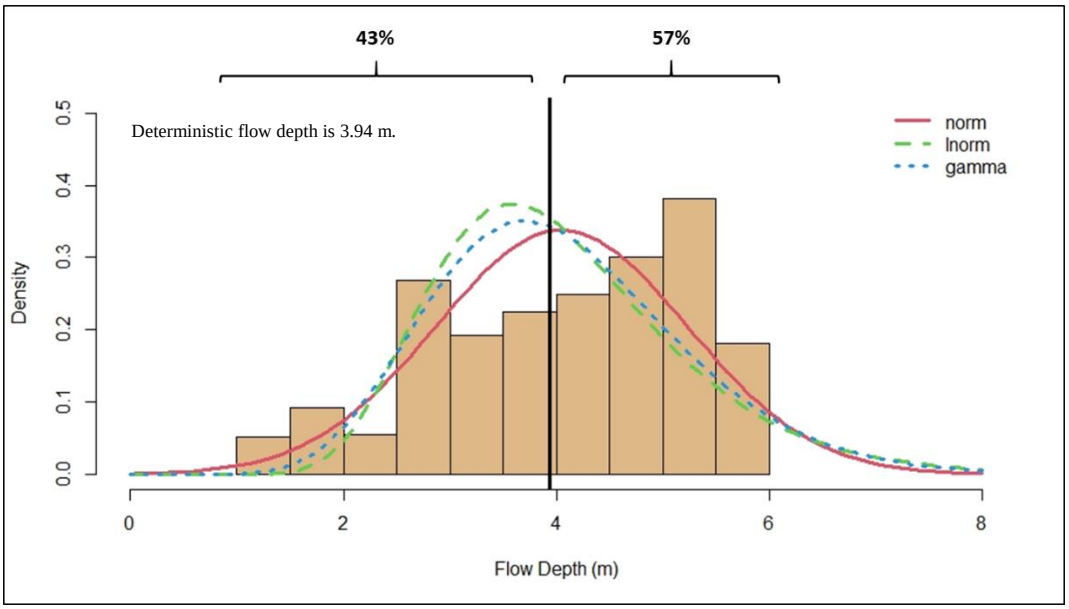

Figure D. 17 Distribution fitting for flow depth Cross-Section 3.3 BD (n: Uniform distribution)

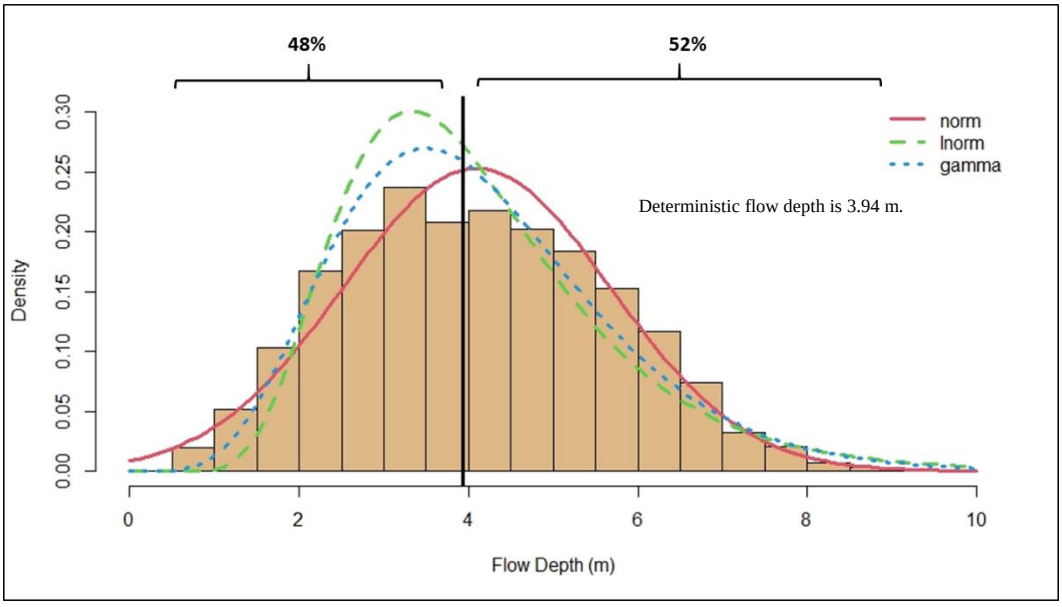

Figure D. 18 Distribution fitting for flow depth Cross-Section 3.3 BD (n: Uniform distribution, Q: Log-Normal distribution)

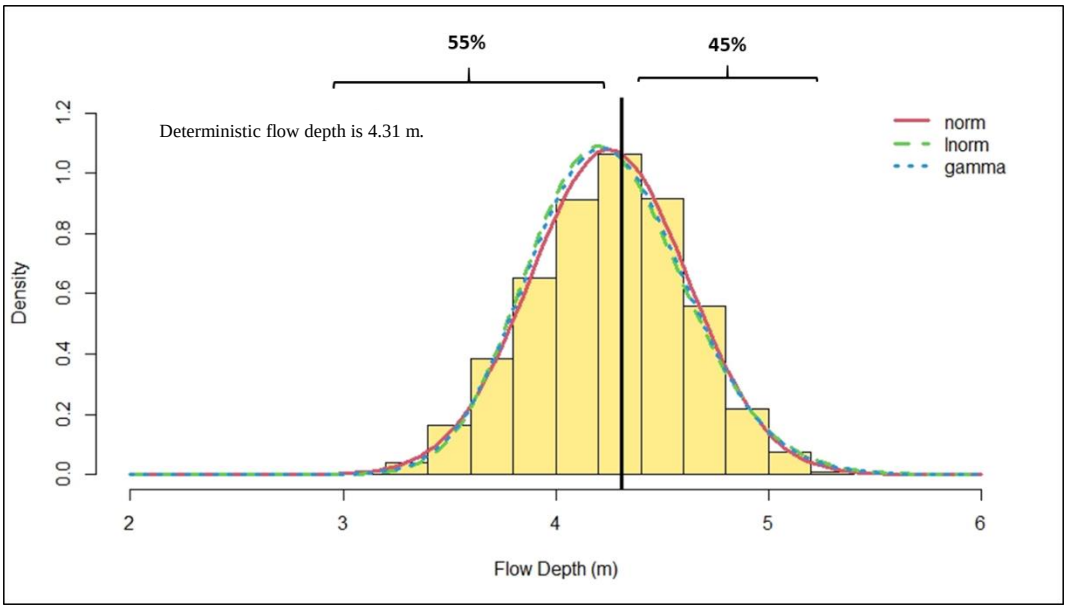

Figure D. 19 Distribution fitting for flow depth Cross-Section 3.3 BU (n: Normal distribution)

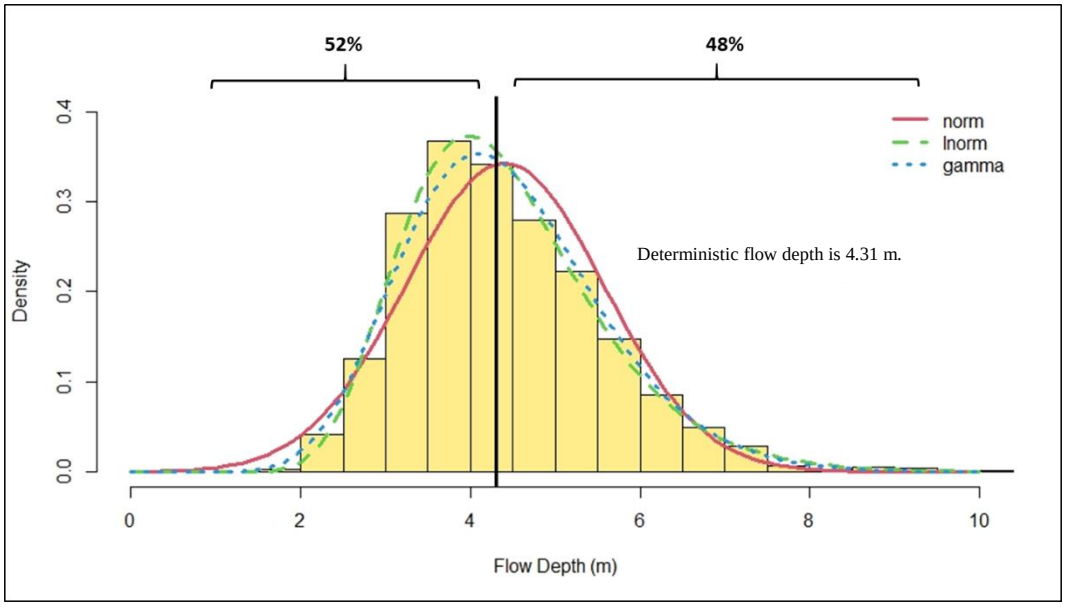

Figure D. 20 Distribution fitting for flow depth Cross-Section 3.3 BU (n: Normal distribution, Q: Log-Normal distribution)

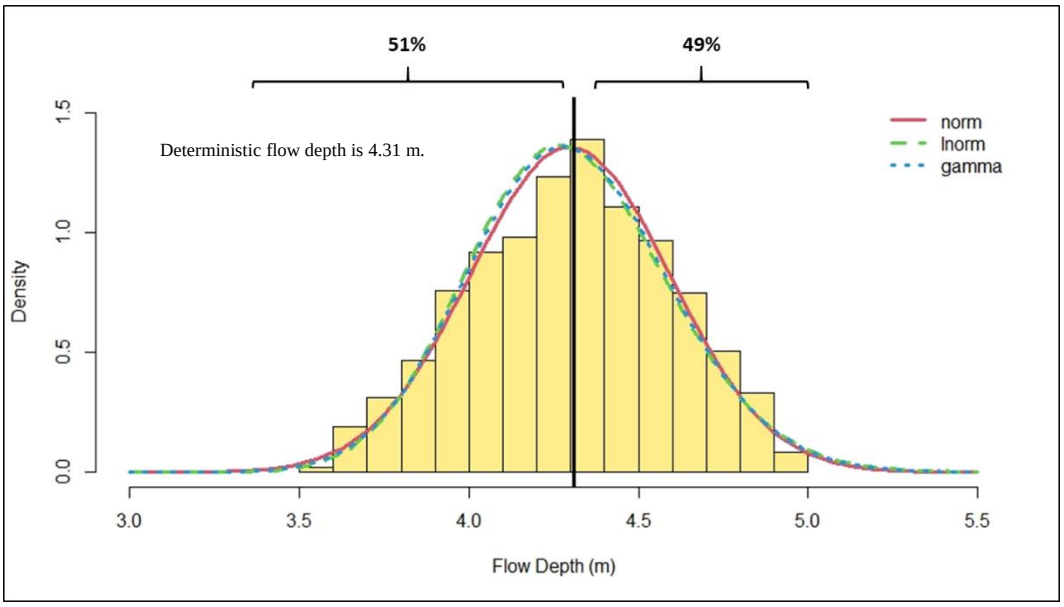

Figure D. 21 Distribution fitting for flow depth Cross-Section 3.3 BU (n: Triangular distribution)

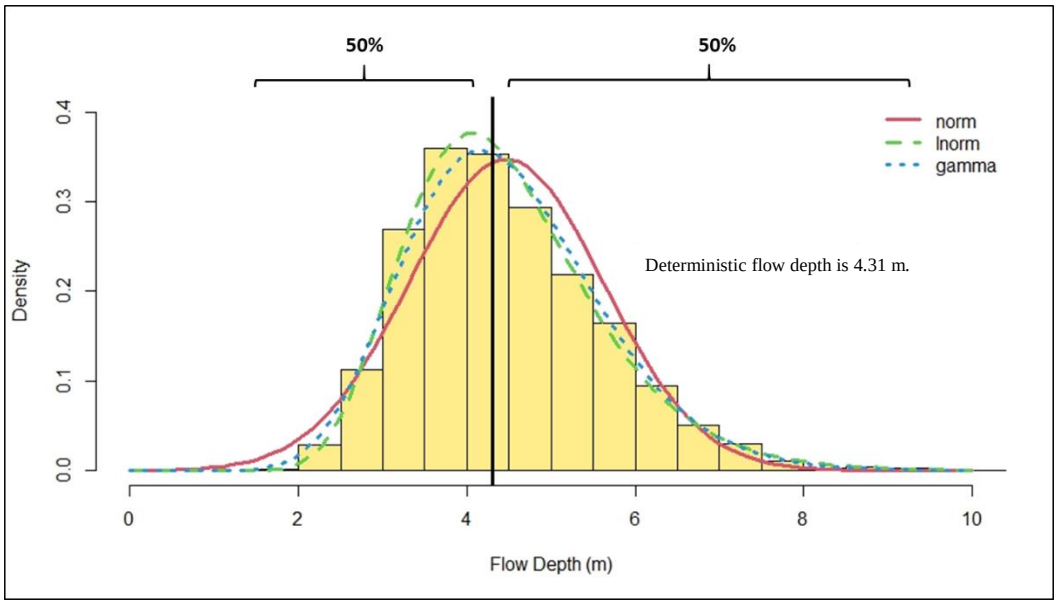

Figure D. 22 Distribution fitting for flow depth Cross-Section 3.3 BU (n: Triangular distribution, Q: Log-Normal distribution)

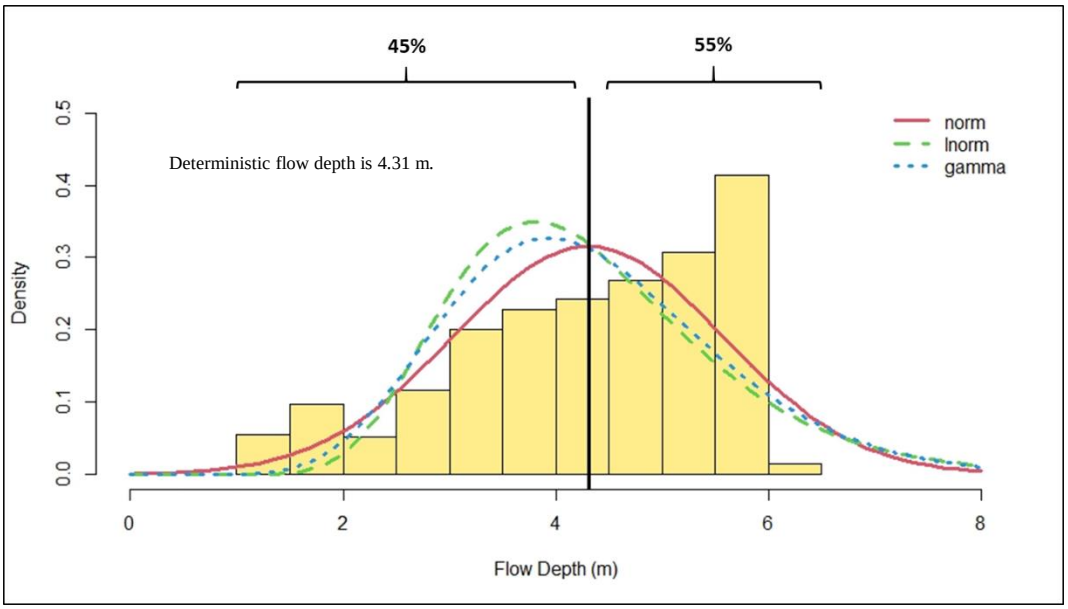

Figure D. 23 Distribution fitting for flow depth Cross-Section 3.3 BU (n: Uniform distribution)

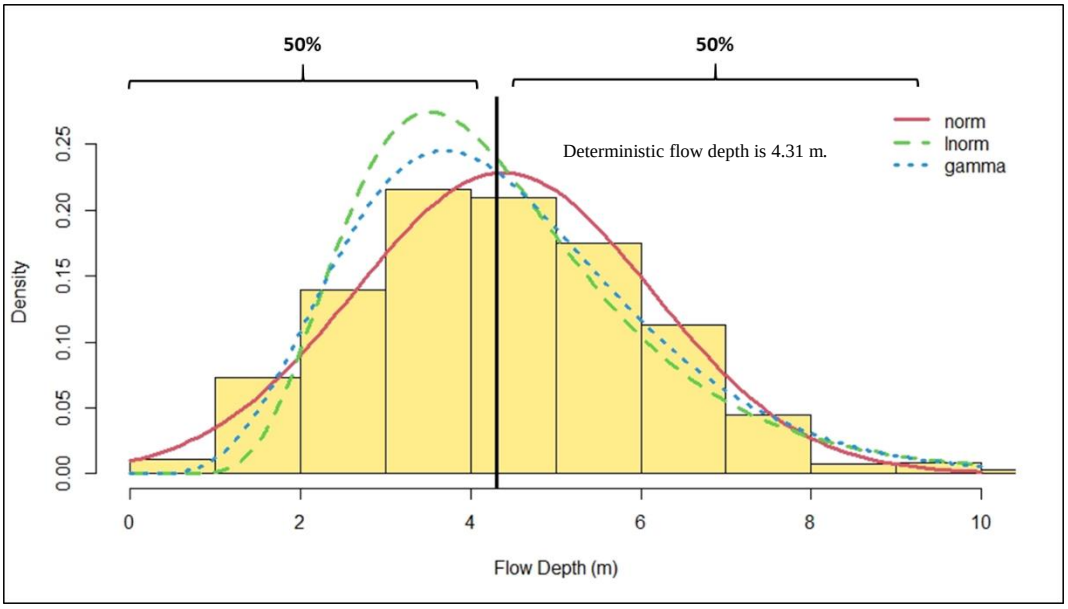

Figure D. 24 Distribution fitting for flow depth Cross-Section 3.3 BU (n: Uniform distribution, Q: Log-Normal distribution)

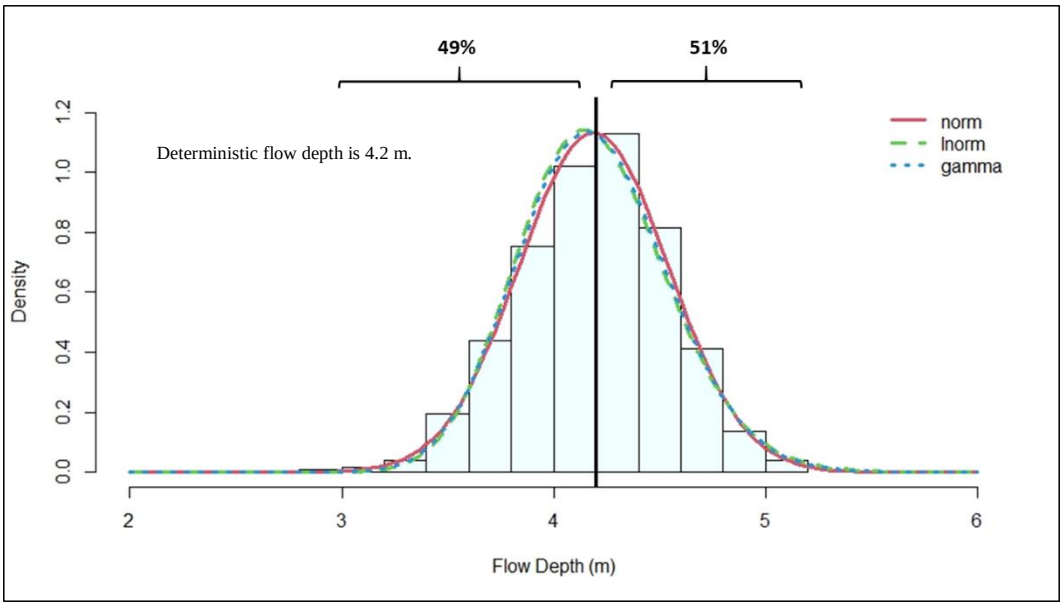

Figure D. 25 Distribution fitting for flow depth Cross-Section 4 (n: Normal distribution)

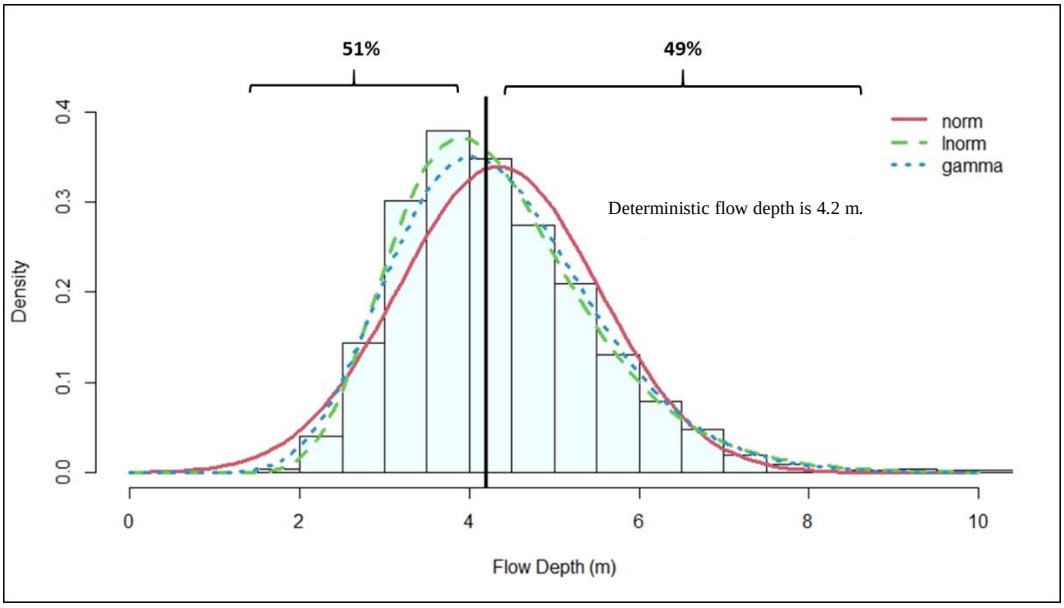

Figure D. 26 Distribution fitting for flow depth Cross-Section 4 (n: Normal distribution, Q: Log-Normal distribution)

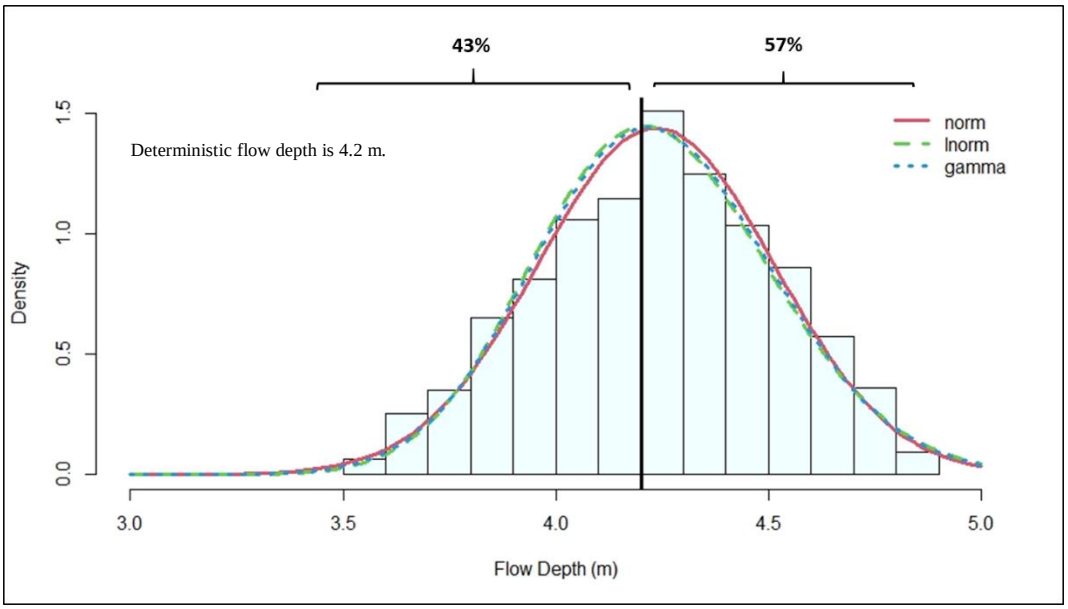

Figure D. 27 Distribution fitting for flow depth Cross-Section 4 (n: Triangular distribution)

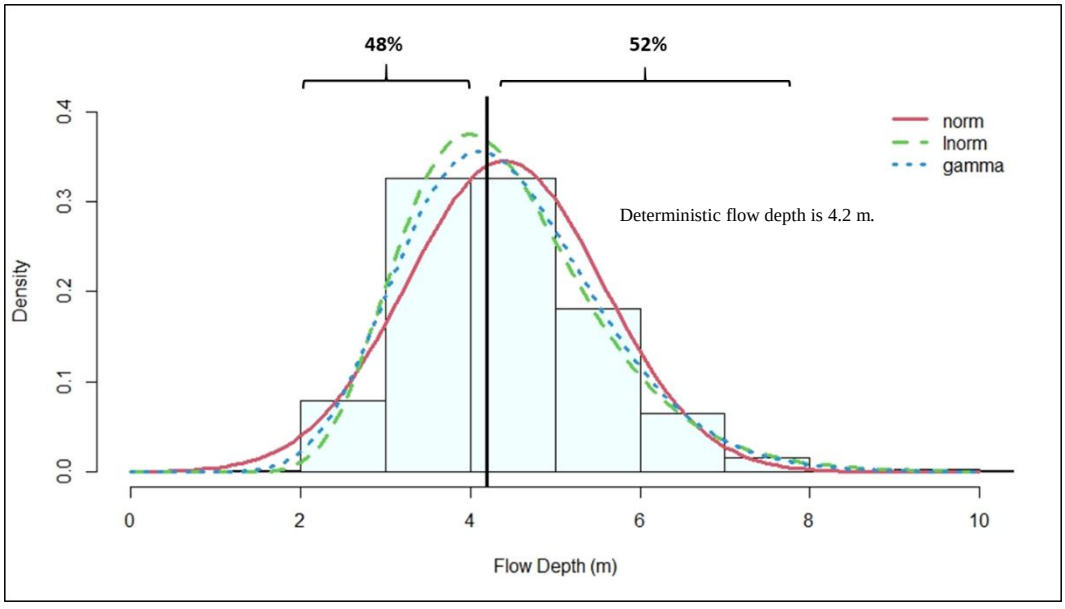

Figure D. 28 Distribution fitting for flow depth Cross-Section 4 (n: Triangular distribution, Q: Log-Normal distribution)

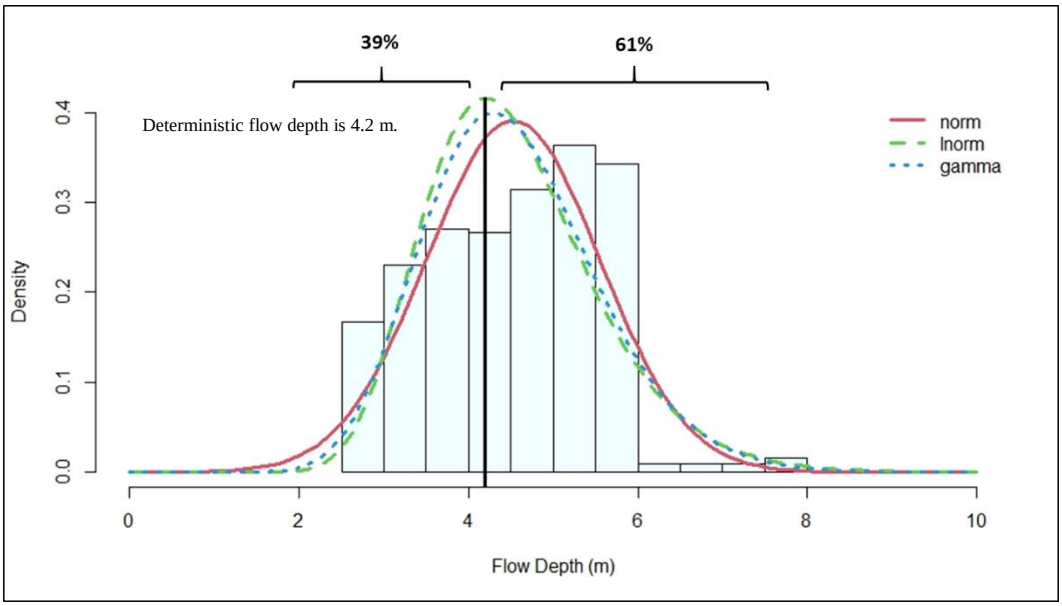

Figure D. 29 Distribution fitting for flow depth Cross-Section 4 (n: Uniform distribution)

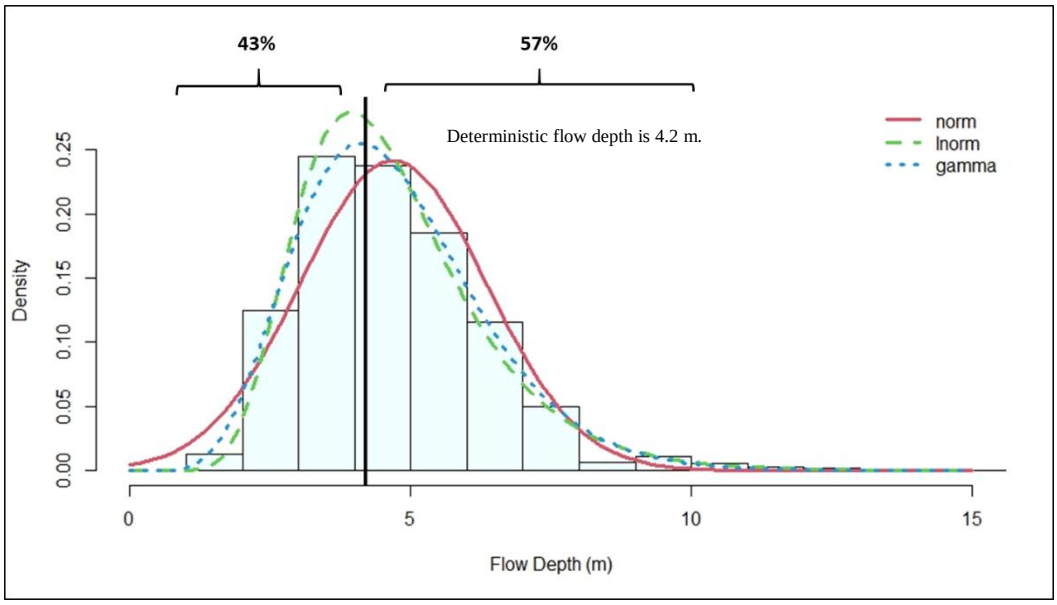

Figure D. 30 Distribution fitting for flow depth Cross-Section 4 (n: Uniform distribution, Q: Log-Normal distribution)

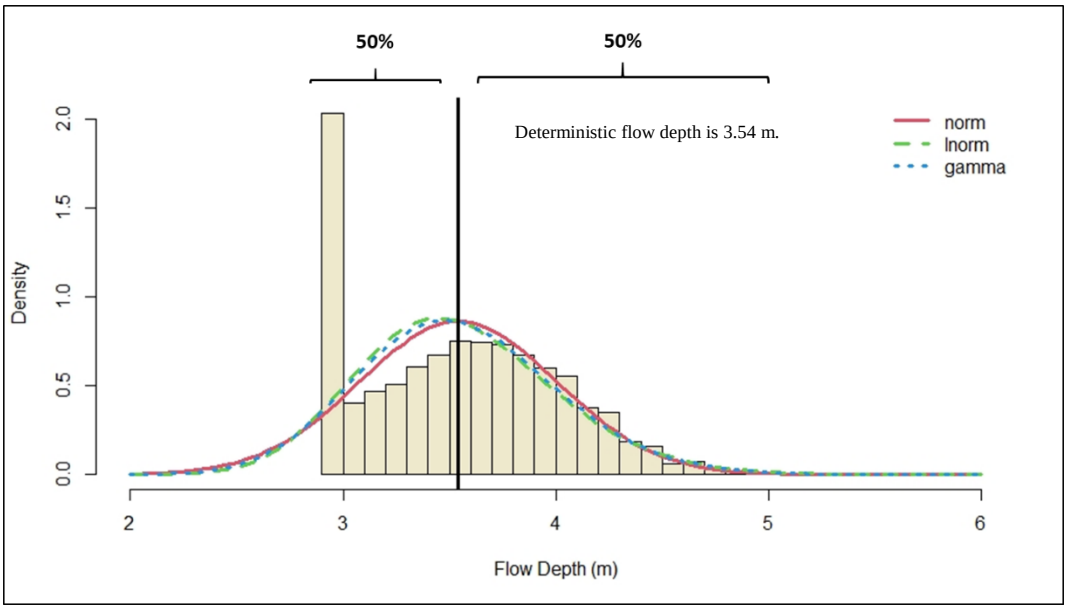

Figure D. 31 Distribution fitting for flow depth Cross-Section 7 (n: Normal distribution)

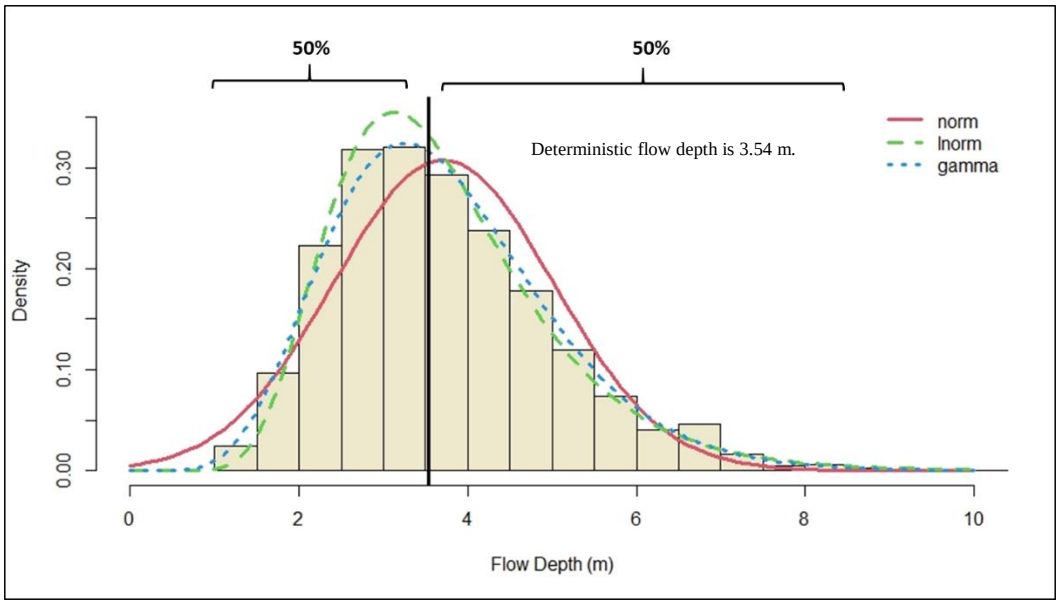

Figure D. 32 Distribution fitting for flow depth Cross-Section 7 (n: Normal distribution, Q: Log-Normal distribution)

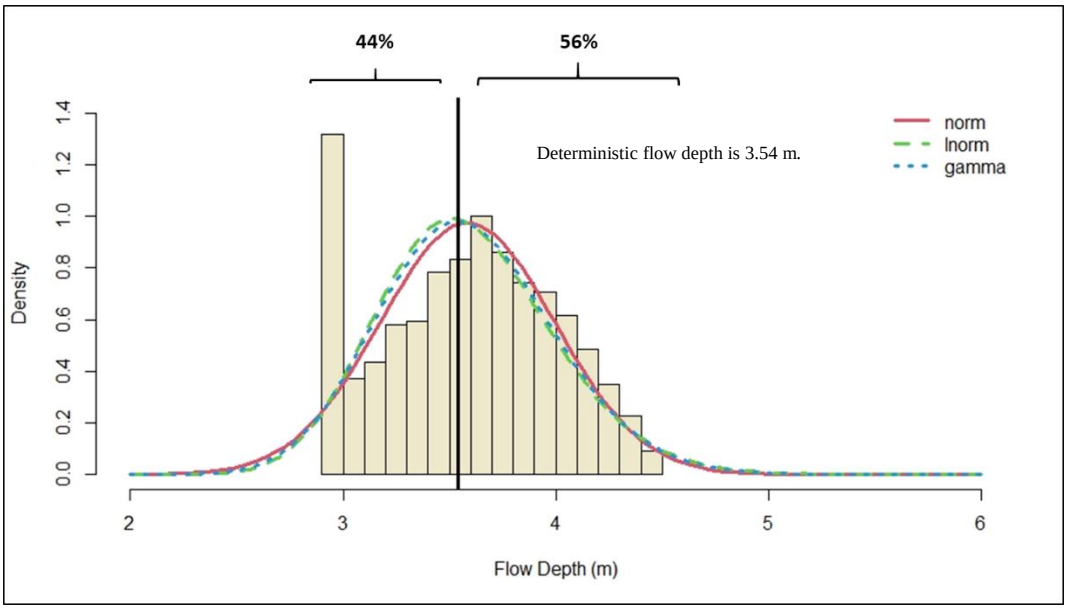

Figure D. 33 Distribution fitting for flow depth Cross-Section 7 (n: Triangular distribution)

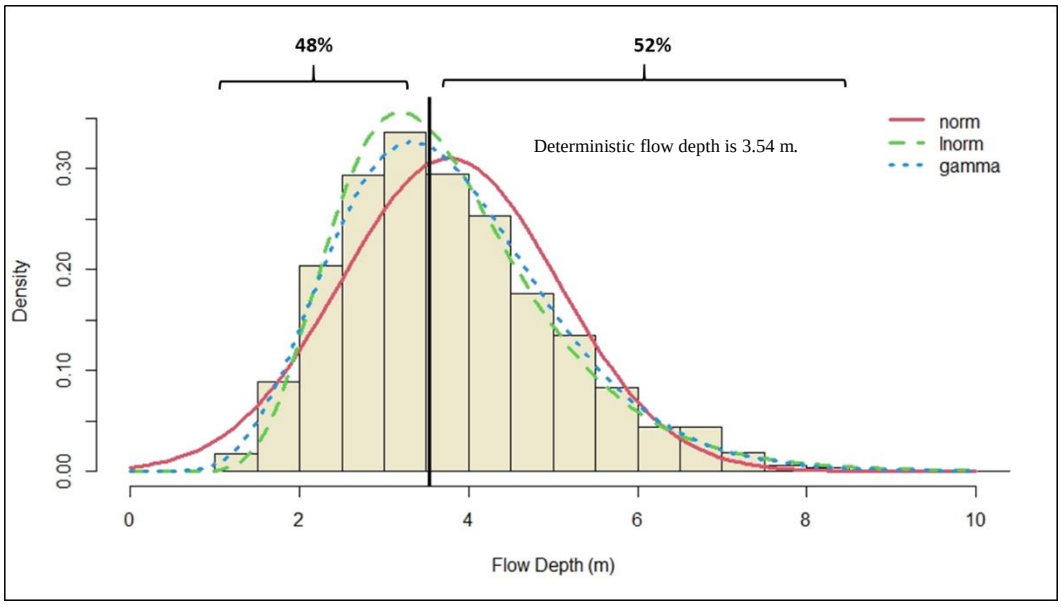

Figure D. 34 Distribution fitting for flow depth Cross-Section 7 (n: Triangular distribution, Q: Log-Normal distribution)

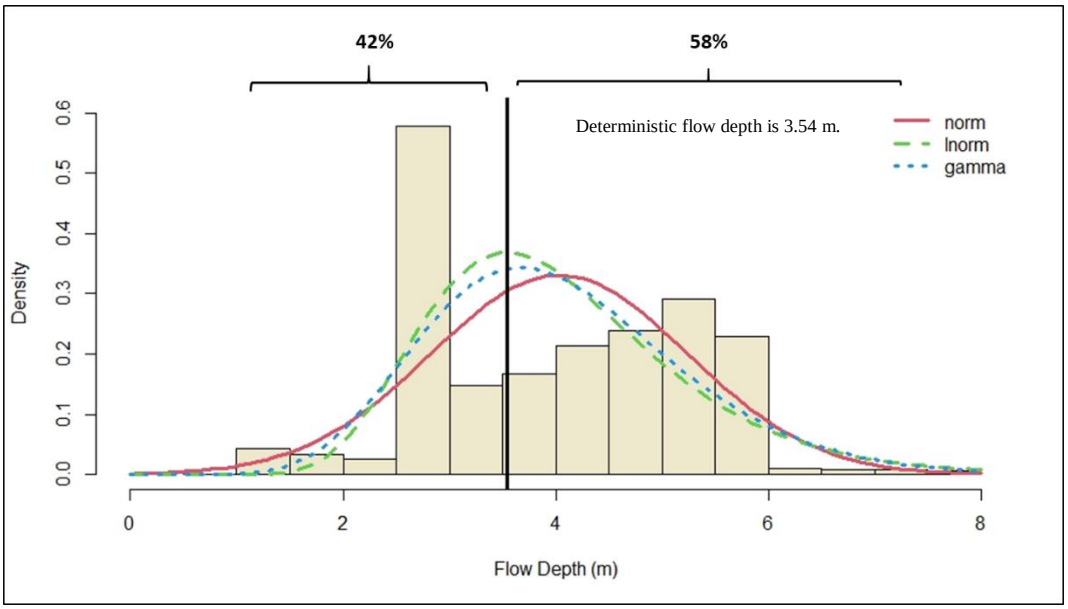

Figure D. 35 Distribution fitting for flow depth Cross-Section 7 (n: Uniform distribution)

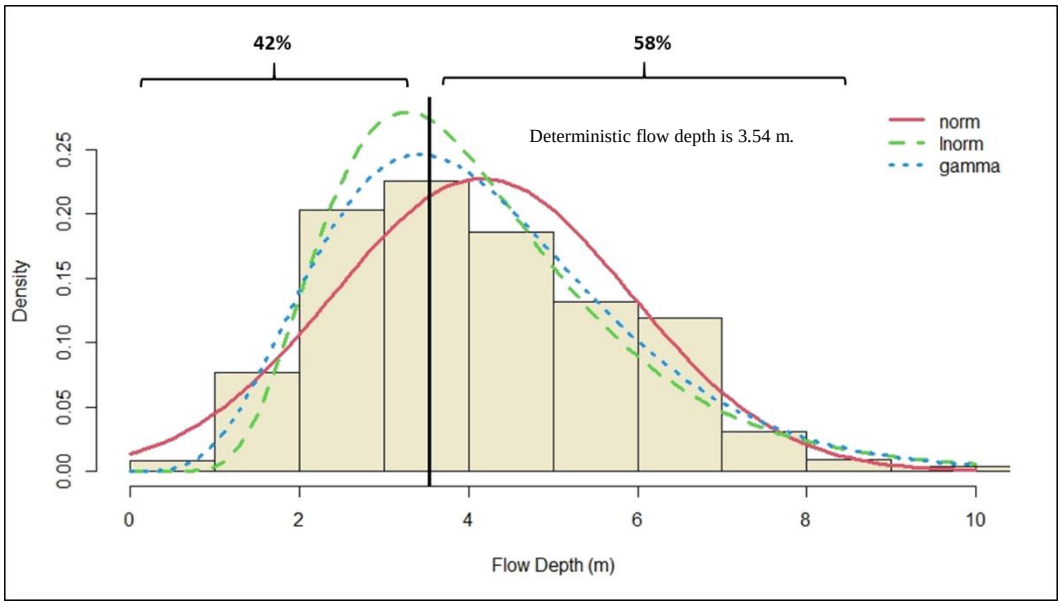

Figure D. 36 Distribution fitting for flow depth Cross-Section 7 (n: Uniform distribution, Q: Log-Normal distribution)

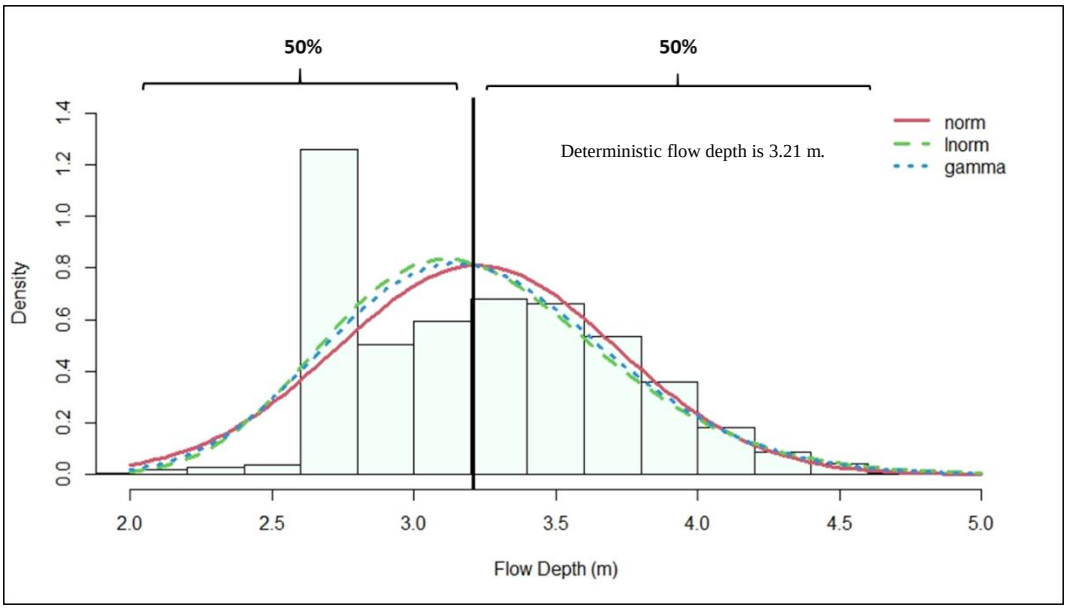

Figure D. 37 Distribution fitting for flow depth Cross-Section 11 (n: Normal distribution)

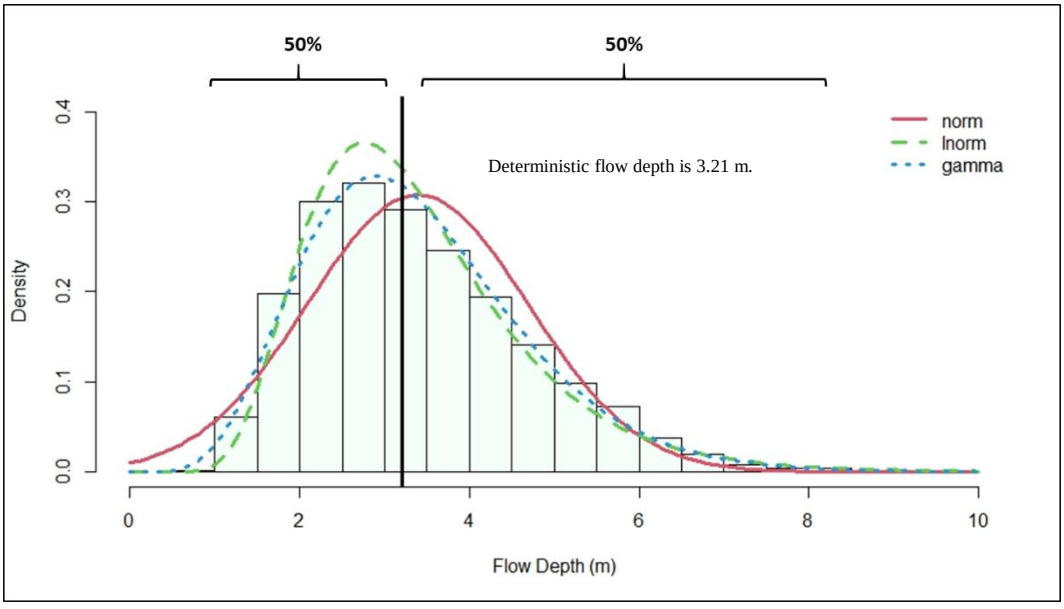

Figure D. 38 Distribution fitting for flow depth Cross-Section 11 (n: Normal distribution, Q: Log-Normal distribution)

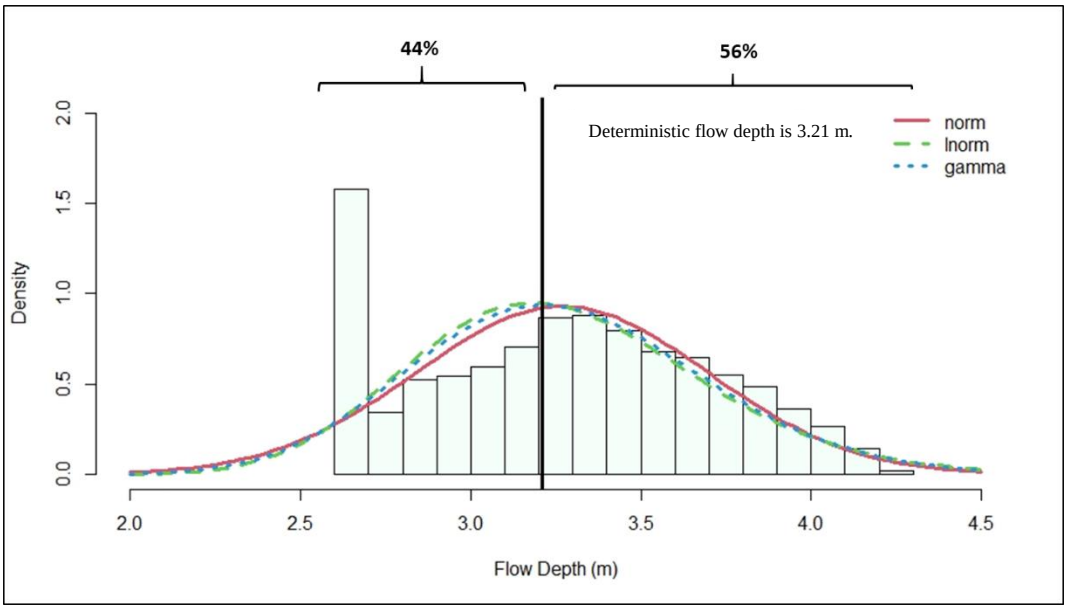

Figure D. 39 Distribution fitting for flow depth Cross-Section 11 (n: Triangular distribution)

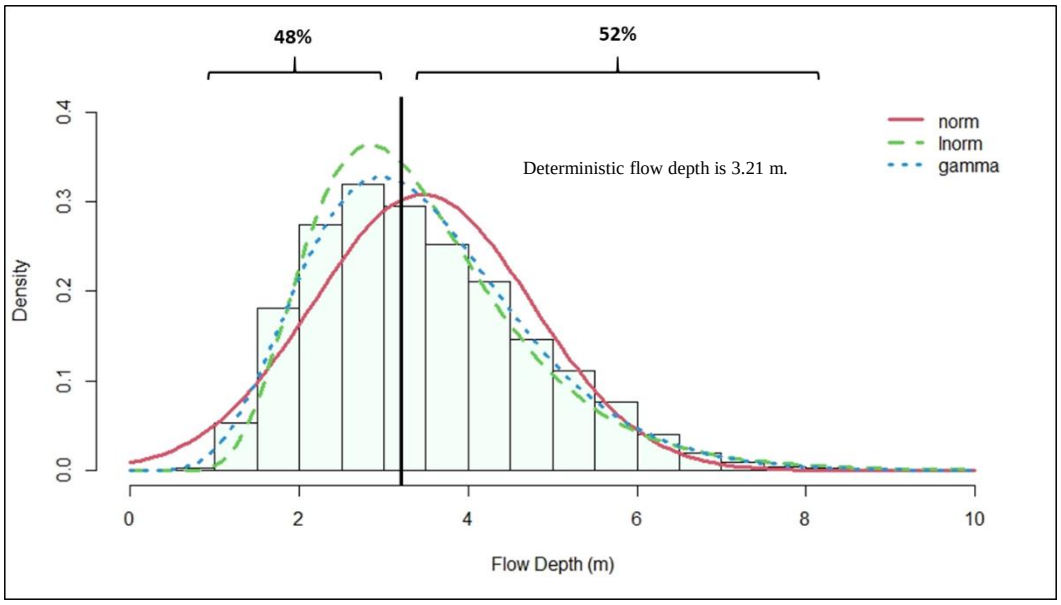

Figure D. 40 Distribution fitting for flow depth Cross-Section 11 (n: Triangular distribution, Q: Log-Normal distribution)

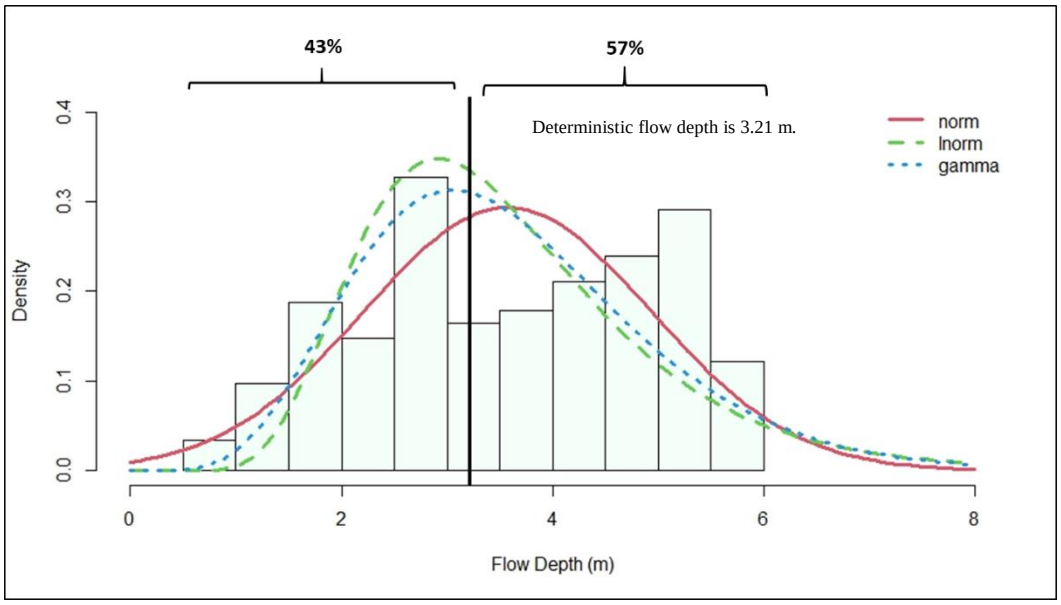

Figure D. 41 Distribution fitting for flow depth Cross-Section 11 (n: Uniform distribution)

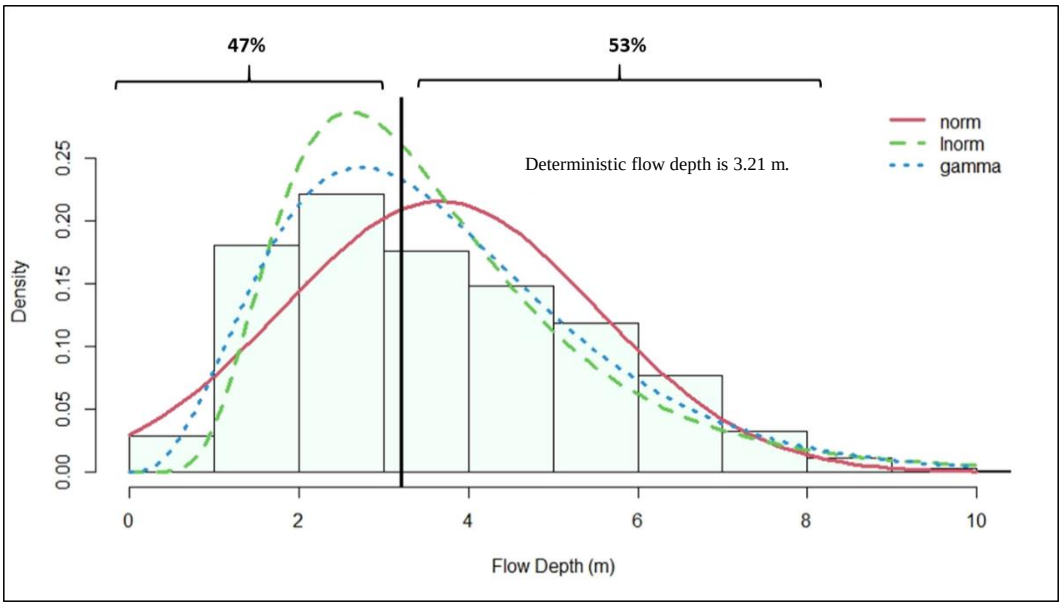

Figure D. 42 Distribution fitting for flow depth Cross-Section 11 (n: Uniform distribution, Q: Log-Normal distribution)